UNIVERSITÀ DI PARMA

UNIVERSITA' DEGLI STUDI DI PARMA

DOTTORATO DI RICERCA IN

"MEDICINA MOLECOLARE"

CICLO XXXVI

PHOSPHORYLATION OF CARDIAC SODIUM CHANNEL ANTICIPATES MANIFESTATIONS OF AGING MYOPATHY

Coordinatore:

Chiar.mo Prof. Prisco Mirandola

Tutor:

Chiar.mo Prof. Emilio Macchi

Dottorando: Emanuele Pizzo

Anni Accademici 2020/2021 – 2022/2023

Content

RIASSUNTO

La disfunzione diastolica e il prolungamento della ripolarizzazione ventricolare si osservano tipicamente negli anziani, tuttavia non e' chiaro se questi fattori sono associati alla progressiva manifestazione della cardiomiopatia dell'invecchiamento. In modelli sperimentali, l'invecchiamento porta ad un aumento della corrente tardiva del sodio (I_{NaL}) nei cardiomiociti, e pertanto abbiamo ipotizzato che questa corrente e' coinvolta nel prolungamento della ripolarizzazione con conseguenze sul rilassamento del miocardio dell'animale anziano. A tal proposito, abbiamo studiato topi wild-type (WT) e animali geneticamente modificati con mutazioni della proteina Nav1.5, che forma i canali ionici del sodio. In particolare, abbiamo utilizzato mutazioni a guadagno di funzione (Gain of Function, GoF) o a perdita di funzione (Loss of Function, LoF) del sito fosforilativo di Nav1.5 che causano, rispettivamente, un aumento e una stabilizzazione della corrente tardiva del sodio. I risultati sono stati ottenuti sia in topi maschi che femmine. Con l'invecchiamento, i topi WT hanno sviluppato un prolungamento della ripolarizzazione (intervallo QT dell'elettrocardiogramma) ed un'alterata funzione diastolica. La protratta ripolarizzazione e la disfunzione diastolica si sono manifestate prematuramente nei topi giovani GoF, e sono progressivamente deteriorate con l'eta'. Invece, gli animali LoF hanno mantenuto una buona funzione contrattile e di rirpolarizzazione durante l'invecchiamento. A livello cellulare, le fasi di contrazione/rilassamento erano prolungate nei miociti WT invecchiati rispetto alle cellule giovani. Invece, il prolungamento della meccanica di contrazione e' comparso prematuramente allo stadio giovanile nei miociti GoF, ed e' progressivamente deteriorato con l'età. Al contrario, miociti LoF hanno mantenuto una buona funzione meccanica durante l'invecchiamento. Collettivamente, questi risultati dimostrano che la fosforilazione della proteina Nav1.5 e la corrente tardiva di sodio modulano il rilassamento dei miociti, costituendo il meccanismo che collega la ripolarizzazione ventricolare ritardata con la disfunzione diastolica.

ABSTRACT

Diastolic dysfunction and delayed ventricular repolarization are typically observed in the elderly, but whether these defects are intimately associated in the progressive manifestation of the aging myopathy remains to be determined. In this regard, aging in experimental animals is coupled with increased late Na^+ current (I_{NaL}) in cardiomyocytes, raising the possibility that I_{NaL} conditions the modality of electrical recovery and myocardial relaxation of the aged heart. For this purpose, aging male and female wild-type (WT) C57Bl/6 mice were studied together with genetically engineered mice with phosphomimetic (gain-of-function, GoF) or ablated (loss-of-function, LoF) mutations of the sodium channel Nav1.5 at Ser571 associated with, respectively, increased and stabilized I_{NaL}. At ~18 months (m) of age, WT mice developed prolonged duration of the QT interval of the electrocardiogram and impaired diastolic left ventricular (LV) filling, defects that were reversed by I_{NaL} inhibition. Prolonged repolarization and impaired LV filling occurred prematurely in adult (~5 m) GoF mutant mice, whereas these alterations were largely attenuated in aging LoF mutant animals. Ca^{2+} transient decay and kinetics of myocyte shortening/relengthening were delayed in aged (~24 m) WT myocytes, with respect to adult cells. In contrast, delayed Ca^{2+} transients and contractile dynamics occurred at adult stage in GoF myocytes and further deteriorated at old age. Conversely, myocyte mechanics were minimally affected in aging LoF cells. Collectively, these results document that Nav1.5 phosphorylation at Ser571 and the late Na^+ current modulates the modality of myocyte relaxation, constituting the mechanism linking delayed ventricular repolarization and diastolic dysfunction.

INTRODUCTION

Aging is the major independent risk factor of chronic heart failure (HF) in people ≥65 years of age (Schwartz & Zipes, 2011; Tsao *et al.*, 2022). Elderly people constitute a large segment of the US population and trends in the patterns of aging predict an increase of the number of individual 65 years or older from ~56 million in 2020, to ~82 million in 2040 (Colby & Ortman, 2015). Advance in overall age is unavoidably coupled with augmented incidence of cardiovascular disease, thus, identification of factors involved in the origin and progression of aging myopathy is critical to develop preventive and therapeutic strategies for elderly patients.

A multitude of structural and functional modifications have been proposed as determinants of aging myopathy (Lakatta, 2003; Li *et al.*, 2020), but factors responsible for the increased incidence of cardiovascular diseases in the elderly remain to be elucidated. Our data in experimental animals indicate that aging is coupled with increase of the late Na^+ current (I_{NaL}) and action potential (AP) prolongation in myocytes, factors centrally involved in the protracted electrical recovery, arrhythmogenicity, declined ventricular compliance, and impaired contractile reserve of the aged heart (Signore *et al.*, 2015; Sorrentino *et al.*, 2016). Specifically, I_{NaL} increases by ~60% in myocytes from aged (26-30 months) mice, with respect to cells from adult (3 months) animals, whereas the AP, measured at 90% repolarization, is prolonged by ~50% in cells from old mice, with respect to young animals (Signore *et al.*, 2015).The adoption of prolonged electrical recovery by the myocardium is a common adaptation to conditions characterized by increased workload (Tomaselli & Marban, 1999; Janse, 2004), a scenario that appears to be operative in the old heart. Long AP promotes Ca^{2+} influx and provides positive inotropic effect to the muscle, sustaining systemic hemodynamic requirements, but enhancing the vulnerability of the heart to electrical disturbances and life-threatening arrhythmias (Janse, 2004; Signore *et al.*, 2013; Signore *et al.*, 2015). Enhanced I_{NaL} with aging contributes to the AP prolongation but it may also raise intracellular Na^+ concentration, which in turn enhances cytoplasmic Ca^{2+} load and contractile force (Pourrier *et al.*, 2014; Kornyeyev *et al.*, 2016), but negatively interferes with myocyte relengthening and diastolic function (Signore *et al.*, 2015; Cervantes *et al.*, 2022).

I_{NaL} is enhanced in inherited and acquired conditions and has emerged as a potential therapeutic drug target for cardiovascular disorders (Moreno & Clancy, 2012; Makielski, 2016). Inhibition of I_{NaL} in cells and tissue from human diseased hearts attenuates diastolic Ca^{2+} and passive tension, respectively (Sossalla *et al.*, 2008; Coppini *et al.*, 2013), partly justifying improvements of diastolic indices seen in patients treated with the I_{NaL} inhibitor ranolazine (Hayashida *et al.*, 1994; Moss *et al.*, 2008; Figueredo *et al.*, 2011; Venkataraman *et al.*, 2012; Maier *et al.*, 2013; Shah *et al.*, 2017). Experimentally, increased I_{NaL} in cardiomyocytes of mice with inducible deletion of *Scn1b* gene, encoding for β1-subunits of the voltage-gated sodium channel, alters Ca^{2+} transient properties and delays kinetics of contraction and relaxation, defects that are corrected by pharmacological reduction of I_{NaL} (Cervantes *et al.*, 2022). Moreover, mice with *Scn1b* deletion have preserved systolic function but impaired diastolic properties and reduced left ventricular (LV) compliance, in the absence of structural modifications of the heart. Importantly, functional defects observed *in vivo* in *Scn1b* null mice are normalized following I_{NaL} inhibition (Cervantes *et al.*, 2022). Thus, clinical and experimental data tend to suggest a causative link between enhanced I_{NaL} and defective myocardial relaxation (Pourrier *et al.*, 2014; Signore *et al.*, 2015). This mechanism is consistent with the reported association between prolonged ventricular repolarization and diastolic dysfunction in patients (Sauer *et al.*, 2012). Therefore, in the elderly, the manifestation of delayed ventricular repolarization (Mangoni *et al.*, 2003; Rabkin *et al.*, 2016) and increased risk of HF with preserved ejection fraction (HFpEF) (Dunlay *et al.*, 2017; Pfeffer *et al.*, 2019) favors the possibility that augmented I_{NaL} contributes to the protracted electrical recovery of the aged myocardium, with important consequences on diastolic performance.

As seen in humans (Schwartz & Zipes, 2011; Dunlay *et al.*, 2017; Pfeffer *et al.*, 2019), diastolic dysfunction occurs in aging rodents (Signore *et al.*, 2015). Mice at ~24 months of age present altered diastolic LV filling, enhanced myocardial stiffness, and impaired relaxation (Signore *et al.*, 2015). Despite the deteriorated diastolic function, systolic indices are preserved at ~24 months, whereas, at later stage, defective cardiac relaxation and compliance are accompanied by poor systolic performance and cavitary dilation (Signore *et al.*, 2015). Importantly, the initial perturbation of LV filling in aging mice is coupled with protracted electrical recovery of the ECG (Signore *et al.*, 2015), as observed in the elderly population (Mangoni *et al.*, 2003; Rabkin *et al.*, 2016).

Therefore, these results strengthen the viability of the aging rodent heart as a platform to model human myocardial senescence.

Cardiac Na^+ channels are primarily composed of the α-subunit Nav1.5 and are characterized by rapid activation upon depolarization and subsequent voltage inactivation, resulting in prompt decline in channel conductance. The late sodium current is a slowly inactivating component of the fast sodium current (I_{Na}), attributed to the incomplete inactivation of subpopulations of Nav1.5 channels (Maltsev *et al.*, 1998). Importantly, magnitude and properties of I_{NaL} are regulated, in part, by post-translational modifications of Nav1.5, including phosphorylation by the Ca^{2+}/calmodulin-dependent protein kinase II (CaMKII) (Wagner *et al.*, 2006; Glynn *et al.*, 2015). In this regard, activity of CaMKII depends on intracellular Ca^{2+} levels, autophosphorylation, nitrosylation, O-GlcNAcylation, and oxidation by reactive oxygen spices (ROS), the latter being augmented with aging (Judge *et al.*, 2005).

In the current study, we have addressed the contribution of Nav1.5 phosphorylation at Ser571 and I_{NaL} to the functional defects occurring in the heart with age progression. Based on clinical and experimental evidence supporting the existence of sex-specific patterns of aging of the heart (Yusifov *et al.*, 2022), cardiac function was evaluated in aging male and female animals, for our mouse lines. Specifically, we used *Scn5a* knock-in mice with mutations of Nav1.5 at Ser571, a site targeted by phosphorylation by CaMKII under stress conditions (Koval *et al.*, 2012; Glynn *et al.*, 2015; Greer-Short *et al.*, 2020). Myocytes from young mice with Nav1.5 phosphomimetic mutation (S571E) have ~80% increased I_{NaL} and preserved transient I_{Na} (Glynn *et al.*, 2015; Greer-Short *et al.*, 2020), with respect to wild-type cells, reiterating features observed in myocytes from aged mice (Signore *et al.*, 2015). In contrast, myocytes from animals with ablated phosphorylation site (S571A) are prevented from increases of I_{NaL} secondary to phosphorylation by CaMKII, and this mouse line was employed to establish the effects of stabilized I_{NaL} in the aging process. Thus, S571E and S571A mouse lines served as I_{NaL} gain-of-function (GoF) and I_{NaL} loss-of-function (LoF) models, respectively, providing important information on the role of the sodium channel and I_{NaL} on the complex adaptations occurring with aging in the heart and cardiomyocyte compartment.

METHODS

All data, materials, and methods of this study are available from the corresponding author upon reasonable request.

Animals. Mice were maintained in accordance with the Guide for Care and Use of Laboratory Animals; animal experiments were approved by the local animal care committees (IACUC) of New York Medical College. Mice were kept on a 12-hour light/dark cycle with water and food ad libitum. When needed, isoflurane (1-1.5%, inhalation) was employed as a methodology of anesthesia. Euthanasia was attained under anesthesia by thoracotomy and removal of the heart.

Male and female C57Bl/6 mice were obtained from Charles River and National Institute of Aging rodent colony. Age-matched genetically engineered male and female mice with phosphomimetic mutation of sodium channel Nav1.5 at Ser571 (S571E) or male and female mice with Ser571 phosphorylation site ablated (S571A) were obtained from the laboratory of Drs. Hund and Mohler and maintained in the facility at New York Medical College. Knock-in mice were generated in C57Bl/6 background (Glynn *et al.*, 2015). Throughout the study, C57Bl/6 mice are referred as wild-type (WT), S571E mice are referred as I_{NaL} gain-of-function (GoF), and S571A mice are referred as I_{NaL} loss-of-function (LoF). For comparison, animals were grouped by age ranges of approximately 3-7 (~5 m), 10-14 (~12 m), 17-21 (~18 m), 23-26 (~24 m), and 28-32 (~30) months, in the attempt to define alterations occurring in the heart with progressive aging in each mouse line, starting from the mature-adult stage (Diaz Brinton, 2012; Radulescu *et al.*, 2021).

In vivo cardiac function. Echocardiography was performed in conscious mice using Acuson Sequoia c512 equipped with a 13 MHz (15L8) linear transducer (Signore *et al.*, 2015; Meo *et al.*, 2016; Sorrentino *et al.*, 2017; Cervantes *et al.*, 2022; Pizzo *et al.*, 2022). By this approach, parasternal short axis view of the left ventricle (LV) was employed to evaluate chamber diameter and wall thickness in diastole and systole, for computation of LV volume, mass, and ejection fraction (EF) (Signore *et al.*, 2015; Meo *et al.*, 2016; Sorrentino *et al.*, 2017). Diastolic function was assessed using pulsed-wave Doppler imaging of the transmitral filling pattern in the apical four-chamber view of the heart (Signore *et al.*, 2015; Meo *et al.*, 2016). Early transmitral filling wave (E wave) and late filling wave due to atrial contraction (A wave) were obtained. Isovolumic

relaxation time was calculated as the time from closure of the aortic valve to the initiation of the E wave (Signore *et al.*, 2015; Meo *et al.*, 2016; Cervantes *et al.*, 2022).

Electrocardiograms (ECGs) were recorded under isoflurane anesthesia by inserting needle electrodes subcutaneously into the mouse limbs (Signore *et al.*, 2015; Meo *et al.*, 2016; Sorrentino *et al.*, 2017; Cervantes *et al.*, 2022; Pizzo *et al.*, 2022). Electrical signals were amplified with a 12 Lead ECG Amplifier (DSI, Ponemah), digitized using a 160 kHz A/D converter (DI-1120 HS, Dataq) and recorded with WinDaq software (Dataq). Surface ECG intervals were measured using LabChart8. Spontaneous cycle length was determined by averaging 25 consecutive R-R intervals. PR interval, QRS duration, and QT interval were measured by determining the earliest onset and latest offset of atrial and ventricular deflections from the averaged cycles (Signore *et al.*, 2015; Meo *et al.*, 2016; Sorrentino *et al.*, 2017; Cervantes *et al.*, 2022). Rate-corrected QT interval (QT_c) was normalized by RR interval duration using Bazett formula ($QT_c = QT/\sqrt{RR}$) (Meo *et al.*, 2016; Sorrentino *et al.*, 2017).

To record ECGs in conscious animals an ECG-tunnel device (Emka Technologies) was employed (Comelli *et al.*, 2020; Cervantes *et al.*, 2022; Pizzo *et al.*, 2022). Animals were placed in a tunnel and ECGs recorded for a period of 10 minutes. Electrical signals were amplified with a 12 Lead ECG Amplifier (DSI, Ponemah), digitized using a 160 kHz A/D converter (DI-1120 HS, Dataq) and recorded with WinDaq software (Dataq). Electrical signals were evaluated offline with LabChart8 for occurrence of rhythm disturbances (Comelli *et al.*, 2020; Cervantes *et al.*, 2022; Pizzo *et al.*, 2022).

Left ventricular (LV) hemodynamics were obtained in anesthetized mice (isoflurane, 1.5%) in the closed chest preparation with a MPVS Ultra system for small animals (Millar Instruments) equipped with a SPR-839 catheter and coupled to a PowerLab/8SP A/D converter (ADInstruments) (Signore *et al.*, 2015; Meo *et al.*, 2016; Sorrentino *et al.*, 2017; Cervantes *et al.*, 2022). The mouse was warmed with a heat lamp; the right carotid artery was exposed, and the pressure transducer was inserted and advanced in the LV cavity. Data were acquired with LabChart8 (ADInstruments) software. For calibration of SPR-839 catheter and evaluation of LV blood volume, manufacturer's instructions were followed. Briefly, cuvette calibration protocol with fresh heparinized, warm blood and in vivo bolus infusion of hypertonic saline solution

(15% NaCl) were performed to compute slope and intercept and to assess parallel conductance. Analysis was performed using LabChart software.

In vivo blockade of the late Na^+ current (I_{NaL}) was achieved by administration of GS967 (Apexbio, 0.5 mg/kg body weight, i.p.) (Comelli *et al.*, 2020; Cervantes *et al.*, 2022) dissolved in USP saline solution. Effects of I_{NaL} inhibition were tested at ~30-60 min after drug administration. For *in vivo* adrenergic stimulation, epinephrine (Sigma-Aldrich, 2 mg/kg body weight, i.p.) was dissolved in USP saline solution and administered to mice (Glynn *et al.*, 2015). Occurrence or arrhythmic events was evaluation for 10 min following adrenergic stimulation.

Ex vivo properties of the mouse heart. For *ex vivo* studies, the ascending aorta was cannulated with PE50 tubing connected to a 23G ¾ needle. Subsequently, hearts were perfused in a Langendorff apparatus (Radnoti). Perfusion was accomplished at a constant pressure of ~80 mmHg with pre-warmed Krebs–Henseleit buffer (KHB; Sigma-Aldrich), containing, in mmol/L: 118 NaCl, 4.7 KCl, 11 glucose, 1.2 $MgSO_4$, 1.2 KH_2PO_4, 1.8 $CaCl_2$ and 25 $NaHCO_3$, gassed with 95% O_2 and 5% CO_2 (pH 7.4) at 37°C (Signore *et al.*, 2013; Signore *et al.*, 2015; Meo *et al.*, 2016; Sorrentino *et al.*, 2017; Meo *et al.*, 2019; Cervantes *et al.*, 2022; Pizzo *et al.*, 2022). The temperature was maintained by immersing the heart in a water-heated glassware reservoir (Radnoti), containing preheated KHB. Hearts were stimulated at 8 Hz (125 ms cycle length) with a 3 ms square pulse at 1.5-2 fold its threshold level (4 channels stimulator, BMS 414, Crescent Electronics; S48, Grass; or ISO-STIM 01M, npi), using a mini-coaxial electrode (Harvard Apparatus).

To assess electrical activity of perfused hearts, monophasic action potentials (MAPs) were recorded using a micro MAP-Tip electrode (Harvard Apparatus) positioned on the LV free wall (Signore *et al.*, 2013; Signore *et al.*, 2015; Meo *et al.*, 2016; Meo *et al.*, 2019; Cervantes *et al.*, 2022). A two-lead mini ECG system (Harvard Apparatus), in which electrodes were placed on the right atrium and apex of the heart, was used to obtain pseudo-ECG (Signore *et al.*, 2013; Signore *et al.*, 2015; Sorrentino *et al.*, 2017; Cervantes *et al.*, 2022; Pizzo *et al.*, 2022). Electrical signals were amplified (6600 Amplifier, Gould Instruments), digitized using a 160 kHz A/D converter (DI-1120 HS, Dataq) and recorded with WinDaq software (Dataq).

Programmed electrical stimulation (PES) was introduced to assess the propensity of the mouse heart to develop ventricular arrhythmias (Signore *et al.*, 2013; Signore *et al.*, 2015; Cervantes *et al.*, 2022). A stimulus generator (STG2004, Multi Channel System) controlled by a PC was coupled with a stimulus isolation unit (ISO-STIM 01M, npi) to apply PES protocols. Initially, a train of 20 pacing stimuli (S1) applied at 125 ms cycle length with an extra stimulus (S2) inserted at the end of the train was employed. The S1–S2 interval was progressively reduced until the S2 stimulus either failed to generate an action potential or induced ectopic events (Signore *et al.*, 2015; Cervantes *et al.*, 2022). The appearance of premature ventricular complexes (PVCs, ectopic beats characterized by atria-ventricular dissociation) ventricular tachycardia (three or more consecutive ectopic beats) and/or ventricular fibrillation was established (Signore *et al.*, 2013; Signore *et al.*, 2015; Cervantes *et al.*, 2022). Data were analyzed with LabChart8 software.

Isolation of adult ventricular cardiomyocytes. With the animal under deep anesthesia (isoflurane) and following administration of heparin (~200 unit, i.p.), thoracotomy was performed, heart was excised, and left ventricular (LV) myocytes were enzymatically dissociated as previously reported (Signore *et al.*, 2013; Signore *et al.*, 2015; Meo *et al.*, 2016; Sacchi *et al.*, 2017; Sorrentino *et al.*, 2017; Borghetti *et al.*, 2018; Shu *et al.*, 2018; Meo *et al.*, 2019). Briefly, the heart was connected to a plastic cannula for retrograde perfusion-the aorta in a Langendorff system (Radnoti), at 37°C. Perfusate consisted of a Ca^{2+}-free solution gassed with 100% O_2. After 5 minutes, 0.1 mmol/L $CaCl_2$, 274 units/ml collagenase (type 2, Worthington Biochemical Corp) and 0.57 units/ml protease (Type XIV, Sigma-Aldrich) were added to the solution which contained in mmol/L: NaCl 126, KCl 4.4, $MgCl_2$ 5, HEPES 20, Glucose 22, Taurine 20, Creatine 5, Na Pyruvate 5 and NaH_2PO_4 5 (pH 7.4). At completion of digestion, atria and right ventricle were dissected and discarded. Remaining LV free wall and septum were separated. Tissue cut in small pieces and these fragments were shaken in re-suspension solution and filtered using a 230 µm sieve (Sigma-Aldrich). For physiological studies, only rod-shaped LV free wall myocytes exhibiting cross striations and showing no spontaneous contractions or contractures were selected; cells were used within 8 hours following enzymatic digestion.

Cell Shortening. Isolated LV myocytes were placed in a perfusion chamber with field stimulation (Warner Instruments) on the stage of an inverted microscope (Swift) for contractility measurements (Signore *et al.*, 2013; Signore *et al.*, 2015; Sorrentino *et al.*, 2016; Shu *et al.*, 2018). Cells were bathed continuously with Tyrode Tyrode solution containing (in mmol/L): NaCl 140, KCl 5.4, $MgCl_2$ 1, HEPES 5, Glucose 5.5 and $CaCl_2$ 1 (pH 7.4, adjusted with NaOH). Tyrode solution was warmed at 37º C. Measurements were collected in field-stimulated cells by a CCD camera (TM-540, Pulnix), video edge detection (VED-205, Crescent Electronics), a 10 kHz A/D converter (DI-155 HS, Dataq), and WinDaq software (Dataq). Contractions were elicited at 1 Hz by rectangular depolarizing pulses, 3 ms in duration and ~1.5-fold threshold in intensity, with platinum electrodes connected to a stimulator (SD9, Grass). For each animal, 35-50 cells were employed to characterize the contractile behavior of cardiomyocytes paced at 1 Hz stimulation rate for various experimental groups. For other tests, variable numbers of cells/animals were employed. To test the effects of increased pacing rates, myocytes were stimulated at 1 Hz and 4 Hz. The late Na^+ current (I_{NaL}) was blocked with 300 nmol/L GS967 (Apexbio) (Cervantes *et al.*, 2022) or with 10 µmol/L mexiletine (Sigma-Aldrich) (Signore *et al.*, 2015; Sorrentino *et al.*, 2016). Parameters of cell shortening and relaxation were analyzed using LabChart8 software.

Ca^{2+} Transients. Isolated LV myocytes were placed in a perfusion chamber with field stimulation (Warner Instruments) on the stage of an upright microscope (BX61WI, Olympus) for evaluation of Ca^{2+} transients (Signore *et al.*, 2013; Signore *et al.*, 2015; Sacchi *et al.*, 2017; Sorrentino *et al.*, 2017). Cells were bathed continuously with Tyrode solution warmed at 37º C. Measurements were collected in field-stimulated cells by IonOptix fluorescence systems (IonOptix) connected to a 10 kHz A/D converter (DI-155 HS, Dataq). Signals were acquired using WinDaq software (Dataq). Ca^{2+} transients were elicited at 1 Hz by rectangular depolarizing pulses, 3 ms in duration and ~1.5-fold threshold in intensity, with platinum electrodes connected to a stimulator (SD9, Grass). For each animal, 55-70 cells were employed to characterize Ca^{2+} transient properties of cardiomyocytes paced at 1 Hz stimulation rate for various experimental groups. Reported trend for Ca^{2+} transient properties were confirmed in cardiomyocytes obtained for a separate group of animals (data not shown). The two sets of experiments were not combined because of slightly different experimental conditions, i.e., lower laboratory room temperature and different fluorescent lamp and

related alignment. To test the effects of increased pacing rates, myocytes were stimulated at 1 Hz and 4 Hz. Ca^{2+} transients were assessed by epifluorescence after loading myocytes with 0.5 µmol/L Fluo-4 AM (Invitrogen). Excitation wavelength was 480 nm with emission collected at 535 nm using a 60x, long distance, water immersion objective (LUMPlanFI, Olympus). Fluorescence excitation was restricted to the central area of the cell using a field diaphragm, whose aperture was maintained constant (Cervantes *et al.*, 2022). Parameters of Ca^{2+} transients were analyzed using LabChart8. For amplitude of Ca^{2+} transients, Fluo signals were expressed as normalized fluorescence (F/F_0), where F_0 is the diastolic fluorescent level subtracted by the background signal measured in the region adjacent to the cell (Signore *et al.*, 2015; Sorrentino *et al.*, 2017). The late Na^+ current (I_{NaL}) was blocked with 300 nmol/L GS967 (Cervantes *et al.*, 2022), or with 10 µmol/L mexiletine (Signore *et al.*, 2015; Sorrentino *et al.*, 2016; Cervantes *et al.*, 2022).

Myocyte Size. Images of LV myocytes fixed in paraformaldehyde were collected with an inverted microscope (CK40, Olympus) equipped with a digital camera (MU1003, Amscope). Cell length and area were evaluated using ImageJ software. Average cell width was calculated by dividing cell area by cell length (long axis). Cell volume was then computed assuming the shape of myocytes as a flattened cylinder with elliptical cross section (Signore *et al.*, 2015; Sorrentino *et al.*, 2016; Cervantes *et al.*, 2022), in which the major axis corresponds to the average cell width and the ratio major-to-minor axis is 1.8, based on previous three dimensional reconstructions for mouse cardiomyocytes (Signore *et al.*, 2015).

Histological Analysis. Mouse hearts were perfused and stored in neutral buffered, 10% formalin solution (Sigma-Aldrich) for histological analysis. Transversal sections of the LV at the mid-ventricular level were embedded in paraffin and sliced to obtain thin sections (~4 mm thickness) (Signore *et al.*, 2015; Cimini *et al.*, 2017; Cervantes *et al.*, 2022). For detection of connective tissue, slides were trichrome-stained (Masson's Trichrome Stain Kit, Mastertech, StatLab) following manufacturer's instruction. Images were acquired using an inverted microscope (CK40, Olympus) with 20x objective equipped with a digital color camera (MU1003, Amscope). Interstitial fibrosis was quantified with respect to total tissue area using ImageJ software (Signore *et al.*, 2015; Sorrentino *et al.*, 2016; Cervantes *et al.*, 2022).

Quantitative RT-PCR. Total cellular RNA was prepared from mouse LV isolated cardiomyocytes utilizing RNeasy Mini Kit (Qiagen) following manufacturer's instructions, as previously reported (Jain *et al.*, 2018; Cervantes *et al.*, 2022). cDNA was obtained from total RNA using Transcriptor High Fidelity cDNA Synthesis Kit (Sigma-Aldrich). Real-time RT-PCR was performed with primers listed in **Table S1 in the Supplemental Data**. The QuantStudio Real-Time PCR system (Applied Biosystems) was employed for quantitative RT-PCR. In each case, cDNA was combined with Fast SYBR™ Green Master Mix (Applied Biosystems) in a 25 µl reaction mix. Cycling conditions were as follow: 95°C for 10 min followed by 40 cycles of amplification (95°C denaturation for 10-15 sec, 60°C annealing and extension for 1 min). The melting curve was then obtained. C_t values were normalized with respect to hypoxanthine guanine phosphoribosyl transferase (*Hprt*).

Western Blotting. Whole protein extracts from snap-frozen LV cardiomyocytes or LV tissue were prepared using RIPA Lysis and Extraction Buffer (Thermo Fisher Scientific), supplemented with a Protease and Phosphatase Inhibitor Cocktail (Sigma-Aldrich). Equivalent of 50 µg of proteins were prepared with SDS Sample Buffer (Sigma-Aldrich), separated on either 4-15% or 7.5% SDS-PAGE (Mini-PROTEAN TGX Stain-Free™ Protein Gels, Biorad) with Tris/Glycine/SDS (Biorad). High molecular weight proteins were separated on 7.5% gels for 4 hours on ice, at constant voltage (90 V). Proteins were transferred onto PVDF membrane (Li-cor) with Tris/Glycine transfer buffer (Biorad) containing 20% or 5% (for high molecular weight proteins) methanol. Subsequently, total protein load was quantified using a protein stain (Revert™ 700, Li-cor). Membranes were washed with Tris Buffered Saline (TBS, Biorad) with 0.1% Tween 20 (Fisher Scientific) blocked with Intercept Blocking Buffer (Lic-cor), for 1 hour at room temperature. Membranes were incubated overnight at 4°C with primary antibodies listed in **Table S2 in the Supplemental Data**, at the indicated dilution. Fluorescent-labeled secondary antibodies (IRDye® 800CW or 680LT Secondary Antibodies) were utilized for signal detection with an infrared imaging system (Odyssey CLx, Li-Cor). Western blotting protocols with various antibodies were optimized before quantitative analysis. For molecular weight identification Chameleon® Kit Pre-stained Protein Ladders (Li-Cor) were employed. Optical density of bands was measured using ImageJ and normalized by the expression of β-actin.

For studies directed to the quantification of sodium channel Nav1.5 and phosphorylation at Ser571, whole LV lysates from mice at 5 and 21 months of age were prepared by flash freezing heart tissue and pulverizing in liquid nitrogen. The ground heart tissue was lysed in PhosphoSafe™ Extraction Buffer (Millipore 71296) supplemented with protease inhibitor cocktail (Millipore P8340) and analyzed using SDS-PAGE and immunoblotting, as previously described (Hund *et al.*, 2014). Briefly, 50 µg of protein was mixed with 4x sample buffer and left at room temperature before gel loading. Samples were loaded in 10% TGX mini-protean gels separated at 100V for 1 hour. Proteins were transferred onto nitrocellulose membranes containing 20% methanol at 30V overnight at 4°C. Membranes were washed with Tris Buffered Saline (TBS, Biorad) with 0.1% Tween 20 and blocked using 2% BSA for 1 hour at room temperature. Membranes were incubated overnight at 4°C with primary antibody. Immunoblotting of phospho Ser571 Nav1.5 and total Nav1.5 was performed using affinity purified custom antibody (Hund *et al.*, 2010) and GAPDH (1:5000, Fitzgerald 10R-G109A) in a 2% BSA/TBST solution. Secondary antibodies conjugated to HRP were incubated for 2 hours at room temperature. Signals were captured using a ChemiDoc MP Imager (BioRad). Optical densities were measured using ImageJ and normalized by expression of GAPDH.

Data analysis. Data are presented as median and interquartile ranges with dot plots. Fold and percentage changes are referred to median values. Investigators performing acquisition and analysis of data had knowledge of mouse genotype. Statistical analysis was performed using GraphPad Prism 9. Data were initially tested for normality (Shapiro-Wilk) and equal variance for assignment to parametric or non-parametric analysis. Parametric tests included Student's *t*-test, paired *t*-test, ordinary one-way analysis of variance (ANOVA) followed by Bonferroni multiple comparisons tests. Non-parametric tests included Mann-Whitney rank sum test and Wilcoxon-signed rank test, Kruskal-Wallis test followed by Dunn's multiple comparisons test (Signore *et al.*, 2015; Meo *et al.*, 2016; Sorrentino *et al.*, 2016; Sorrentino *et al.*, 2017; Borghetti *et al.*, 2018; Comelli *et al.*, 2020; Cervantes *et al.*, 2022; Pizzo *et al.*, 2022). For categorical data analysis, Fisher's exact or Chi-square tests for trend were used (Comelli *et al.*, 2020; Cervantes *et al.*, 2022; Pizzo *et al.*, 2022). For survival curves, Gehan–Breslow–Wilcoxon and log-rank (Mantel–Cox) tests were employed (Comelli *et al.*, 2020; Cervantes *et al.*, 2022; Pizzo *et al.*, 2022). $P<0.05$ was considered significant.

RESULTS

Aging and Sodium Channel Status Delay Cardiac Repolarization

To evaluate age-related alterations of the electrical repolarization of the heart and contribution of the late Na^+ current to the process, electrocardiograms (ECGs) were collected in animals at different age (**Supplemental Fig. S1A**), in the anesthetized state. Ventricular repolarization was quantified by the QT interval duration of the ECG and the rate-corrected QT_c., parameters that yielded comparable results. Data were acquired in: *i)* C57Bl/6 (wild-type, WT) male mice, who are characterized by an ~60% increase in I_{NaL} in cardiomyocyte with aging (Signore *et al.*, 2015); *ii)* male mice with phosphomimetic mutation of sodium channel Nav1.5 at Ser571, leading to an ~80% increase in I_{NaL} in cardiomyocytes in the adult stage (I_{NaL} gain-of-function mutation, GoF) (Glynn *et al.*, 2015); and *iii)* male mice with Ser571 phosphorylation site ablated, preventing I_{NaL} increases under stress condition (I_{NaL} loss-of function, LoF) (Glynn *et al.*, 2015). Animals were studied starting from the mature-adult stage (3-6 months, ~5 m) (Diaz Brinton, 2012; Radulescu *et al.*, 2021), and then at 11-14 (~12 m), 17-20 (~18 m), and 23-26 (~24 m) months of age.

With respect to mice at ~5 months (m), QT interval was prolonged by ~20% in WT animals at ~18 and ~24 m (**Fig. 1 A and 1B**). In contrast, no significant alterations of QT interval duration occurred with age in GoF and LoF animals. However, at ~5 and ~12 m of age, GoF mice had longer QT interval, in comparison to age-matched WT and LoF animals (**Fig. 1 A and 1B**). Importantly, QT interval duration was comparable between WT and GoF mice at ~18 and ~24 months but was shorter in LoF animals (**Fig. 1B**). For each of the three mouse lines, QT interval duration was similar for age-matched male and female mice (**Supplemental Fig. S2**). Consequently, age- and genotype-related trends of ventricular repolarization detected in male mice were also observed in female animals (**Supplemental Fig. S3**).

Atrio-ventricular conduction, assessed by the PR interval duration, was prolonged with aging in female and male mice for the three genotypes, but differences did not reach statistical significance for male GoF animals. Similarly, ventricular conduction, assessed by the duration of the QRS complex, tended to be prolonged in aging mice (**Supplemental Fig. S1 and S3**).

To establish the contribution of I_{NaL} to the observed differences in ventricular repolarization, ECGs were collected in subgroups of mice at baseline (Base) and ~30 minutes after administration of GS967, an inhibitor of the late Na^+ current (Comelli *et al.*, 2020; Cervantes *et al.*, 2022). Inhibition of I_{NaL} had no effects on QT interval duration in WT animals at ~5 m but shortened ventricular repolarization in WT mice at ~18 and ~24 months of age (**Fig. 1C and 1E**). In GoF animals, GS967 shortened QT interval at all age ranges (**Fig. 1D and 1F**), whereas inhibition of I_{NaL} had no major consequences on the QT interval of LoF mice (**Fig. 1G**). Atrio-ventricular and ventricular conduction velocities, (PR and QRS intervals) were not affected by the drug (**Supplemental Fig. S4**). Effects of GS967 on ventricular repolarization observed in male animals were also detected in cohorts of female mice **(Supplemental Fig. S5)**.

Thus, aging is coupled with delayed ventricular repolarization, which is normalized following pharmacological inhibition of I_{NaL}. Mice with I_{NaL} gain-of-function mutation anticipate the manifestation of protracted electrical recovery occurring with aging, whereas animals with I_{NaL} loss-of-function mutation are protected from the age-related changes of ventricular repolarization and are insensitive to the corrective effects of I_{NaL} inhibition.

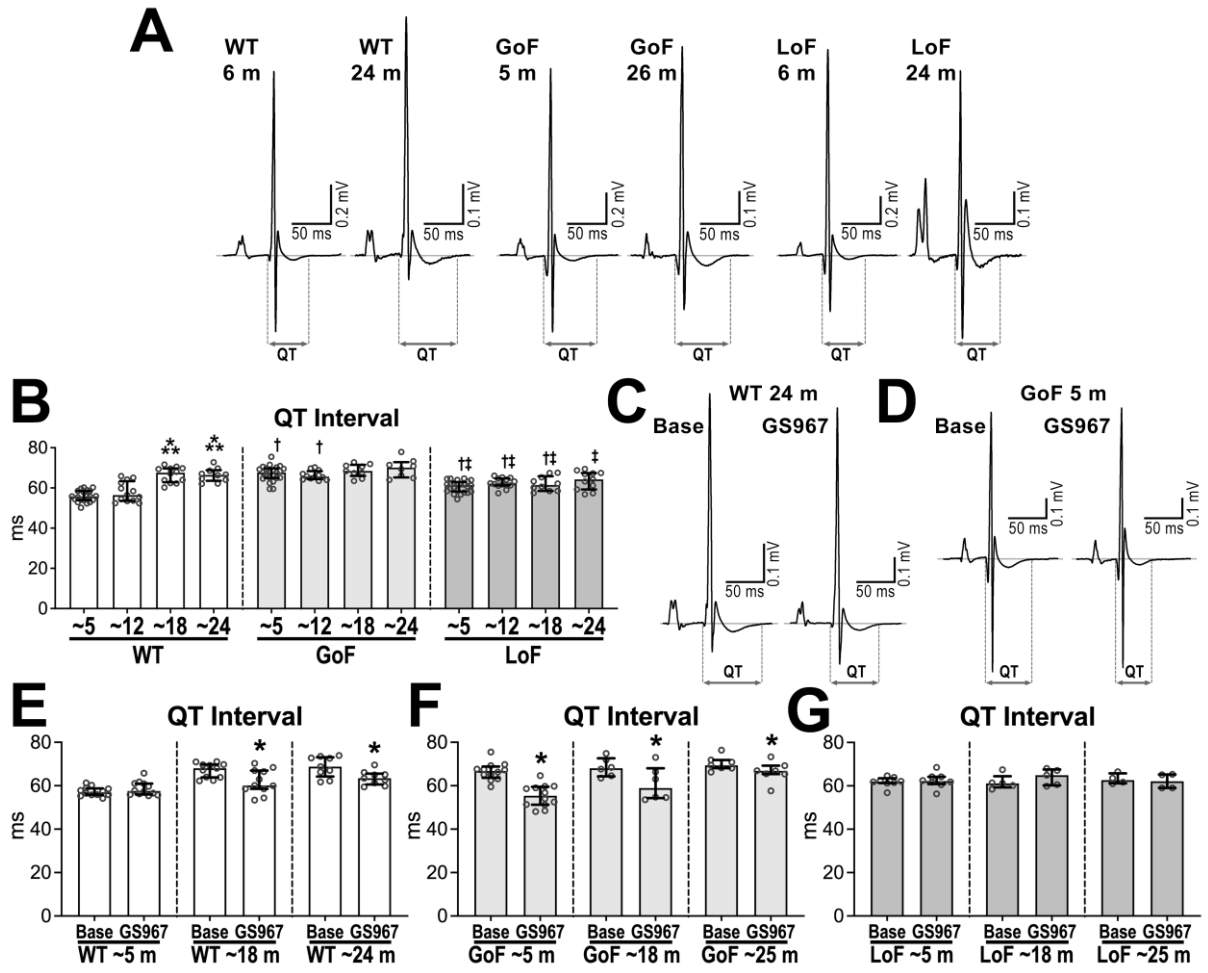

Fig 1. Aging and I_{NaL} alter electrical repolarization of male mice. A, ECGs obtained in anesthetized adult and aged mice. **B,** Quantitative data for WT, GoF, and LoF mice at ~5 (n=20-24), ~12 (n=12-14), ~18 (n=9-12), and ~24 m (n=8-11). Data are median and interquartile ranges with dot plots. *P<0.05 vs. ~5, **P<0.05 vs. ~12, †P<0.05 vs. age-matched WT, ‡P<0.05 vs. age-matched GoF, using one-way ANOVA, followed by Bonferroni multiple comparison test. **C, D,** ECGs in a WT mouse at 24 m (**C**) and a GoF mouse at 5 m (**D**), before (Base, left traces) and after administration of the I_{NaL} inhibitor GS967 (0.5 mg/kg body weight, right traces). **E-G,** Quantitative data for QT interval duration of ECGs obtained in WT mice (**E**) at ~5 m (n=12), ~18 m (n=11), and ~24 m (n=9), in GoF mice (**F**) at ~5 m (n=12), ~18 m (n=6), and ~25 m (n=7), and in LoF mice (**G**) at ~5 m (n=8), ~18 m (n=5), and 25 m (n=4) before (Base) and after administration of GS967. Data are median and interquartile ranges with dot plots. *P<0.05 vs. Base, using paired *t*-test. **H-J,** Quantitative data for the fraction of aging mice presenting isolated or multiple PVCs (black segment) and mice free of events (upper segment) in the conscious state. Data for WT (**H**), GoF (**I**), and LoF (**J**) mice at

~4 (n=54, 49, 20, respectively), ~12 (n= 24, 20, 15, respectively), ~18 (n= 41, 20, 19, respectively), ~24 (n= 30, 21, 12, respectively), and ~30 m (n= 7, 29, 11, respectively) are reported. For each genotype, P value using Chi-square test for trend is reported. **K,** Fraction of aging mice presenting ventricular tachycardia (VT, black segment) following epinephrine challenge (2 mg/kg, body weight, i.p.) in the conscious state. Data for male GoF and LoF mice at 20-27 m (n=7 and 9, respectively) and for female GoF and LoF mice at 20-27 m (n=9 and 6, respectively) are reported. *P<0.05 vs. GoF with both Fisher's exact test and Chi-square test. **L and M,** Survival curves for male GoF (n=394) and LoF (n=163) mice (**L**) and for female GoF (n=308) and LoF (n=138) mice (**M**). For the two sexes, survival curves for the two genotypes were different (P<0.05) using Gehan-Breslow-Wilcoxon test but only for female Log-rank (Mantel-Cox) test. For completeness, data reported in panel H, I, L, and M include a fraction of WT and GoF animals that were employed in a previous report (Comelli et al., 2020) (Comelli *et al.*, 2020).

Aging and Sodium Channel Status and Susceptibility to Arrhythmias

To establish whether the delayed electrical repolarization occurring in aged mice and animals with I_{NaL} gain of function was coupled with occurrence of ventricular ectopic events, ECGs were collected in aging male mice in the conscious state over a period of 10 min **(Supplemental Fig. S6)**. Aging was coupled with a progressive increase in the fraction of WT, GoF, and LoF male mice presenting one or multiple premature ventricular complexes (PVCs), but no significant differences were observed among genotypes **(Fig. 2A-F)**. Similar trends occurred in female animals **(Supplemental Fig. S6C and S6D)**.

Based on previous findings that adult mice with phosphomimetic mutation of Ser571 are susceptible to arrhythmia at the cellular and animal level in the presence of β-adrenergic stimulation (Glynn *et al.*, 2015), occurrence of ventricular tachycardia was established in GoF and LoF aged mice (20-27 months of age) exposed to epinephrine challenge. With respect to GoF animals, the occurrence of ventricular tachycardia following epinephrine administration was reduced in LoF mice (**Fig. 2D and Supplemental Fig. S7A and S7B**). Notably, for several of the aged GoF mice that developed VT with epinephrine test, pretreatment with the I_{NaL} inhibitor GS967 prevented the occurrence of VT when adrenergic challenge was repeated (**Supplemental Fig. S7C**).

To obtain information on the possibility that mice with altered sodium channel function develop lethal arrhythmic events not captured during the ECG acquisition, we computed and compared probability of survival of aging GoF and LoF animals raised and maintained in our colony. Interestingly, for both male and female animals, Kaplan-Meier survival curves were different for the two genotypes, with indication that probability of survival was enhanced in LoF mice with respect to GoF animals **(Fig. 2E, and 2F)**. No significant differences were observed when comparing survival curves of the two mutant mice with respect to previously collected curves for C57Bl/6 animals (Comelli *et al.*, 2020) (data not shown).

Thus, aging is associated with enhanced occurrence of ventricular ectopic events, which, however, appears not directly correlated to I_{NaL} function.

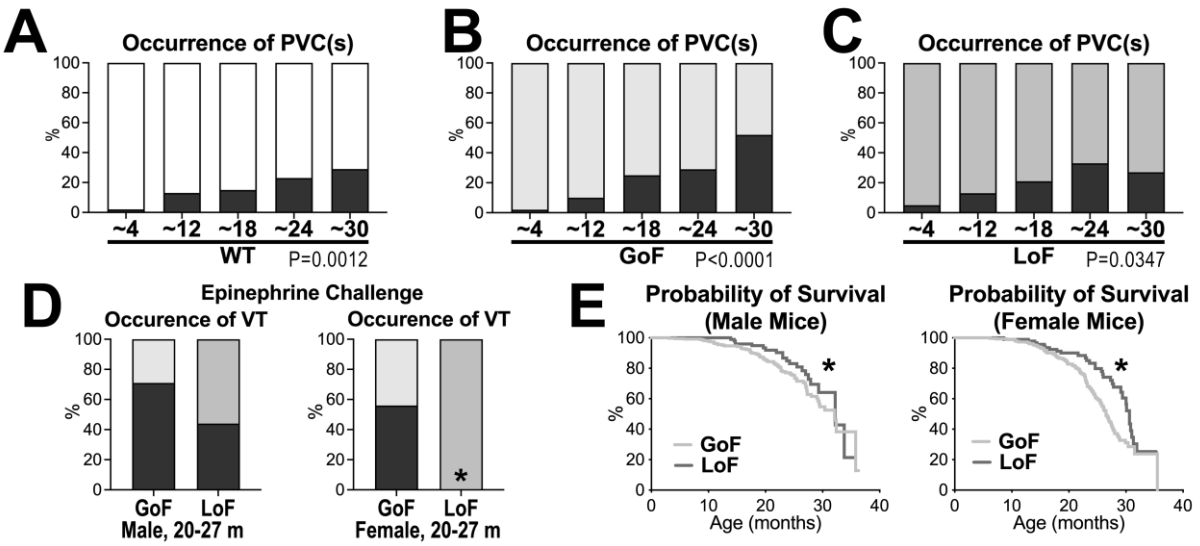

Fig 2. Aging and I_{NaL} alter vulnerability of the heart to arrhythmias. A-C, Quantitative data for the fraction of aging mice presenting isolated or multiple PVCs (black segment) and mice free of events (upper segment) in the conscious state. Data for WT (**A**), GoF (**B**), and LoF (**C**) mice at ~4 (n=54, 49, 20, respectively), ~12 (n= 24, 20, 15, respectively), ~18 (n= 41, 20, 19, respectively), ~24 (n= 30, 21, 12, respectively), and ~30 m (n= 7, 29, 11, respectively) are reported. For each genotype, P value using Chi-square test for trend is reported. **D,** Fraction of aging mice presenting ventricular tachycardia (VT, black segment) following epinephrine challenge (2 mg/kg, body weight, i.p.) in the conscious state. Data for male GoF and LoF mice at 20-27 m (n=7 and 9, respectively) and for female GoF and LoF mice at 20-27 m (n=9 and 6, respectively) are reported. *P<0.05 vs. GoF with both Fisher's exact test and Chi-square test. **E and F,** Survival curves for male GoF (n=394) and LoF (n=163) mice (**E**) and for female GoF (n=308) and LoF (n=138) mice (**F**). For the two sexes, survival curves for the two genotypes were different (P<0.05) using Gehan-Breslow-Wilcoxon test but only for female Log-rank (Mantel-Cox) test. For completeness, data reported in panel H, I, L, and M include a fraction of WT and GoF animals that were employed in a previous report (Comelli et al., 2020) (Comelli *et al.*, 2020).

Aging and Sodium Channel Status Alter the Electrical Properties of the Ventricular Myocardium

To evaluate whether alterations of QT interval duration observed *in vivo* were associated with changes in the late repolarization phase of the LV action potential (AP), local monophasic APs (MAPs) were collected *ex vivo* using perfused hearts from male animals at 11-13 months (~12 m) and 22-26 months (~24 m) of age. In WT hearts, duration of the MAP to 90% repolarization (MAPD90) was longer at ~24 m, with respect to ~12 m (**Fig. 3A and 3B)**. In contrast, no changes with age were observed for MAPD90 in hearts from GoF and LoF animals. However, at ~12 m, MAPD90 was prolonged in GoF hearts with respect to WT and LoF organs. Additionally, MAPD90 was comparable in WT and GoF hearts at ~24 months, but shorter in organs from LoF mice.

To obtain additional information on the effects of aging and modulation of I_{NaL} function on the propensity of the ventricular muscle to develop arrhythmias, inducibility of ectopic events in perfused hearts was tested using programmed electrical stimulation (PES). The delivery of trains of pacing stimuli (S1) followed by an extra stimulus (S2) at progressively shorter S1-S2 interval (S1-S2 protocol) resulted in occurrence of ectopic events in 14-31% of the perfused hearts, but no significant differences were detected among organs from the three groups of mice at ~12 m and ~24 m (**Fig. 3C and 3D)**.

Thus, protracted ventricular recovery occurring with aging and with I_{NaL} gain of function is associated with prolonged action potential duration of the myocardium and appears not to interfere with the propensity of the cardiac muscle to develop ectopic events.

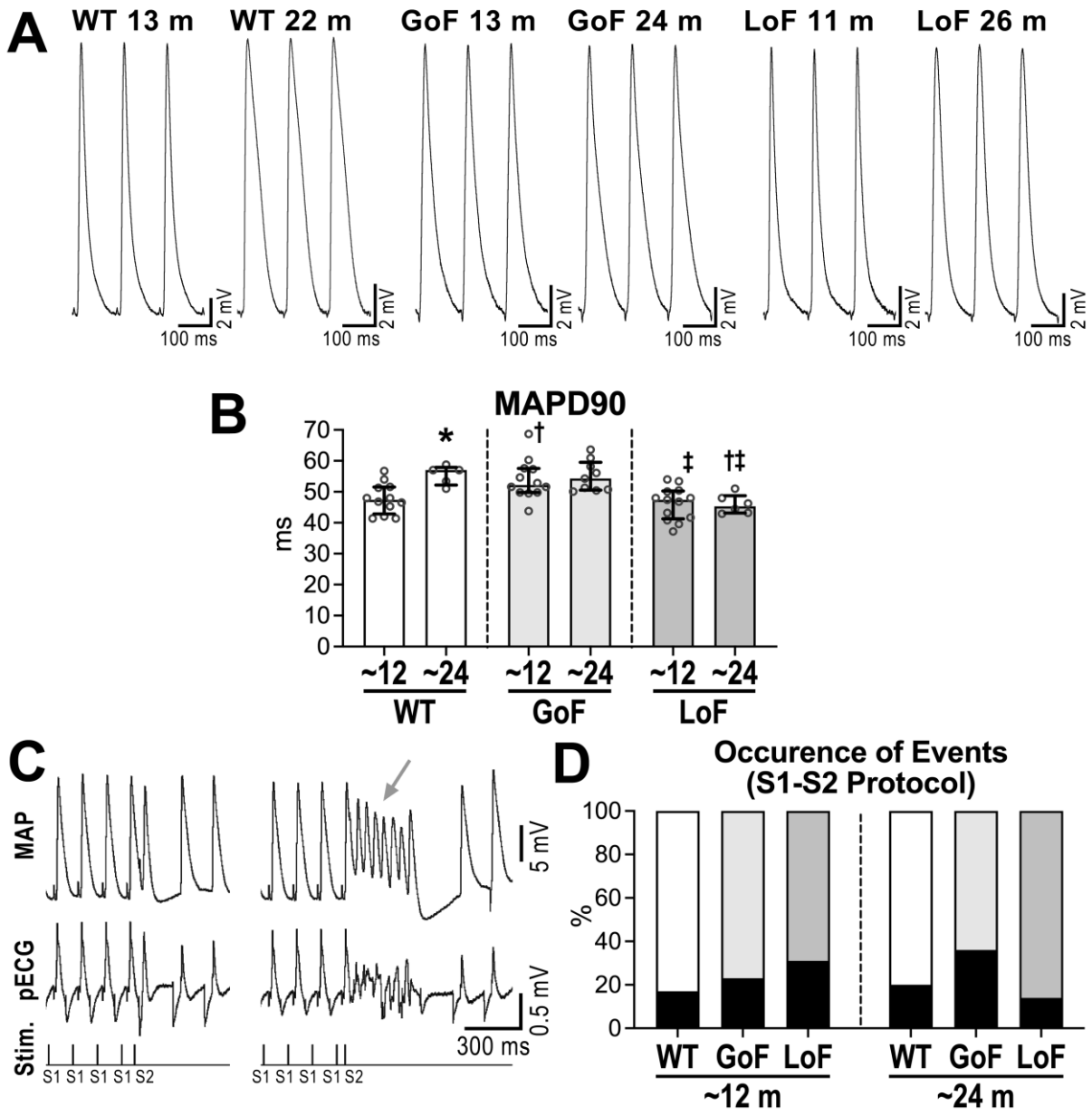

Fig 3. Aging and I_{NaL} alter electrical properties of the ventricular myocardium. A, Monophasic APs obtained from the LV myocardium of perfused hearts from adult and aged WT, GoF and LoF male mice stimulated at 8 Hz. **B,** Quantitative data for time to 90% repolarization of the MAP (MAP90) obtained in the LV myocardium of WT, GoF, and LoF male mice at 11-13 m (~12 m, n=12-13) and at 22-26 m (~24 m, n=5-9). Data are median and interquartile ranges with dot plots. *P<0.05 vs. ~12 m, using unpaired *t*-test; †P<0.05 vs. age-matched WT, ‡P<0.05 vs. age-matched GoF, using one-way ANOVA, followed by Bonferroni multiple comparison test. **C,** Traces reporting representative MAPs, pseudo-ECG (pECG) and stimulation protocol (Stim.) for a heart from a GoF mouse at 11 m of age. The extra stimulus originated ectopic events at

short S1-S2 interval (left traces, gray arrow). **D,** Quantitative data for the occurrence of ectopic events (black segment) by programmed electrical stimulation (S1-S2 protocol) in WT, GoF, and LoF hearts from mice at ~12 m, (n=12-13) and at ~24 m (n=5-11).

Aging and Sodium Channel Status Interfere with Diastolic Function

To evaluate age-related alterations of ventricular function and contribution of the late Na^+ current to the process, echocardiography and transmitral flow Doppler imaging were conducted in conscious WT, GoF, and LoF male mice, at various age ranges. Specifically, LV volumetric and filling parameter were employed to assess systolic and diastolic indices of LV performance, together with gross LV anatomical properties (Meo *et al.*, 2016; Sorrentino *et al.*, 2017; Cervantes *et al.*, 2022). Male animals from ~3 to ~30 months of age were employed (**Supplemental Fig. S8A**).

For WT, GoF, and LoF mice, LV ejection fraction (EF) was preserved with age and, when considered age-matched animals, no differences among genotypes were observed (**Supplemental Fig. S8**). Anatomically, LV end-diastolic volume (LVEDV) increased in the three groups of mice at ~30 m of age, with respect to animals at ~5 m, whereas progressive increase of LV mass occurred at ~18 months and older age (**Fig. 4A**). For the various age ranges, GoF mice had larger LV mass with respect to LoF animals, but normalization of LV mass by body weight tempered differences between these two genotypes (**Supplemental Fig. S8D**).

For each genotype, LVEDV and LV mass tended to be reduced in female mice, with respect to corresponding age-matched male animals (**Supplemental Fig. S9**). Moreover, for female mice, although no significant alterations in EF and LVEDV were detected with age, LV mass increased in old hearts, as detected in male animals (**Supplemental Fig. S10**).

By transmitral flow Doppler echocardiography, the ratio between peak velocity of the early passive and peak velocity of the active LV filling (E wave/A wave, or E/A ratio) was comparable in WT male mice at ~5 m and ~12 m. However, with respect to mice at ~5 m, E/A ratio decreased in WT animals by 23-26% at ~18, ~24, and ~30 m (**Fig. 4B and 4C, and Supplemental Fig. S11**). Concomitantly, with respect to WT mice at ~5 m, isovolumic relaxation time (IVRT), the time interval between aortic valve closure and mitral valve opening, was preserved at ~12 m but increased by 20-38% at ~18, ~24, and ~30 m (**Fig. 4D**). These findings are consistent with progressive impairment of diastolic function with aging.

With respect to age-matched WT animals, GoF mice at ~5 and ~12 m of age, had ~10% lower E/A ratio and ~10% prolonged IVRT (**Fig. 4B-D**). These parameters

remained relatively preserved up to ~24 m in GoF mice, but further deteriorated at ~30 m. Importantly, LoF mice had shorter IVRT with respect to age-matched GoF animals at ~5 m to ~24 m. Also, IVRT was shorter in LoF mice with respect to age-matched WT animals at ~18 m and ~24 m. However, at ~30 m, both IVRT and E/A ratio worsened in LoF mice.

Overall, for three genotypes, E/A ratio and IVRT in female mice were comparable to values observed in age-matched male mice (**Supplemental Fig. S12**). Thus, alterations of LV filling properties with aging and sodium channel mutations occurring in male animals were also observed in female mice (**Supplemental Fig. S13**).

To establish the contribution of I_{NaL} to the impairment of diastolic function observed in aged WT mice and in GoF adult animals, echocardiographic imaging was conducted in subgroups of mice at baseline (Base) and ~30 minutes after administration of the I_{NaL} inhibitor GS967 (**Fig. 5A and 5B)**. This intervention had no major effects on heart rate or ejection fraction for the various groups of animals (**Supplemental Fig. S14**). By Doppler imaging, I_{NaL} inhibition did not alter diastolic filling indices in adult WT mice at ~5 months of age. However, in WT mice at ~18 and ~26 m, GS967 ameliorated E/A ratio (16% and 22% increase, respectively) and reduced IVRT (-4%, -10%, respectively) (**Fig. 5C and 5D and Supplemental Fig. S15**). Moreover, in GoF mice at ~5, ~18, and ~26 months of age, all characterized by depressed LV filling, I_{NaL} inhibition increased E/A ratio (+23%, +18%, 36%, respectively) and reduced IVRT (-18%, -10%, -15%, respectively) (**Fig. 5E and 5F and Supplemental Fig. S15**). In contrast, no major consequences were observed on LV filling following administration of GS967 in LoF animals at ~5, ~18, and ~24 months of age (**Fig. 5G and 5H and Supplemental Fig. S15**). When considering female mice at ~18 m, inhibition of I_{NaL} ameliorated LV diastolic filling in WT and GoF mice but had no detectable consequences on LoF animals (**Supplemental Fig. S16**), mirroring effects observed in male animals.

To obtain additional information on alterations of ventricular function associated with aging and in the presence of phosphomimetic or stabilized sodium channels, LV hemodynamics were obtained in WT, GoF, and LoF male mice at ~5 to ~30 months of age. In WT mice, LV developed pressure was preserved with aging, but attenuations in maximal rate of pressure raise (dP/dt_{max}) and decay (dP/dt_{min}), and prolongation of

the time constant of pressure decline (tau) were observed when comparing WT mice at ~5 months with animals at ~18 m or older age (**Supplemental Fig. S17**). For both GoF and LoF animals, there were no major age-related alterations in LV hemodynamics. However, GoF mice tended to have attenuated dP/dt_{max} and dP/dt_{min}, and prolonged tau with respect to WT and/or LoF animals, mostly at adult stage (~5 m and ~12 m).

Thus, aging is coupled with progressive LV hypertrophy, impairment of LV relaxation and pattern of diastolic filling, but preservation of systolic performance. Gain of I_{NaL} function anticipates diastolic defects, whereas loss of I_{NaL} function and I_{NaL} inhibition, respectively, delay and reverse impairments of myocardial function occurring with age.

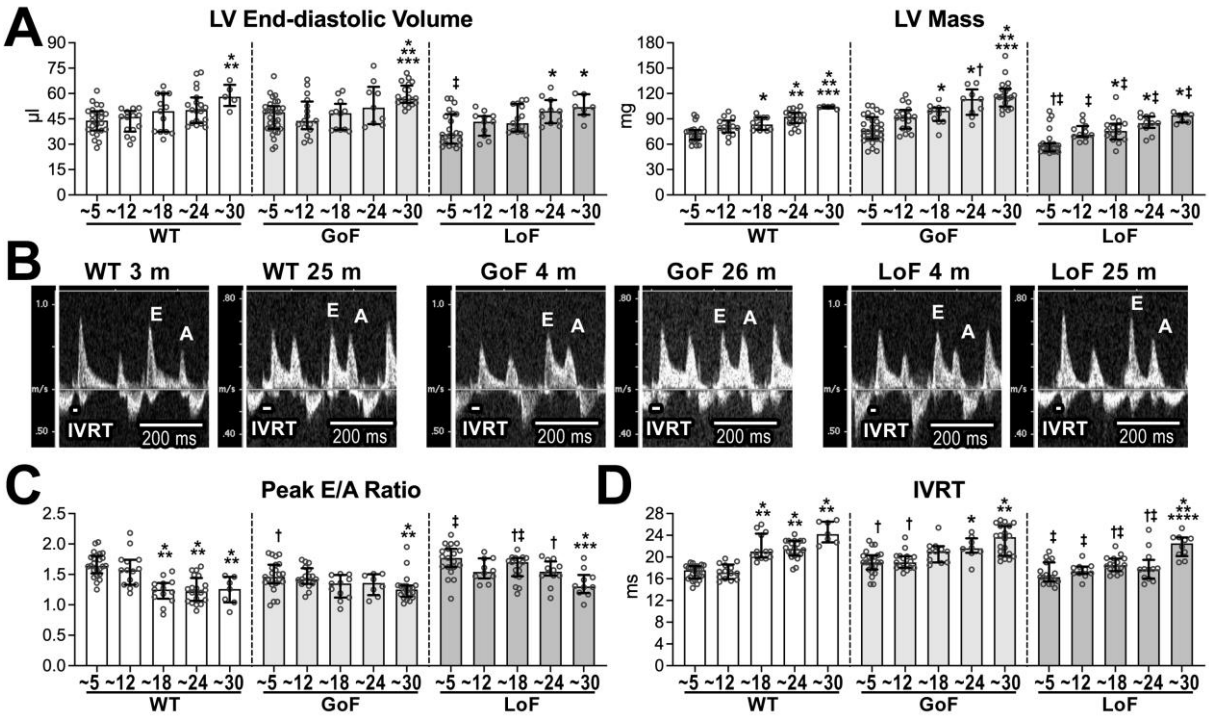

Fig 4. Aging and I_{NaL} alter the pattern of diastolic LV filling of male mice. A, Quantitative data for LV anatomical parameters obtained by echocardiography in WT, GoF, and LoF mice at ~5 (n=23-30), ~12 (n=11-16), ~18 (n=12-15), ~24 (n=9-19), and ~30 m (n= 5-20). Data are median and interquartile ranges with dot plots. *P<0.05 vs. ~5, **P<0.05 vs. ~12, ***P<0.05 vs. ~18, †P<0.05 vs. age-matched WT, ‡P<0.05 vs. age-matched GoF. Data were tested by one-way ANOVA, followed by Bonferroni multiple comparison test or by Kruskal-Wallis, followed by Dunn's multiple comparison test. **B,** Transmitral flow Doppler echocardiograms for adult and aged WT, GoF, and LoF mice. **C, D,** Quantitative data for transmitral flow Doppler echocardiographic parameters obtained in WT, GoF, and LoF mice at ~5 (n=19-24), ~12 (n=10-17), ~18 (n=11-17), ~24 (n=8-20), and ~30 m (n=7-20). Data are median and interquartile ranges with dot plots. *P<0.05 vs. ~5, **P<0.05 vs. ~12, ***P<0.05 vs. ~18, ****P<0.05 vs. ~24, †P<0.05 vs. age-matched WT, ‡P<0.05 vs. age-matched GoF. Data were tested by one-way ANOVA, followed by Bonferroni multiple comparison test or by Kruskal-Wallis, followed by Dunn's multiple comparison test.

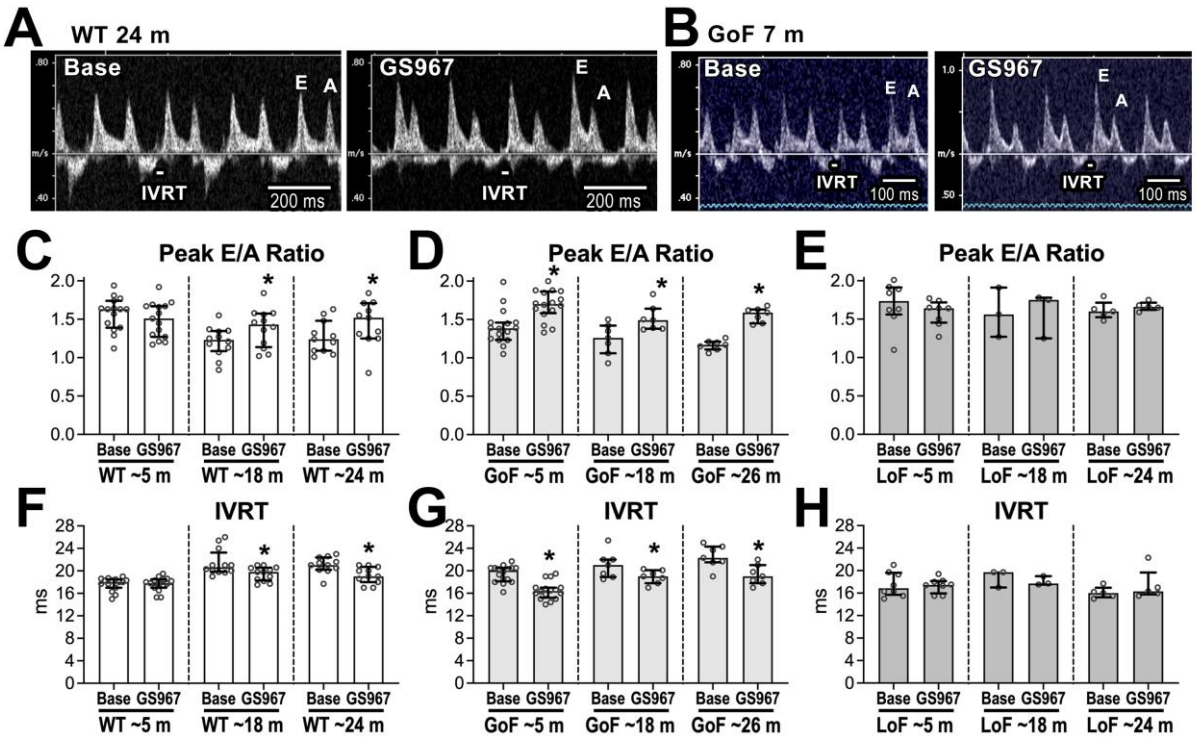

Fig 5. Blockade of I_{NaL} and the pattern of diastolic LV filling of male mice. A, B, Transmitral flow Doppler echocardiograms for a male WT mouse at 24 m of age (**A**) and a GoF mouse at 7 m of age (**B**), before (Base, **left** panels) and after administration of the I_{NaL} inhibitor GS967 (0.5 mg/kg body weight, i.p., **right** panels). **C-H,** Quantitative data for transmitral flow Doppler echocardiographic parameters obtained in WT mice (**C, D**) at 3-6 m (~5 m, n=15), 18-19 m (~18 m, n=12), and 24-26 m of age (~24 m, n=11), in GoF mice (**E, F**) at 5-8 m (~5 m, n=16), 18-19 m (~18 m, n=7), and 26-28 m of age (~26 m, n=7), and in in LoF mice (**G, H**) at 3-5 m (~5 m, n=8), 18-20 m (~18 m, n=3), and 23-25 m of age (~24 m, n=5) before (base) and after administration of GS967. Data are median and interquartile ranges with dot plots. *P<0.05 vs. Base in the same genotype, using paired *t*-test or Wilcoxon test.

Aging and Sodium Channel Status Affect Structural Properties of the Myocardium

To evaluate the structural properties of the myocardium of aging mice and animals with I_{NaL} gain- and loss-of-function mutations, myocardial interstitial fibrosis, myocyte size, and expression of hypertrophic markers were assessed in WT, GoF, and LoF male mice using histological sections and isolated cell preparations. Analysis was restricted to age ranges that were found to be associated with absence and appearance of defects in diastolic function in WT male mice.

Histologically, level of interstitial fibrosis in the LV myocardium was comparable for the three groups of mice at 4-7 months of age (~5 m). However, collagen deposition in the myocardium differently increased at 18-20 months of age (~20 m) in WT (2.2-fold increase), GoF (1.9-fold increase), and LoF mice (1.7-fold increase). Consequently, interstitial fibrosis at ~20 m was comparable in WT and GoF animals but was lower (-17%) in LoF mice, with respect to GoF animals (**Fig. 6A**).

For mice at 5-6 months (~5 m), myocyte size was larger in GoF hearts with respect to cells from WT (12%) and LoF mice (+21%) (**Fig. 6B and Supplemental Fig. S18**). Myocyte volume increased for the three groups of animals at 19-24 months of age (~20 m), and size of cells remained larger in GoF hearts with respect to cells from WT (29%) and LoF mice (+23%).

By RT-PCR, with respect to myocytes obtained from mice at 3-6 months (~5 m), the expression of *Myh7*, the gene encoding for the hypertrophic marker β-myosin heavy chain (β-MHC), increased in cells of WT, GoF, and LoF animals at 19-26 months (~22 m) (**Fig. 6C**). Moreover, the expression of *Nppa* gene, encoding for atrial natriuretic peptide (ANP), another hypertrophic marker, was enhanced in GoF myocytes at ~5 m, with respect to age-matched WT cells. Also, expression of *Nppa* gene increased in LoF myocytes with age.

Thus, aging is coupled with structural remodeling of the heart, a process that involves myocyte hypertrophy, increased expression of fetal genes, and augmented interstitial fibrotic deposition. These modifications tend to be augmented in mice with I_{NaL} gain-of-function with respect to those with loss-of function mutation.

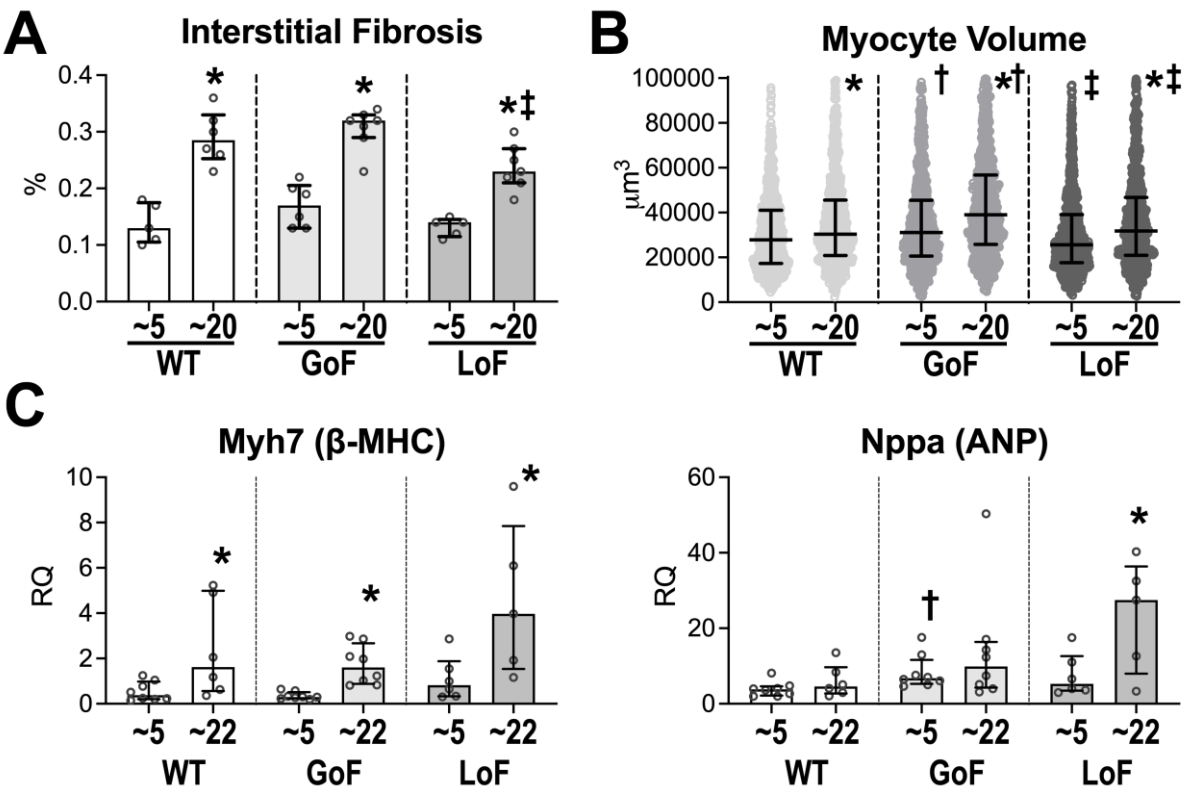

Fig 6. Aging alters LV structure of male mice. A, Quantitative data for level of interstitial fibrosis in the LV myocardium of WT, GoF, and LoF mice at 5-7 m (~5, n=5-6) and 18-20 m (~20, n=6-7), assessed by trichrome staining in tissue sections. Data are median and interquartile ranges with dot plots. *P<0.001 vs. ~5 using *t*-test. ‡P<0.05 vs. age-matched GoF, using one-way ANOVA, followed by Bonferroni multiple comparison test. **B,** Quantitative data for volume of myocytes obtained from WT, GoF, and LoF mice at 5-7 m (~5, n=757, 889, and 777 cells from 5 WT, 6 GoF mice, and LoF mice, respectively) and 19-24 m (~20, n=754, 764, and 766 cells from 5 WT, 5 GoF, and 5 LoF mice, respectively). Data are median and interquartile ranges with dot plots. *P<0.0001 vs. ~5 using Mann-Whitney test. †P<0.0001 vs. age-matched WT, ‡P<0.0001 vs. age-matched GoF, using Kruskal-Wallis, followed by Dunn's multiple comparison test. **C,** Quantitative data for expression of genes related to hypertrophic markers β myosin heavy chain (β-MHC) and atrial natriuretic peptide (ANP) in myocytes from WT, GoF, and LoF mice at 3-6 m (~5, n=6-8) and 19-26 m (~22, n=5-8). Data are median and interquartile ranges with dot plots. RQ: relative quantity with respect to hypoxanthine guanine phosphoribosyl transferase (*Hprt*). *P<0.05 vs. ~5 using unpaired *t*-test or Mann-Whitney test. †P<0.05 vs. age-matched WT using Kruskal-Wallis, followed by Dunn's multiple comparison test.

Aging and Sodium Channel Status Alter the Kinetics of Ca^{2+} Cycling and Cell Mechanics of Myocytes

To evaluate the effects of aging and contribution of the sodium channels to the contractile behavior of aging cardiomyocytes, properties of cell shortening and intracellular Ca^{2+} cycling were assessed in isolated cells under field stimulation, at 1 and 4 Hz pacing rates. Myocytes from the LV free wall of WT, GoF, and LoF male mice at 3-7 months (~6 m) and 22-28 months (~24 m) of age were employed.

With respect to myocytes from WT mice at ~6 m, cells from WT animals at ~24 m stimulated at 1 Hz presented reduced fractional cell shortening (-16%), prolonged time to peak contraction (+26%), and delayed time to 50% relaxation (+44%) (**Fig. 7A and 7B**). Similarly, reduced fractional cell shortening (-15%) and prolongation of time to peak contraction (+42%) and time to 50% relaxation (+58%) occurred in GoF myocytes with aging. In contrast, for LoF myocytes, fractional cell shortening was not affected by aging, and modest prolongations of time to peak (+18%) and 50% relaxation (+26%) were observed. Myocytes from GoF mice at ~6 m and ~24 m, had protracted time to peak contraction and time to 50% relaxation, with respect to cells from age-matched WT and LoF mice. Comparable alterations with aging and among genotypes in the kinetics of contraction and relaxation were also seen in cells stimulated at 4 Hz pacing rate (**Supplemental Fig. S19**).

Using cells loaded with the Ca^{2+} indicator Fluo-4 and stimulated at 1 Hz, kinetics of Ca^{2+} transients, quantified as the time necessary for the Ca^{2+} transient to reach 50% of its decay, were protracted in GoF myocytes at ~6 m with respect to cells from age-matched WT (+10%) and LoF (+4%) mice (**Fig. 8A and 8B**). From ~6 m to ~24 m, kinetics of Ca^{2+} transients were delayed in WT (+20%) and GoF (+8%) myocytes, but not in LoF cells. Thus, at ~24 m, duration Ca^{2+} transient decay was comparable in WT and GoF cells but was ~10% shorter in myocytes from LoF mice. Amplitude of Ca^{2+} transients was comparable for cells of the three genotypes at ~6 m, whereas at ~24 m LoF myocytes had greater amplitude with respect to their adult counterpart, and in comparison to age-matched WT and GoF cells (**Fig. 8B**).

To establish whether altered kinetics of Ca^{2+} transient decay occurring with age and in GoF myocytes are associated with defective cytosolic Ca^{2+} clearance, Ca^{2+} levels were evaluated in response to the acute increase in stimulation rate from 1 Hz to 4 Hz

(Cervantes *et al.*, 2022). The increase in stimulation rate was coupled with elevation of diastolic fluorescent signal, indicative of the increased diastolic Ca^{2+} level. The increase in diastolic fluorescence was augmented by 42% in myocytes from WT mice at ~24 m, with respect to cells from ~5 m WT animals (**Fig. 9A and 9B**). For GoF myocytes at ~5 m, the frequency-induced diastolic fluorescent elevation was ~40% larger with respect to age-matched WT and LoF. A similar increase was observed in cells from aged GoF mice. In contrast, LoF myocytes at ~5 m had diastolic fluorescent elevation comparable to age-matched WT cells, and no changes were observed with age. Thus, for myocytes from LoF mice at ~24 m, the elevation of diastolic fluorescence elicited by the higher pacing rate was attenuated by >46%, with respect to cells from age-matched WT and GoF mice, respectively.

The increase in stimulation rate from 1 Hz to 4 Hz was also coupled by diastolic cell contracture (i.e., reduction of diastolic cell length). For cells from WT animals, the level of cell contracture was increased by 79% in cells from mice at ~24 m, with respect to cells from animals at ~5 m (**Fig. 9C and 9D**). For myocytes from GoF mice at ~5 m, the frequency-induced cell contracture was >65% greater, with respect to cells from age-matched WT and LoF animals. Moreover, cell contracture in GoF myocytes further increased by 69% in myocytes from mice at ~24 m. For LoF myocytes at ~5 m, frequency-induced cell contracture was comparable to levels found in age-matched WT cells, and no significant changes were observed with age. Thus, for myocytes from aged LoF mice, cell contracture was attenuated by ~50%, with respect to cells from age-matched GoF mice.

To clarify the role of I_{NaL} in the delayed kinetics of Ca^{2+} transient and cell shortening observed in myocytes from aged WT animals and GoF mice, measurements were performed in cells in the absence and presence of the I_{NaL} inhibitor GS967. Properties of cell contraction and relaxation and Ca^{2+} transient decay were not affected in myocytes from adult WT mice (~5 months) exposed to GS967. In contrast, myocytes from aged WT mice (~24 months) bathed with GS967 had shorter time to peak contraction (7% reduction), reduced time to 50% relaxation (19% reduction), and faster Ca^{2+} transient decay (8% reduction), with respect to cells not exposed to the I_{NaL} inhibitor (**Fig. 10A and 10B**). Importantly, for cells obtained from adult (~5 m) and aged (~24 m) GoF mice, GS967 shortened time to peak contraction (3% and 20%,

respectively), cell relaxation (9%, 24%, respectively), and Ca^{2+} transient decay (5% and 13%, respectively) (**Fig. 10C and 10D**). The amplitude of Ca^{2+} transient and fractional cell shortening were not affected by I_{NaL} inhibition (**Supplemental Fig. S20**). Importantly, in myocytes from adult and aged LoF mice, GS967 had no detectable effects on mechanical and Ca^{2+} cycling kinetics (**Fig. 10E and 10F**). Moreover, mexiletine, another inhibitor of I_{NaL}, had comparable effects to those of GS967 in myocytes from adult GoF mice (**Supplemental Fig. S21**).

Thus, myocyte aging results in delayed kinetics of Ca^{2+} transients and cell contraction and relaxation. These defects, which affect rate adaptation of Ca^{2+} clearance and myocyte relengthening, are exacerbated with I_{NaL} gain-of-function mutation but are minimized with I_{NaL} loss-of-function mutation or following I_{NaL} inhibition.

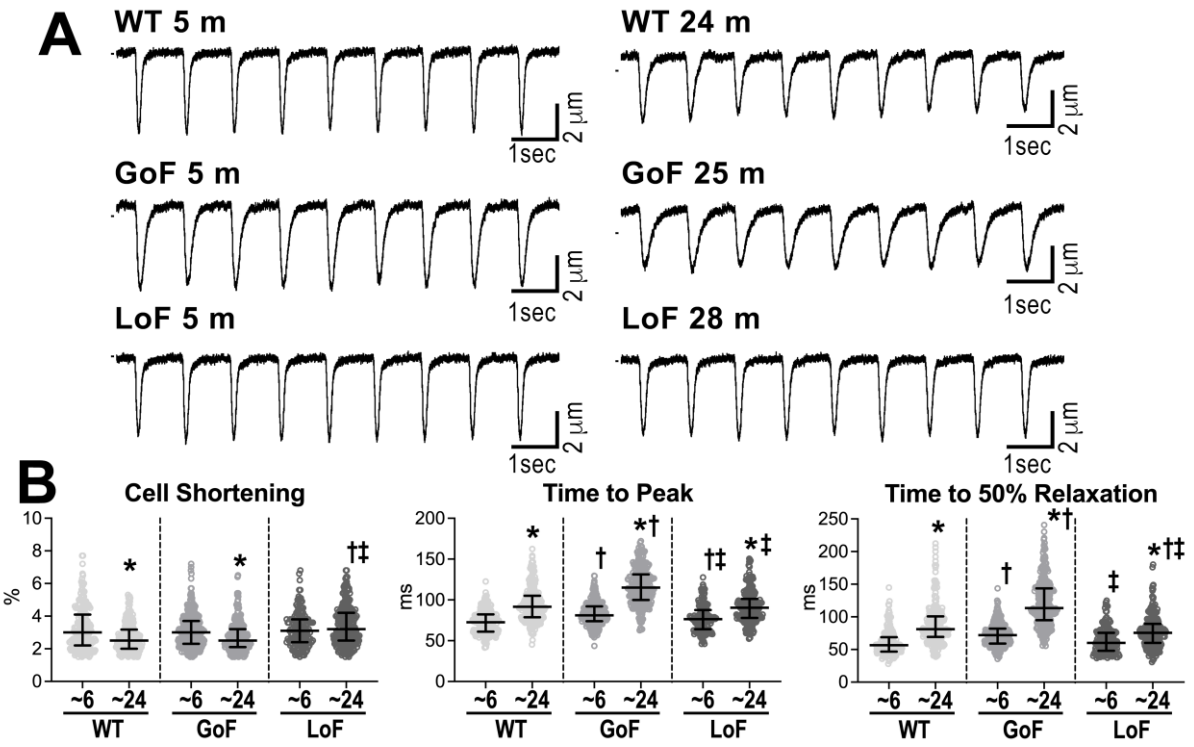

Fig 7. Aging and I_{NaL} alters myocyte mechanics. A, Cell shortening traces from myocytes from adult and aged male mice. **B,** Quantitative data for cell shortening properties of LV myocytes from male WT, GoF, and LoF mice at 4-7 m (~6, n=227, 326, 173 cells from 5 WT, 7 GoF, and 4 LoF mice, respectively) and 22-28 m (~24, n=284, 286, 270, cells from 6 WT, 6 GoF, and 6 LoF mice, respectively). Quantitative data are median and interquartile ranges with dot plots. *P<0.05 vs. ~6 using Mann-Whitney test. †P<0.0001 vs. age-matched WT, ‡P<0.05 vs. age-matched GoF, using Kruskal-Wallis, followed by Dunn's multiple comparison test.

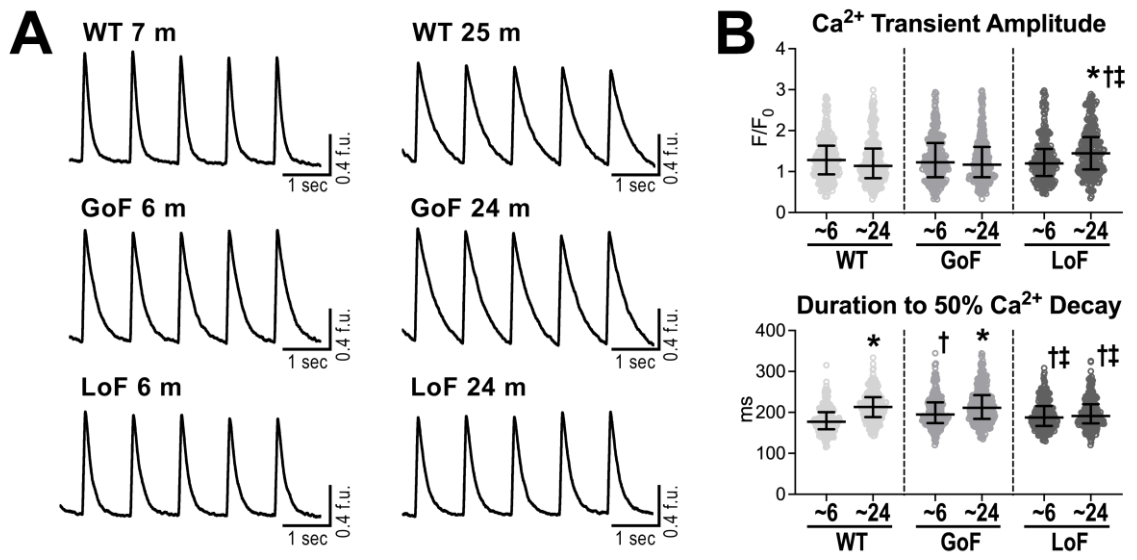

Fig 8. Aging and I_{NaL} alters Ca^{2+} homeostasis of cardiomyocytes. A, Traces of Ca^{2+} transients from myocytes from adult and aged male mice. **B,** Quantitative data for Ca^{2+} transient properties of LV myocytes from WT, GoF, and LoF male mice at 3-7 m (~6, n=266, 280, 259 cells from 4 WT, 4 GoF, and 4 LoF mice, respectively) and 23-28 m (~24, n=278, 340, 280 cells from 4 WT, 5 GoF, and 4 LoF mice, respectively). Quantitative data are median and interquartile ranges with dot plots. *P<0.05 vs. ~6 using Mann-Whitney test. †P<0.0001 vs. age-matched WT, ‡P<0.05 vs. age-matched GoF, using Kruskal-Wallis, followed by Dunn's multiple comparison test.

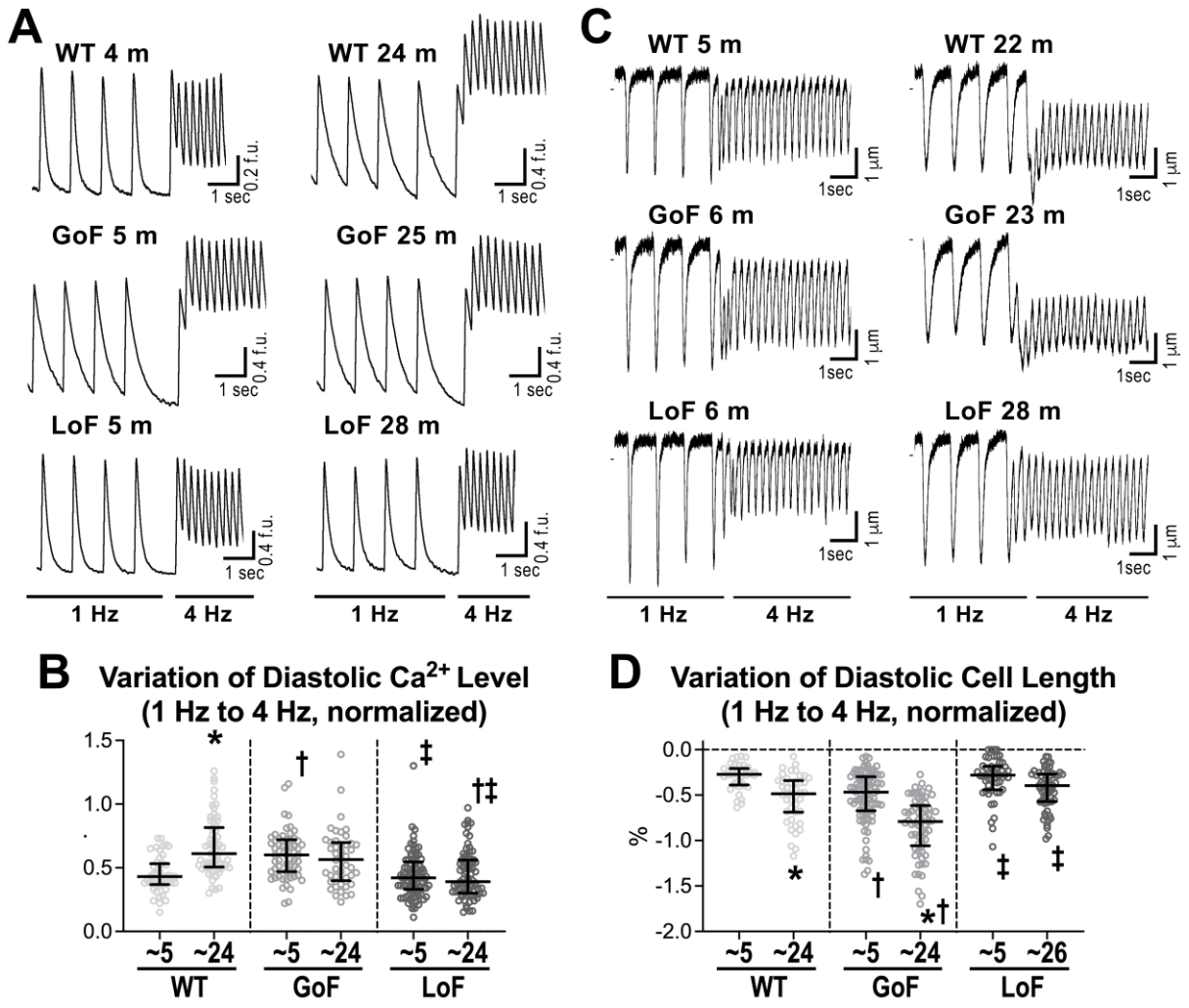

Fig 9. Aging and I_{NaL} alter the response of cardiomyocytes to increase in pacing rate. A, Traces of Ca^{2+} transients from myocytes from adult and aged male mice stimulated at 1 Hz and 4 Hz. f.u., fluorescent units. **B,** Quantitative data for variation of diastolic Ca^{2+} upon stimulation at 4 Hz, which is expressed as fraction of Ca^{2+} transient amplitude. Data for myocytes from WT, GoF, and LoF male mice at 3-7 m (~5, n=46, 59, and 88 cells from 3 WT, 5 GoF, and 5 LoF mice, respectively) and 22-28 m (~24, n=61, 44, and 75 cells from 4 WT, 6 GoF, and 6 LoF mice, respectively) are median and interquartile ranges with dot plots. *P<0.0001 vs. ~5 using Mann-Whitney test. †P<0.0001 vs. age-matched WT, ‡P<0.01 vs. age-matched GoF, using Kruskal-Wallis, followed by Dunn's multiple comparison test. **C,** Cell shortening traces from myocytes from adult and aged male mice stimulated at 1 Hz and 4 Hz. **D,** Quantitative data for variation of diastolic cell length and at 4 Hz with respect to 1 Hz in myocytes from WT, GoF, and LoF male mice at 3-7 m (~5, n=38, 92, and 50 cells from 3 WT, 9 GoF, and 6 LoF mice, respectively) and 22-28 m (~24, n=43, 63, and 62 cells from 4 WT, 5 GoF,

and 5 LoF mice, respectively). Data are median and interquartile ranges with dot plots. *P<0.0001 vs. ~5 using unpaired *t*-test or Mann-Whitney test. †P<0.0001 vs. age-matched WT, ‡P<0.001 vs. age-matched GoF, using Kruskal-Wallis, followed by Dunn's multiple comparison test.

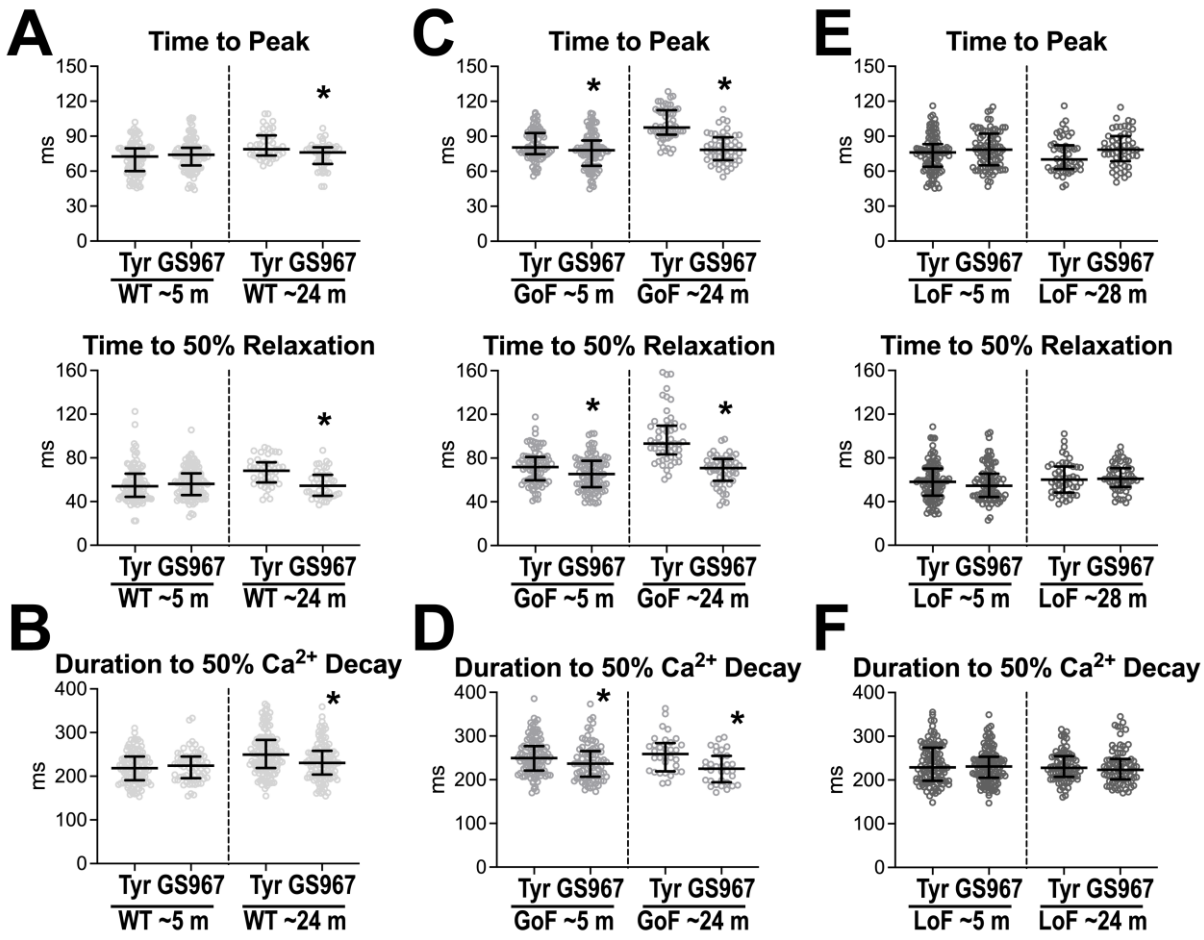

Fig 10. Aging and I_{NaL} alter cell mechanics and Ca^{2+} homeostasis of cardiomyocytes. A-F, Quantitative data for cell shortening and Ca^{2+} transient properties of LV myocytes stimulated at 1 Hz in the absence (Tyrode solution, Tyr) and presence of the I_{NaL} inhibitor GS967 (300 nmol/L). **A,** Data for cell shortening of myocytes from WT male mice at 4-6 m (~5 m, n=5) in the absence (n=103) and presence of GS967 (n=113) and myocytes from WT male mice at 24-28 m (~24 m, n=2) in the absence (n=42) and presence of GS967 (n=45). **B,** Data for Ca^{2+} transients of myocytes from WT male mice at 5 m (~5 m, n=5) in the absence (n=110) and presence of GS967 (n=64) and myocytes from WT male mice at 21-28 m (~24 m, n=6) in the absence (n=134) and presence of GS967 (n=112). **C,** Data for cell shortening of myocytes from GoF male mice at 5-6 m (~5 m, n=4) in the absence (n=81) and presence of GS967 (n=96) and myocytes from GoF male mice at 24-25 m (~24 m, n=3) in the absence (n=53) and presence of GS967 (n=51). **D,** Data for Ca^{2+} transients of myocytes from GoF male mice at 3-6 m (~5 m, n=4) in the absence (n=108) and presence of GS967 (n=79) and myocytes from GoF male mice at 24-25 m (~24 m,

n=3) in the absence (n=32) and presence of GS967 (n=32). **E,** Data for cell shortening of myocytes from LoF male mice at 5-7 m (~5 m, n=4) in the absence (n=110) and presence of GS967 (n=85) and myocytes from LoF male mice at 28 m (~28 m, n=3) in the absence (n=48) and presence of GS967 (n=53). **F,** Data for Ca^{2+} transients of myocytes from LoF male mice at 5-7 m (~5 m, n=4) in the absence (n=104) and presence of GS967 (n=120) and myocytes from LoF male mice at 21-28 m (~24 m, n=5) in the absence (n=79) and presence of GS967 (n=77). Data are median and interquartile ranges with dot plots. *P<0.05 vs. Tyr in the same experimental group using unpaired *t*-test or Mann-Whitney test.

Aging, Sodium Channel Status, and regulatory proteins

In order to gain information on putative molecular alterations contributing to the functional remodeling of aged cardiomyocytes from wild-type mice and animals with I_{NaL} gain- or loss-of-function mutations, levels of kinases affecting post-translational status of proteins involved excitation-contraction coupling, including sodium channel, were evaluated by Western blotting in myocytes from mice at ~5 and ~22 m (**Supplemental Fig. S22A**). Importantly, using LV tissue from WT mice, phosphorylation level of Nav1.5 at Ser571 tended to be enhanced with age (p=0.053), while expression of Nav1.5 was comparable in the myocardium of young and old WT animals (**Fig. 11A and 11B**).

In WT myocytes, expression of the cAMP-dependent protein kinase (PKA) was preserved with age, but phosphorylation status of the catalytic subunit of PKA was reduced at ~22 m, with respect to cells at ~5 m (**Fig. 11C and 11D**). Moreover, in WT myocytes, levels of the Ca^{2+}/calmodulin-dependent protein kinase II (CaMKII) declined at ~22 m, with respect to cells at ~5 m. However, the relative expression of the phosphorylated and oxidized CaMKII were, respectively, not altered and increased in old cells (**Fig. 11E and 11F**).

For GoF animals, both PKA and CaMKII levels were reduced in myocytes at ~22 m, with respect to cells from mice at ~5 m, but these changes did not occur in cells from LoF mice (**Supplemental Fig. S22B-E**). Moreover, using small cohorts of adult and old animals, there was no indication that oxidized CaMKII was affected with aging in GoF and LoF mice. Relative level of phosphorylated CaMKII was, however, reduced in old LoF animals (**Supplemental Fig. S22C and S22E**).

To establish whether increased CaMKII oxidation observed in aged WT myocytes was coupled with cellular alterations consistent with enhanced oxidative stress, transcripts for enzymes involved in the production of reactive oxygens species (ROS), and components of the antioxidant defense were evaluated. Transcripts for *Nox4* and *Cybb* genes, encoding for NADPH oxidase 4 and cytochrome B-245, which contribute to ROS generation (Ago *et al.*, 2010), and *Homox1* gene, encoding for heme oxygenase 1 (HO-1), whose expression is part of the cellular response to elevated ROS levels (Abraham & Kappas, 2005), were enhanced in myocytes from WT mice at ~22 m, in comparison to cells at ~5 m (**Fig. 11G and Supplemental Fig. S23A**). In contrast,

transcript levels of ROS-related enzyme NADPH oxidase 1 (*Nox1*) and the antioxidant enzymes superoxide dismutase 1 and 2 (*Sod1* and *Sod2*) were similar in adult and old myocytes (**Supplemental Fig. S23B**). Moreover, cells from GoF and LoF mice at ~5 m had more abundant expression of ROS-related genes with respect to cells from age-matched WT mice. However, the expression profile of ROS-associated genes for aging GoF and LoF myocytes followed the pattern observed in aging WT cells.

Thus, aging affects active forms of kinases modulating electromechanical function in cardiomyocytes and is coupled with expression of genes associated with oxidative stress. I_{NaL} gain and loss of function mutations tend to interfere with age-related alterations in active kinases but do not affect expression of ROS-associated genes with aging.

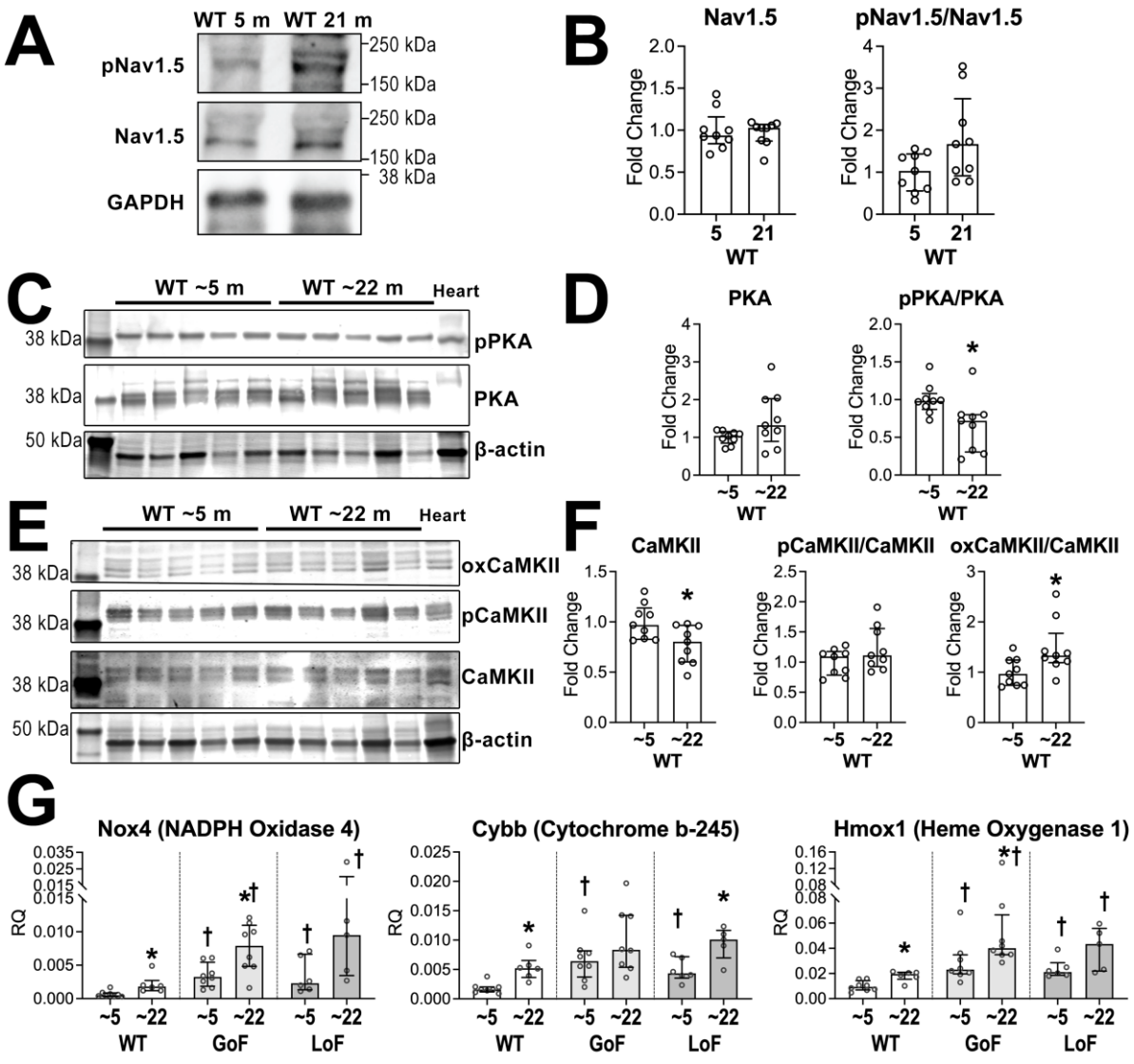

Fig 11. Aging and I_{NaL} alter status of regulatory proteins in myocytes. A, Expression of phosphorylated (Ser571, pNav1.5) and total Nav1.5 proteins in LV myocardium of WT male mice, by Western blotting. GAPDH is the loading condition. Tissue was obtained from mice at 5 and 21 m of age. **B**, Quantitative data for expression of total Nav1.5 and pNav1.5-to-Nav1.5 ratio in the LV myocardium of WT mice at 5 (n=9) and ~21 m (n=9). Data are median and interquartile ranges with dot plots as fold changes with respect to 5 m. **B**, Expression of phosphorylated (pPKA) and total PKA proteins in LV myocytes of WT male mice at ~5 and ~22 m of age, by Western blotting. For reported images, blots for heart tissue are the far-right lanes and β-actin is the loading condition. **C**, Quantitative data for expression of total PKA and pPKA-to-PKA ratio in LV myocytes of WT, GoF, and LoF mice at ~5 (n=9) and ~22 m

(n=9). Data are median and interquartile ranges with dot plots as fold changes with respect to ~5 m. *P<0.05 vs. ~5 using unpaired *t*-test. **D**, Expression of phosphorylated (pCaMKII), oxidized (oxCaMKII), and total CaMKII proteins in LV myocytes of WT male mice at ~5 and ~22 m of age. **E**, Quantitative data for expression of total CaMKII, pCaMKII-to-CaMKII ratio, and oxCaMKII-to-CaMKII ratio in LV myocytes of WT mice at ~5 (n=9) and ~22 m (n=9). Data are median and interquartile ranges with dot plots as fold changes with respect to ~5. *P<0.05 vs. ~5 using unpaired *t*-test or Mann-Whitney test. **F**, Quantitative data for expression of genes related to enzymes involved in ROS production and antioxidant defense in cardiomyocytes from WT, GoF, and LoF male mice at ~5 (n=8, 8, 6, respectively) and at ~22 m (n=6, 8, 5, respectively). Transcript levels for *Nox4*, encoding for NADPH oxidase 4, *Cybb*, encoding for cytochrome B-245, and *Homox1*, encoding for and heme oxygenase 1 (HO-1) are median and interquartile ranges. RQ: relative quantity with respect to hypoxanthine guanine phosphoribosyl transferase (*Hprt*). *P<0.05 vs. ~5 using unpaired *t*-test or Mann-Whitney test. †P<0.05 vs. age-matched WT using Kruskal-Wallis, followed by Dunn’s multiple comparison test.

DISCUSSION

Results of the current study document that the progressive impairment of cardiac function with aging in rodents is associated with protracted electrical recovery and structural alterations of the myocardium, together with defective Ca^{2+} cycling and mechanical properties of cardiomyocytes. WT mice at ~18 months, estimated to reflect humans at ~64 years of age (Diaz Brinton, 2012), begin to manifest impaired diastolic LV filling and prolonged QT interval, defects that are attenuated by acute inhibition of I_{NaL}. Importantly, mice with increased I_{NaL} (gain-of-function mice), due to phosphomimetic mutation of Nav1.5 at Ser571, prematurely exhibit diastolic impairment and prolonged ventricular repolarization. In contrast, animals harboring a mutation preventing enhancement of I_{NaL} via phosphorylation of Nav1.5 at Ser571 (loss-of-function mice) are resilient to age-related alterations of cardiac function. Thus, these results strengthen the notion that sodium channel status is integral part of the cardiac aging phenotype.

Prolongation of the QT interval with age appears to be strictly related to the delayed repolarization of the ventricular action potential of the aged myocardium, as previously reported in rodents (Capasso *et al.*, 1983; Signore *et al.*, 2015) and large mammals (Sorrentino *et al.*, 2016). Importantly, our current results substantiate the central role of I_{NaL} in the protracted ventricular recovery and delayed action potential repolarization occurring with age. This was documented by the ability of GS967 to normalize the QT interval of aged mice together with findings that LoF animals, protected from I_{NaL} enhancement (Glynn *et al.*, 2015), fail to adopt prolonged action potential and lengthened QT interval at old age. These results are corroborated by previous studies reporting that the delayed electrical recovery of aged animals, myocardium, and myocytes is corrected following I_{NaL} inhibition, with ranolazine or mexiletine (Signore *et al.*, 2015; Sorrentino *et al.*, 2016). Interestingly, GoF mice with increased I_{NaL} and action potential prolongation in myocytes, have long QT interval duration at young stage (Glynn *et al.*, 2015; Comelli *et al.*, 2020), and no further alterations occur with aging. Thus, results obtained from our two mouse lines with mutations of Nav1.5 together with findings in wild-type animals suggest that the Ser571 site, phosphorylated by CaMKII, is centrally involved in the electrical remodeling of the aged, murine heart.

Protracted electrical recovery of aged WT mice is coupled with increased incidence of ventricular ectopic events. However, results obtained in animals with I_{NaL} gain- or loss-of-function mutations attenuate the causative association between modality of repolarization and occurrence of extra-systolic beats, in the settings of myocardial aging in rodents. In fact, GoF and LoF mice have preserved QT interval duration as they age, but ventricular ectopy is equally enhanced. Moreover, when considering age-matched animals presenting normal or altered I_{NaL} function and repolarization properties, no substantial differences were observed in the *in vivo* occurrence of PVCs in the unstimulated state, or in the inducibility of arrhythmias in the *ex vivo* heart. In spite of these results, experiments in cohorts of aged mice revealed that epinephrine challenge induced ventricular tachycardia in GoF animals, whereas LoF mice were less predisposed to the occurrence of triggered events. Thus, because autonomic inputs to the heart are altered with aging (Comelli *et al.*, 2020), the possibility remains that imbalanced sympathovagal tone and increased I_{NaL} form the substrate for adverse electrical disturbances in old mice, a factor that may partly account for the unfavorable survival pattern of aging GoF animals, with respect to LoF mice. Overall, these findings suggest that the age-related incidence of ventricular ectopy is independent of modification of I_{NaL}, which, however, modulates the vulnerability of the heart to ventricular tachycardia.

Defective diastolic LV filling and depressed myocardial relaxation appear in both male and female WT mice at 18-20 months of age in combination with delayed ventricular repolarization. Additionally, at this age range, mechanical and electrical modifications are coupled with myocyte and ventricular hypertrophy, expression of hypertrophic markers, and increased interstitial fibrosis, factors that have been recognized as key modulators of passive muscle stiffening and reduced chamber compliance. Interestingly, our results provide information on the relative contribution of structural and electrical remodeling of the myocardium to the manifestation of impaired diastolic function occurring with age. In fact, despite augmented LV mass, myocyte size, and interstitial fibrosis, aged LoF mice with preserved QT interval duration are protected from the deteriorated diastolic function occurring in age-matched WT animals. In contrast, adult (~5 months) GoF mice, with relatively normal myocardial structure but defective repolarization, display impaired ventricular filling, supporting the notion that enhanced I_{NaL} and delayed electrical recovery are important contributors of diastolic

performance. These findings were substantiated by pharmacological interventions aimed at inhibiting I_{NaL} and restoring ventricular repolarization, which resulted in amelioration of LV ventricular filling pattern in GoF mice and aged WT animals.

Impaired diastolic function observed in old WT mice is coupled with altered kinetics of contraction and relaxation of cardiomyocytes, together with delayed Ca^{2+} transient decay, and defective intracellular Ca^{2+} clearance. Similar alterations of myocyte mechanics were found in adult GoF mice, characterized by impaired diastolic performance. In contrast, preservation of diastolic properties in aged LoF mice is coupled with limited modifications of the kinetics of cell mechanics and intracellular Ca^{2+} homeostasis in myocytes. Importantly, the close relationship between functional behavior at the cellular and organ levels is corroborated by the finding that interventions aimed at inhibiting I_{NaL} are equally effective in ameliorating kinetics of myocyte shortening/relengthening and the *in vivo* LV filling pattern, for aged animals and GoF mice. Therefore, these results strengthen the fundamental role of the myocyte compartment in conditioning the modality of myocardial relaxation and LV filling of the aged heart.

The notion that enhanced I_{NaL} and prolonged electrical recovery cause defective ventricular relaxation and impaired LV filling, is substantiated by experimental findings in mice with inducible deletion of *Scn1b*, the gene encoding for the β1-subunits of the voltage-gated sodium channel, which results in increased I_{NaL} in cardiomyocytes. As observed for GoF animals studied here, mice with *Scn1b* deletion have prolonged QT interval duration together with impaired diastolic properties and reduced LV compliance, without structural modifications of the myocardium (Cervantes *et al.*, 2022) Importantly, myocytes with *Scn1b* deletion have delayed kinetics of Ca^{2+} transient, cell shortening, and cell relaxation, defects that are corrected by inhibition of I_{NaL}, resulting in normalization of diastolic indices *in vivo* (Cervantes *et al.*, 2022). Clinical information linking I_{NaL} gain-of-function mutations with defective diastolic properties of the heart are scanty. However, it has been reported that patients with inherited long QT syndrome secondary to *SCN5A* mutation have impaired diastolic function (Moss *et al.*, 2008; Hummel *et al.*, 2013), a feature that is apparent at early stages of development (Clur *et al.*, 2018). Moreover, it was found that in the human myocardium obtained from patients suffering from pathologies associated with

enhanced late Na^+ current, myocardial relaxation and passive tensions are ameliorated following I_{NaL} inhibition (Sossalla *et al.*, 2008; Coppini *et al.*, 2013). Overall, these findings, together with current results support the role of the sodium channels and late Na^+ current as key modulators of myocardial relaxation of the mammalian heart.

Mechanisms linking late Na^+ current and modality of cell and myocardial relaxation in the context of cardiac aging appear to be intimately associated with the process of cytosolic Ca^{2+} clearance. In fact, the chronic modulation of I_{NaL} in mice with gain and loss of function mutations, and the acute pharmacological inhibition of I_{NaL} in aged animals, affect Ca^{2+} transient decay, which in turn conditions myocyte relengthening and diastolic function. The enhanced Na^+ entry mediated by I_{NaL} and prolonged AP duration may increase $[Na^+]_i$, attenuating Ca^{2+} extrusion via NCX, on the one hand, but also promoting activity of the Na^+/K^+ ATPase, which may limit ATP utilization for Ca^{2+} re-uptake into the SR via SERCA, on the other (Pourrier *et al.*, 2014; Kornyeyev *et al.*, 2016). Moreover, increased $[Na^+]_i$ also favors extrusion of Ca^{2+} from the mitochondrial matrix via the mitochondrial NCX affecting ATP supply to the cell (Maack *et al.*, 2006) and SERCA action. Thus, the process affecting diastolic function of the aged heart appears to be partly accounted by perturbation of intracellular Na^+ and Ca^{2+} homeostasis, which can be corrected, in principle, by targeting ion channels and transporters and/or related regulatory proteins.

Molecular events underlying I_{NaL} enhancement with aging remains to be fully clarified. The Ser571 of Nav1.5 is one the known sites targeted by CaMKII and phosphorylated in rodent, canine, and human myocardium under stress conditions, which result in increased I_{NaL} (Koval *et al.*, 2012; Glynn *et al.*, 2015). Importantly, the elevated expression of ROS-related gene and augmented oxidation of CaMKII in aged cardiomyocytes found in WT mice, strengthen the possibility that oxidative stress is among the triggering factors for the robust phosphorylation of Nav1.5 at Ser571 and, at least in part, the electromechanical remodeling of aged cells. Interestingly, old LoF mice are partly protected from the deterioration of myocyte function in spite of the elevated expression of ROS-related genes. Thus, resistance to phosphorylation of Nav1.5 at Ser571 may confer protection to aging myocytes by attenuating the cascade of deleterious events associated with elevated cytosolic Na^+ and Ca^{2+} ions.

The acute inhibition of the late Na^+ current restores relaxation of cardiomyocyte and diastolic function *in vivo* in the settings of aging, but the long-term consequences of I_{NaL} attenuation remain to be determined. Interestingly, mice with I_{NaL} loss-of-function mutation are protected from the age-associated prolongation of the electrical repolarization and the appearance of diastolic defects. Moreover, changes of interstitial fibrosis and myocyte size with age are attenuated in LoF mice, with respect to alterations observed in WT and GoF animals. These positive features, together with the ameliorated probability of survival, suggest that loss of I_{NaL} function effectively tempers the manifestations of the aging myopathy.

Our in vivo tests support the notion that aging similarly affects cardiac performance in male and female mice. While body weight, LV mass, and LV cavitary dimension are key indices of sexual dimorphisms that are preserved throughout animal lifespan, both male and female mice undergo anatomical and electrical remodeling with aging, together with appearance of defects in diastolic properties. Importantly, results collected in mutant animals and following pharmacological interventions, substantiate the key role of sodium channel status and late Na^+ current in the deteriorated function of the male and female aging heart.

CONCLUSIONS

In conclusion, results of the current study document that the sodium channels modulate myocardial relaxation and diastolic function, a process that is centrally involved in the manifestations of functional defects of the aged heart. These observations offer a new perspective of the cellular and molecular mechanisms that define the etiology of the aging myopathy and putative interventions aimed at delaying, and possibly reversing, heart failure in the elderly.

REFERENCES

Abraham NG & Kappas A. (2005). Heme oxygenase and the cardiovascular-renal system. *Free Radic Biol Med* **39,** 1-25.

Ago T, Kuroda J, Pain J, Fu C, Li H & Sadoshima J. (2010). Upregulation of Nox4 by hypertrophic stimuli promotes apoptosis and mitochondrial dysfunction in cardiac myocytes. *Circ Res* **106,** 1253-1264.

Borghetti G, Eisenberg CA, Signore S, Sorrentino A, Kaur K, Andrade-Vicenty A, Edwards JG, Nerkar M, Qanud K, Sun D, Goichberg P, Leri A, Anversa P, Eisenberg LM, Jacobson JT, Hintze TH & Rota M. (2018). Notch signaling modulates the electrical behavior of cardiomyocytes. *Am J Physiol Heart Circ Physiol* **314,** H68-H81.

Capasso JM, Malhotra A, Remily RM, Scheuer J & Sonnenblick EH. (1983). Effects of age on mechanical and electrical performance of rat myocardium. *Am J Physiol* **245,** H72-81.

Cervantes DO, Pizzo E, Ketkar H, Parambath SP, Tang S, Cianflone E, Cannata A, Vinukonda G, Jain S, Jacobson JT & Rota M. (2022). Scn1b expression in the adult mouse heart modulates Na(+) influx in myocytes and reveals a mechanistic link between Na(+) entry and diastolic function. *Am J Physiol Heart Circ Physiol* **322,** H975-H993.

Cimini M, Cannata A, Pasquinelli G, Rota M & Goichberg P. (2017). Phenotypically heterogeneous podoplanin-expressing cell populations are associated with the lymphatic vessel growth and fibrogenic responses in the acutely and chronically infarcted myocardium. *PLoS One* **12,** e0173927.

Clur SB, Vink AS, Etheridge SP, Robles de Medina PG, Rydberg A, Ackerman MJ, Wilde AA, Blom NA, Benson DW, Herberg U, Donofrio MT & Cuneo BF. (2018). Left Ventricular Isovolumetric Relaxation Time Is Prolonged in Fetal Long-QT Syndrome. *Circ Arrhythm Electrophysiol* **11,** e005797.

Colby SL & Ortman JM. (2015). Projections of the Size and Composition of the U.S. Population: 2014 to 2060.

Comelli M, Meo M, Cervantes DO, Pizzo E, Plosker A, Mohler PJ, Hund TJ, Jacobson JT, Meste O & Rota M. (2020). Rhythm dynamics of the aging heart: an experimental study using conscious, restrained mice. *Am J Physiol Heart Circ Physiol* **319,** H893-H905.

Coppini R, Ferrantini C, Yao L, Fan P, Del Lungo M, Stillitano F, Sartiani L, Tosi B, Suffredini S, Tesi C, Yacoub M, Olivotto I, Belardinelli L, Poggesi C, Cerbai E & Mugelli A. (2013). Late sodium current inhibition reverses electromechanical dysfunction in human hypertrophic cardiomyopathy. *Circulation* **127,** 575-584.

Diaz Brinton R. (2012). Minireview: translational animal models of human menopause: challenges and emerging opportunities. *Endocrinology* **153,** 3571-3578.

Dunlay SM, Roger VL & Redfield MM. (2017). Epidemiology of heart failure with preserved ejection fraction. *Nat Rev Cardiol* **14,** 591-602.

Figueredo VM, Pressman GS, Romero-Corral A, Murdock E, Holderbach P & Morris DL. (2011). Improvement in left ventricular systolic and diastolic performance during ranolazine treatment in patients with stable angina. *J Cardiovasc Pharmacol Ther* **16,** 168-172.

Glynn P, Musa H, Wu X, Unudurthi SD, Little S, Qian L, Wright PJ, Radwanski PB, Gyorke S, Mohler PJ & Hund TJ. (2015). Voltage-Gated Sodium Channel Phosphorylation at Ser571 Regulates Late Current, Arrhythmia, and Cardiac Function In Vivo. *Circulation* **132,** 567-577.

Greer-Short A, Musa H, Alsina KM, Ni L, Word TA, Reynolds JO, Gratz D, Lane C, El-Refaey M, Unudurthi S, Skaf M, Li N, Fedorov VV, Wehrens XHT, Mohler PJ & Hund TJ. (2020). Calmodulin kinase II regulates atrial myocyte late sodium current, calcium handling, and atrial arrhythmia. *Heart Rhythm* **17,** 503-511.

Hayashida W, van Eyll C, Rousseau MF & Pouleur H. (1994). Effects of ranolazine on left ventricular regional diastolic function in patients with ischemic heart disease. *Cardiovasc Drugs Ther* **8,** 741-747.

Hummel YM, Wilde AA, Voors AA, Bugatti S, Hillege HL & van den Berg MP. (2013). Ventricular dysfunction in a family with long QT syndrome type 3. *Europace* **15,** 1516-1521.

Hund TJ, Koval OM, Li J, Wright PJ, Qian L, Snyder JS, Gudmundsson H, Kline CF, Davidson NP, Cardona N, Rasband MN, Anderson ME & Mohler PJ. (2010). A beta(IV)-spectrin/CaMKII signaling complex is essential for membrane excitability in mice. *J Clin Invest* **120,** 3508-3519.

Hund TJ, Snyder JS, Wu X, Glynn P, Koval OM, Onal B, Leymaster ND, Unudurthi SD, Curran J, Camardo C, Wright PJ, Binkley PF, Anderson ME & Mohler PJ. (2014). beta(IV)-Spectrin regulates TREK-1 membrane targeting in the heart. *Cardiovasc Res* **102,** 166-175.

Jain S, Puri N, Rana A, Sirianni N, Mopidevi B & Kumar A. (2018). Metabolic Syndrome Induces Over Expression of the Human AT1R: A Haplotype-Dependent Effect With Implications on Cardio-Renal Function. *Am J Hypertens* **31,** 495-503.

Janse MJ. (2004). Electrophysiological changes in heart failure and their relationship to arrhythmogenesis. *Cardiovasc Res* **61,** 208-217.

Judge S, Jang YM, Smith A, Hagen T & Leeuwenburgh C. (2005). Age-associated increases in oxidative stress and antioxidant enzyme activities in cardiac interfibrillar mitochondria: implications for the mitochondrial theory of aging. *FASEB J* **19,** 419-421.

Kornyeyev D, El-Bizri N, Hirakawa R, Nguyen S, Viatchenko-Karpinski S, Yao L, Rajamani S & Belardinelli L. (2016). Contribution of the late sodium current to intracellular sodium and calcium overload in rabbit ventricular myocytes treated by anemone toxin. *Am J Physiol Heart Circ Physiol* **310,** H426-435.

Koval OM, Snyder JS, Wolf RM, Pavlovicz RE, Glynn P, Curran J, Leymaster ND, Dun W, Wright PJ, Cardona N, Qian L, Mitchell CC, Boyden PA, Binkley PF, Li C, Anderson ME, Mohler PJ & Hund TJ. (2012). Ca2+/calmodulin-dependent protein kinase II-based regulation of voltage-gated Na+ channel in cardiac disease. *Circulation* **126,** 2084-2094.

Lakatta EG. (2003). Arterial and cardiac aging: major shareholders in cardiovascular disease enterprises: Part III: cellular and molecular clues to heart and arterial aging. *Circulation* **107,** 490-497.

Li H, Hastings MH, Rhee J, Trager LE, Roh JD & Rosenzweig A. (2020). Targeting Age-Related Pathways in Heart Failure. *Circ Res* **126,** 533-551.

Maack C, Cortassa S, Aon MA, Ganesan AN, Liu T & O'Rourke B. (2006). Elevated cytosolic Na+ decreases mitochondrial Ca2+ uptake during excitation-contraction coupling and impairs energetic adaptation in cardiac myocytes. *Circ Res* **99,** 172-182.

Maier LS, Layug B, Karwatowska-Prokopczuk E, Belardinelli L, Lee S, Sander J, Lang C, Wachter R, Edelmann F, Hasenfuss G & Jacobshagen C. (2013). RAnoLazIne for the treatment of diastolic heart failure in patients with preserved ejection fraction: the RALI-DHF proof-of-concept study. *JACC Heart Fail* **1,** 115-122.

Makielski JC. (2016). Late sodium current: A mechanism for angina, heart failure, and arrhythmia. *Trends Cardiovasc Med* **26,** 115-122.

Maltsev VA, Sabbah HN, Higgins RS, Silverman N, Lesch M & Undrovinas AI. (1998). Novel, ultraslow inactivating sodium current in human ventricular cardiomyocytes. *Circulation* **98,** 2545-2552.

Mangoni AA, Kinirons MT, Swift CG & Jackson SH. (2003). Impact of age on QT interval and QT dispersion in healthy subjects: a regression analysis. *Age Ageing* **32,** 326-331.

Meo M, Meste O, Signore S & Rota M. (2019). Novel Methods for High-resolution Assessment of Cardiac Action Potential Repolarization. *Biomed Signal Process Control* **51,** 30-41.

Meo M, Meste O, Signore S, Sorrentino A, Cannata A, Zhou Y, Matsuda A, Luciani M, Kannappan R, Goichberg P, Leri A, Anversa P & Rota M. (2016). Reduction in Kv Current Enhances the Temporal Dispersion of the Action Potential in Diabetic Myocytes: Insights From a Novel Repolarization Algorithm. *J Am Heart Assoc* **5**.

Moreno JD & Clancy CE. (2012). Pathophysiology of the cardiac late Na current and its potential as a drug target. *J Mol Cell Cardiol* **52,** 608-619.

Moss AJ, Zareba W, Schwarz KQ, Rosero S, McNitt S & Robinson JL. (2008). Ranolazine shortens repolarization in patients with sustained inward sodium current due to type-3 long-QT syndrome. *J Cardiovasc Electrophysiol* **19,** 1289-1293.

Pfeffer MA, Shah AM & Borlaug BA. (2019). Heart Failure With Preserved Ejection Fraction In Perspective. *Circ Res* **124,** 1598-1617.

Pizzo E, Berrettoni S, Kaul R, Cervantes DO, Di Stefano V, Jain S, Jacobson JT & Rota M. (2022). Heart Rate Variability Reveals Altered Autonomic Regulation in Response to Myocardial Infarction in Experimental Animals. *Front Cardiovasc Med* **9,** 843144.

Pourrier M, Williams S, McAfee D, Belardinelli L & Fedida D. (2014). CrossTalk proposal: The late sodium current is an important player in the development of diastolic heart failure (heart failure with a preserved ejection fraction). *J Physiol* **592,** 411-414.

Rabkin SW, Cheng XJ & Thompson DJ. (2016). Detailed analysis of the impact of age on the QT interval. *J Geriatr Cardiol* **13,** 740-748.

Radulescu CI, Cerar V, Haslehurst P, Kopanitsa M & Barnes SJ. (2021). The aging mouse brain: cognition, connectivity and calcium. *Cell Calcium* **94,** 102358.

Sacchi V, Wang BJ, Kubli D, Martinez AS, Jin JK, Alvarez R, Jr., Hariharan N, Glembotski C, Uchida T, Malter JS, Yang Y, Gross P, Zhang C, Houser S, Rota M & Sussman MA. (2017). Peptidyl-Prolyl Isomerase 1 Regulates Ca2+ Handling by Modulating Sarco(Endo)Plasmic Reticulum Calcium ATPase and Na2+/Ca2+ Exchanger 1 Protein Levels and Function. *J Am Heart Assoc* **6**.

Sauer A, Wilcox JE, Andrei AC, Passman R, Goldberger JJ & Shah SJ. (2012). Diastolic electromechanical coupling: association of the ECG T-peak to T-end interval with echocardiographic markers of diastolic dysfunction. *Circ Arrhythm Electrophysiol* **5,** 537-543.

Schwartz J & Zipes D. (2011). Cardiovascular disease in the elderly. In *Braunwald's Heart Disease: A Textbook of Cardiovascular Medicine 9th ed*, ed. Bonow R, Mann D, Zipes D, Libby P & eds., pp. 1727-1753. Saunders, Philadelphia, Pa.

Shah NR, Cheezum MK, Veeranna V, Horgan SJ, Taqueti VR, Murthy VL, Foster C, Hainer J, Daniels KM, Rivero J, Shah AM, Stone PH, Morrow DA, Steigner ML, Dorbala S, Blankstein R & Di Carli MF. (2017). Ranolazine in Symptomatic Diabetic Patients Without Obstructive Coronary Artery Disease: Impact on Microvascular and Diastolic Function. *J Am Heart Assoc* **6**.

Shu C, Huang H, Xu Y, Rota M, Sorrentino A, Peng Y, Padera RF, Jr., Huntoon V, Agrawal PB, Liu X & Perrella MA. (2018). Pressure Overload in Mice With Haploinsufficiency of Striated Preferentially Expressed Gene Leads to Decompensated Heart Failure. *Front Physiol* **9,** 863.

Signore S, Sorrentino A, Borghetti G, Cannata A, Meo M, Zhou Y, Kannappan R, Pasqualini F, O'Malley H, Sundman M, Tsigkas N, Zhang E, Arranto C, Mangiaracina C, Isobe K, Sena BF, Kim J, Goichberg P, Nahrendorf M, Isom LL, Leri A, Anversa P & Rota M. (2015). Late Na(+) current and protracted electrical recovery are critical determinants of the aging myopathy. *Nat Commun* **6,** 8803.

Signore S, Sorrentino A, Ferreira-Martins J, Kannappan R, Shafaie M, Del Ben F, Isobe K, Arranto C, Wybieralska E, Webster A, Sanada F, Ogorek B, Zheng H, Liu X, Del Monte F, D'Alessandro DA, Wunimenghe O, Michler RE, Hosoda T, Goichberg P, Leri A, Kajstura J, Anversa P & Rota M. (2013). Inositol 1, 4, 5-trisphosphate receptors and human left ventricular myocytes. *Circulation* **128,** 1286-1297.

Sorrentino A, Borghetti G, Zhou Y, Cannata A, Meo M, Signore S, Anversa P, Leri A, Goichberg P, Qanud K, Jacobson JT, Hintze TH & Rota M. (2017). Hyperglycemia induces defective Ca2+ homeostasis in cardiomyocytes. *Am J Physiol Heart Circ Physiol* **312,** H150-H161.

Sorrentino A, Signore S, Qanud K, Borghetti G, Meo M, Cannata A, Zhou Y, Wybieralska E, Luciani M, Kannappan R, Zhang E, Matsuda A, Webster A, Cimini M, Kertowidjojo E, D'Alessandro DA, Wunimenghe O, Michler RE, Royer C, Goichberg P, Leri A, Barrett EG, Anversa P, Hintze TH & Rota M. (2016). Myocyte repolarization modulates myocardial function in aging dogs. *Am J Physiol Heart Circ Physiol* **310,** H873-890.

Sossalla S, Wagner S, Rasenack EC, Ruff H, Weber SL, Schondube FA, Tirilomis T, Tenderich G, Hasenfuss G, Belardinelli L & Maier LS. (2008). Ranolazine improves diastolic dysfunction in isolated myocardium from failing human hearts--role of late sodium current and intracellular ion accumulation. *J Mol Cell Cardiol* **45,** 32-43.

Tomaselli GF & Marban E. (1999). Electrophysiological remodeling in hypertrophy and heart failure. *Cardiovasc Res* **42,** 270-283.

Tsao CW, Aday AW, Almarzooq ZI, Alonso A, Beaton AZ, Bittencourt MS, Boehme AK, Buxton AE, Carson AP, Commodore-Mensah Y, Elkind MSV, Evenson KR, Eze-Nliam C, Ferguson JF, Generoso G, Ho JE, Kalani R, Khan SS, Kissela BM, Knutson KL, Levine DA, Lewis TT, Liu J, Loop MS, Ma J, Mussolino ME, Navaneethan SD, Perak AM, Poudel R, Rezk-Hanna M, Roth GA, Schroeder EB, Shah SH, Thacker EL, VanWagner LB, Virani SS, Voecks JH, Wang NY, Yaffe K & Martin SS. (2022). Heart Disease and Stroke Statistics-2022 Update: A Report From the American Heart Association. *Circulation* **145,** e153-e639.

Venkataraman R, Chen J, Garcia EV, Belardinelli L, Hage FG, Heo J & Iskandrian AE. (2012). Effect of ranolazine on left ventricular dyssynchrony in patients with coronary artery disease. *Am J Cardiol* **110,** 1440-1445.

Wagner S, Dybkova N, Rasenack EC, Jacobshagen C, Fabritz L, Kirchhof P, Maier SK, Zhang T, Hasenfuss G, Brown JH, Bers DM & Maier LS. (2006). Ca2+/calmodulin-dependent protein kinase II regulates cardiac Na+ channels. *J Clin Invest* **116,** 3127-3138.

Yusifov A, Woulfe KC & Bruns DR. (2022). Mechanisms and implications of sex differences in cardiac aging. *J Cardiovasc Aging* **2**.

SUPPLEMENTAL MATERIAL

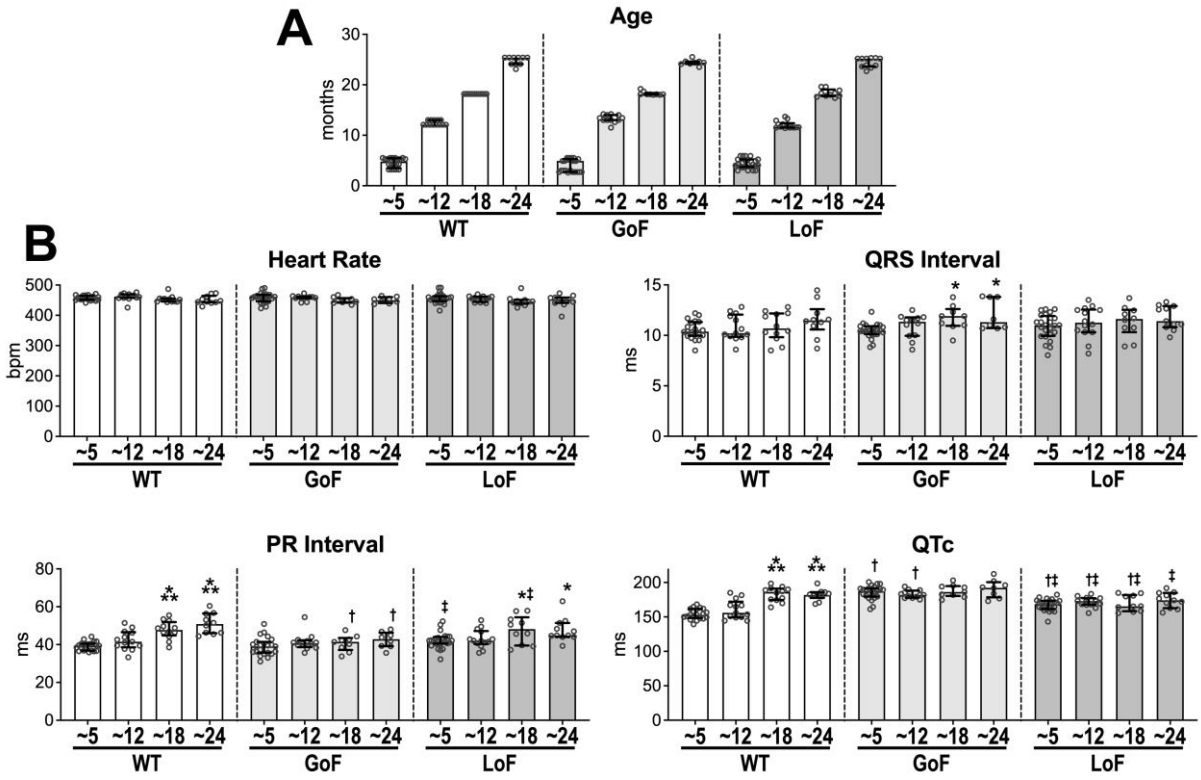

Supplemental Fig S1. Electrocardiographic properties of aging male mice. A, Age of male mice included in electrocardiographic studies. **B,** Quantitative data for electrocardiographic parameter in anesthetized WT, GoF, and LoF male mice at 3-6 m (~5 m, n=20, 23, 24, respectively), 11-14 m (~12 m, n=13, 12, 14, respectively), 17-20 m (~18 m, n=12, 9, 10, respectively), and 23-26 m of age (~24 m, n=10, 8, 11, respectively). Data are shown as median and interquartile ranges with dot plots. *P<0.05 vs. ~5 m, **P<0.05 vs. ~12 m, †P<0.05 vs. age-matched WT, ‡P<0.05 vs. age-matched GoF using one-way ANOVA, followed by Bonferroni multiple comparison test.

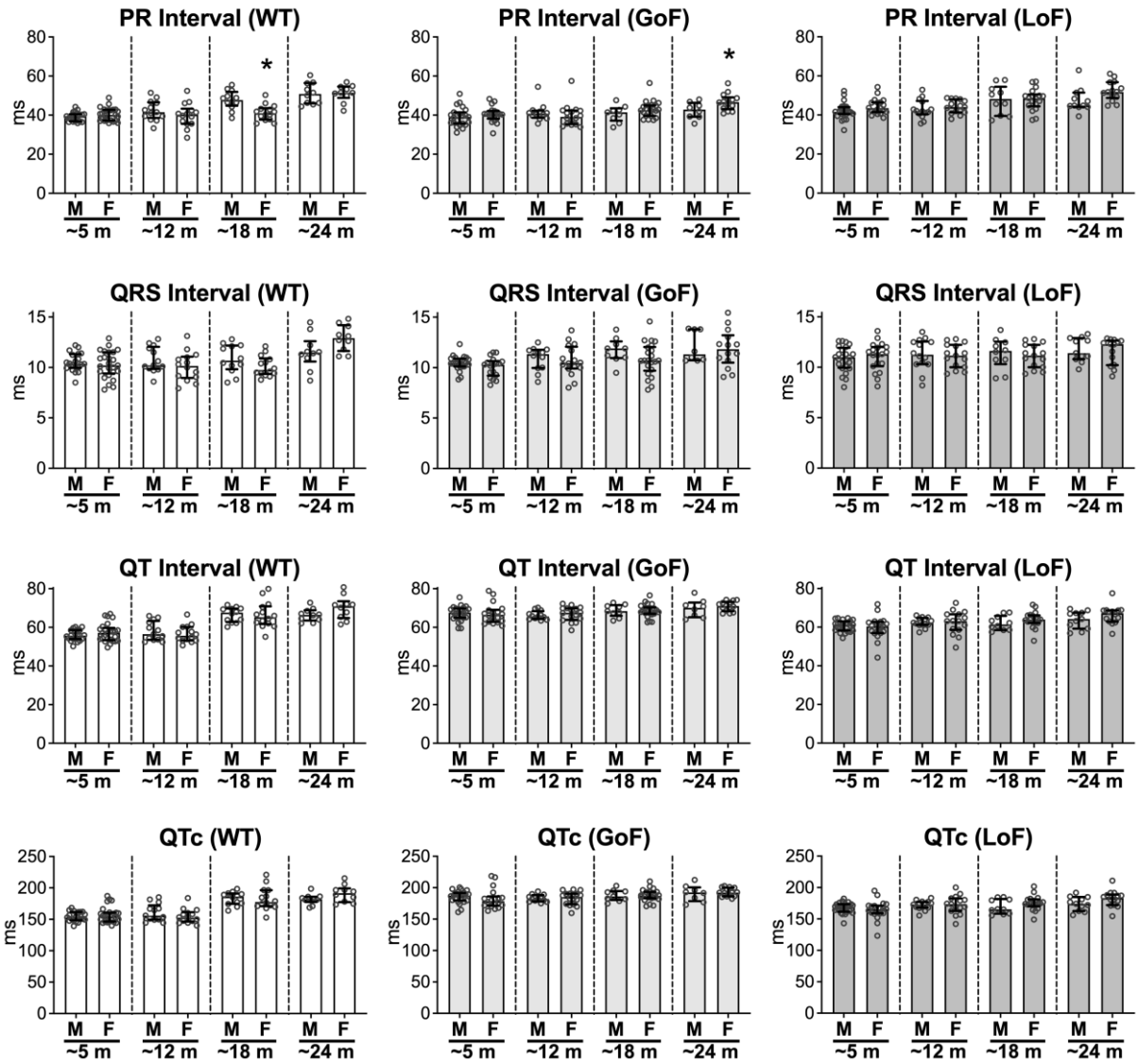

Supplemental Fig S2. Comparison of the electrocardiographic properties of age-matched male and female mice. Electrophysiological properties of age-matched male (M) and female (F) mice. Data are shown as median and interquartile ranges with dot plots. *P<0.05 vs. male using unpaired *t*-test or Mann-Whitney test. Presented data is reported in figures illustrating, for each sex, alterations of electrophysiological properties occurring with aging.

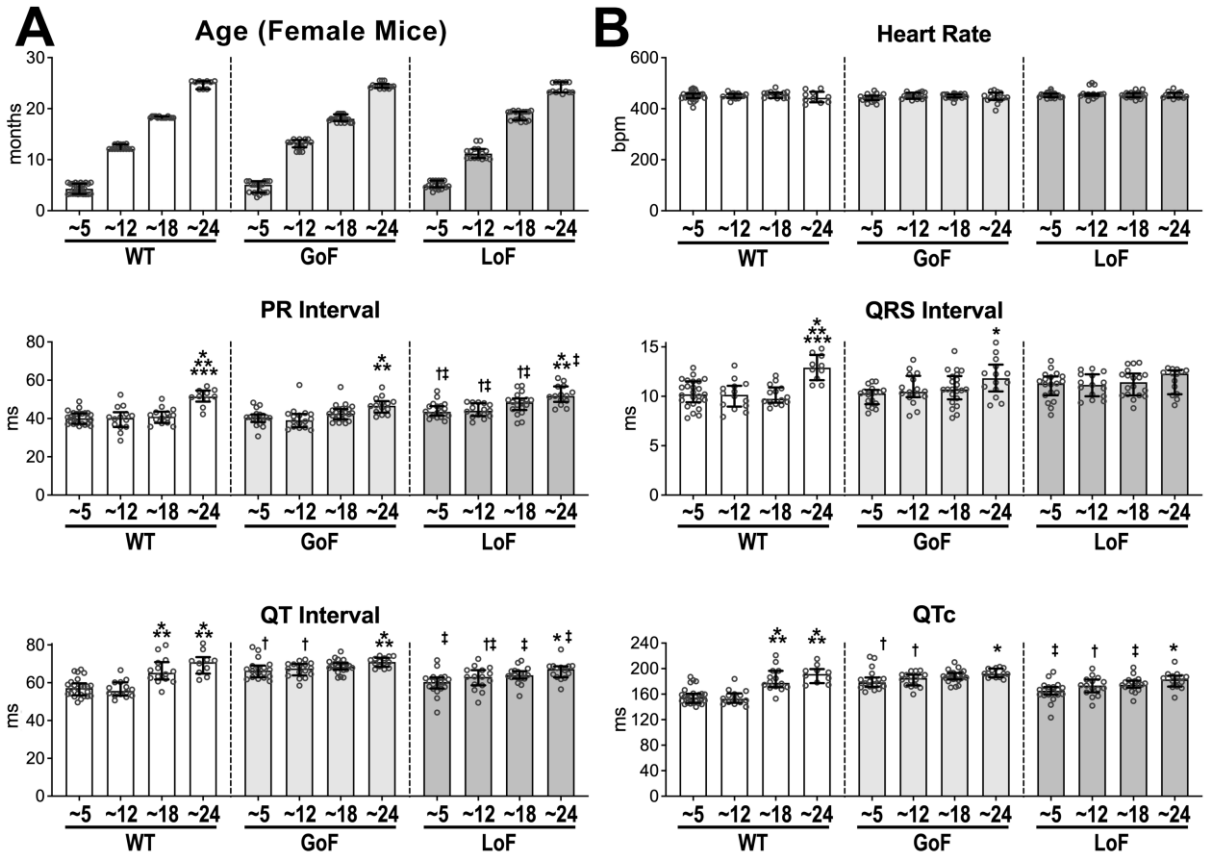

Supplemental Fig S3. Electrocardiographic properties of aging female mice. A, Age of female mice included in electrocardiographic studies. **B,** Quantitative data for electrocardiographic parameter in anesthetized WT, GoF, and LoF female mice at 3-6 m (~5, n=25, 18, 19, respectively), 10-14 m (~12, n=14, 16, 15, respectively), 17-20 m (~18, n=14, 22, 18, respectively), and 23-26 m of age (~24, n=10, 14, 14, respectively). Data are shown as median and interquartile ranges with dot plots. *P<0.05 vs. ~5, **P<0.05 vs. ~12, ***P<0.05 vs. ~18, †P<0.05 vs. age-matched WT, ‡P<0.05 vs. age-matched GoF. Data were tested by one-way ANOVA, followed by Bonferroni multiple comparison test or by Kruskal-Wallis, followed by Dunn's multiple comparison test.

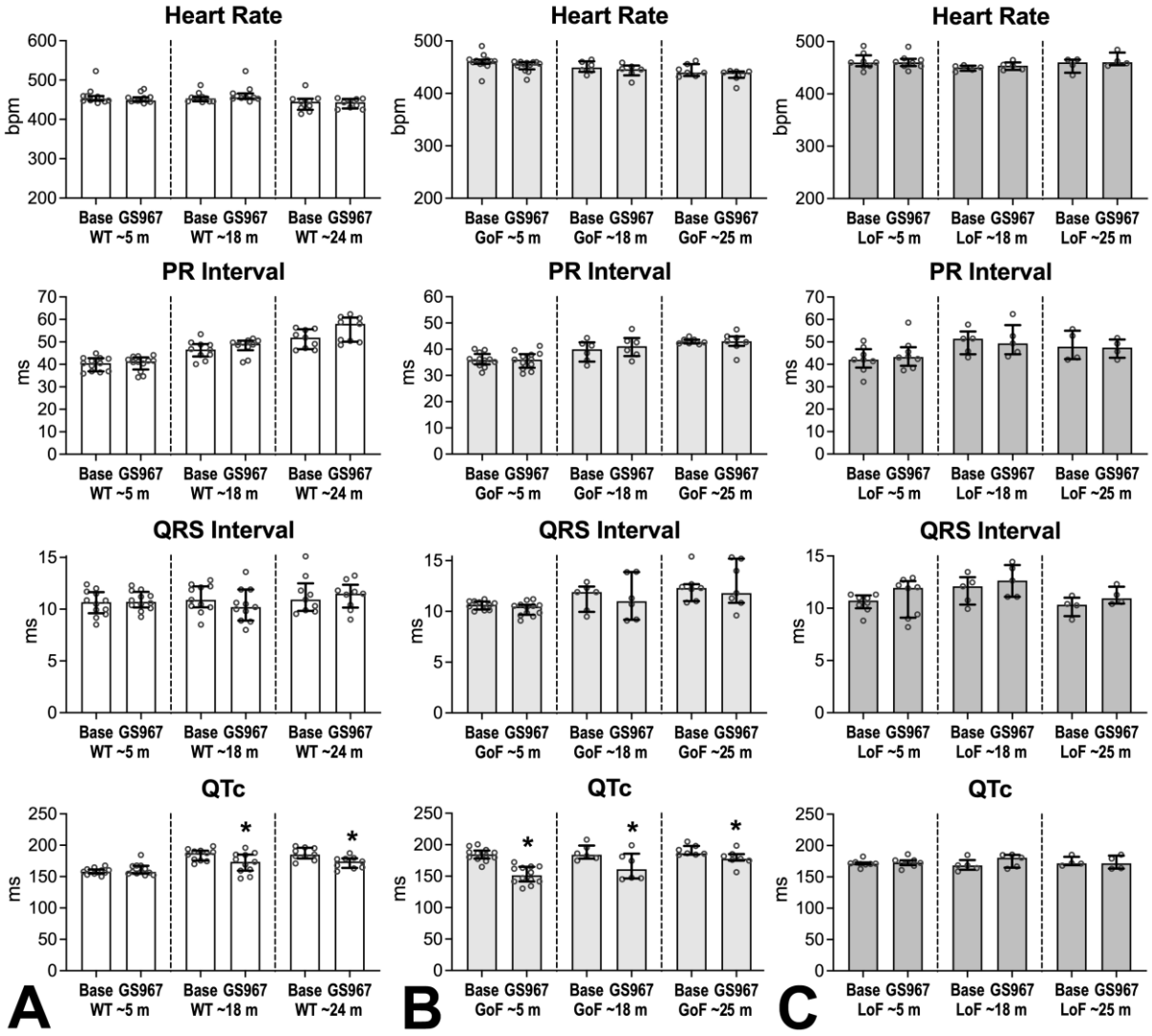

Supplemental Fig S4. Late Na^+ current and ventricular repolarization of male mice. A, Quantitative data for electrocardiographic parameters obtained in anesthetized male WT mice at 3-6 m (~5 m, n=12), 18-19 m (~18 m, n=11), and 24-26 m of age (~24 m, n=9) before (Base) and after administration of GS967. Data are shown as median and interquartile ranges with dot plots. **B,** Quantitative data for electrocardiographic parameters obtained in anesthetized male GoF mice at 5-6 m (~5 m, n=12), 18 m (~18 m, n=6), and 25-28 m of age (~25 m, n=7) before (Base) and after administration of GS967. Data are shown as median and interquartile ranges with dot plots. **C,** Quantitative data for electrocardiographic parameters obtained in anesthetized male LoF mice at 3-5 m (~5 m, n=8), 18-21 m (~18 m, n=5), and 25-27 m of age (~25 m, n=4) before (Base) and after administration of GS967. Data are shown as median and interquartile ranges with dot plots.

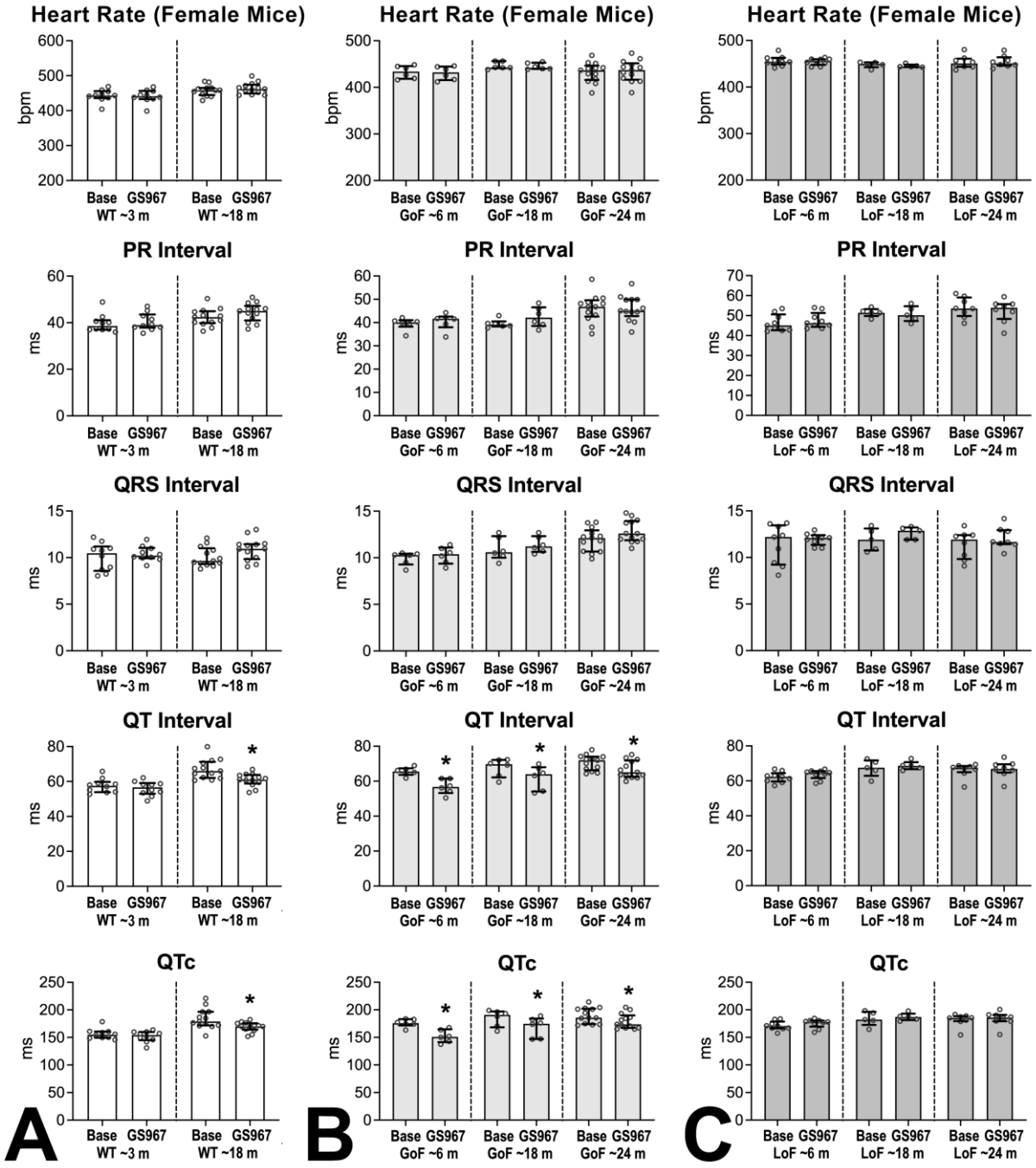

Supplemental Fig S5. Late Na^+ current and ventricular repolarization of female mice. A, Quantitative data for electrocardiographic parameters obtained in anesthetized female WT mice at 3 m (~3 m, n=10) and 18-19 m of age (~18 m, n=13) before (Base) and after administration of GS967. Data are shown as median and interquartile ranges with dot plots. *P<0.001 vs. Base, using paired *t*-test. **B,** Quantitative data for electrocardiographic parameters obtained in anesthetized female GoF mice at 6 m (~6 m, n=6), 18-20 m (~18 m, n=6), and 24-28 m of age (~24 m, n=13) before (Base) and after administration of GS967. Data are shown as median

and interquartile ranges with dot plots. *P<0.01 vs. Base, using paired *t*-test. **C,** Quantitative data for electrocardiographic parameters obtained in anesthetized female LoF mice at 5-7 m (~6 m, n=9), 17-20 m (~18 m, n=5), and 21-25 m of age (~24 m, n=8) before (Base) and after administration of GS967. Data are shown as median and interquartile ranges with dot plots.

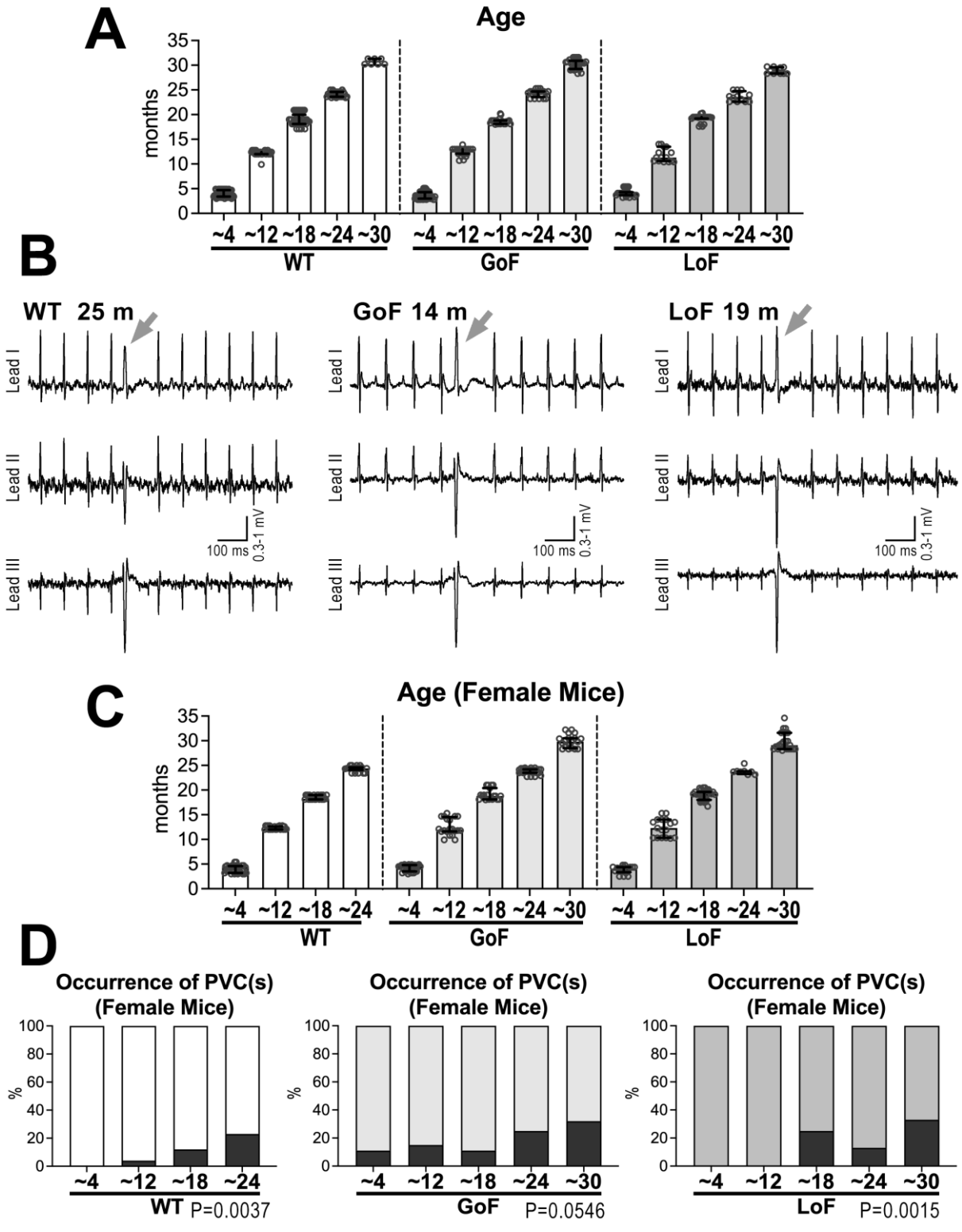

Supplemental Fig S6. Aging and occurrence of ventricular ectopic events. A, Age of male mice included in electrocardiographic studies in the conscious state. **B,** ECG traces for WT, GoF, and LoF female mice showing premature ventricular complexes (PVC; gray arrow). **C,** Age of female mice included in electrocardiographic studies in

the conscious state. **D**, Quantitative data for the fraction of aging female mice presenting isolated or multiple PVCs (black segment) and mice free of events (upper segment). Data for WT, GoF, and LoF female mice at 3-5 m (~4, n=29, 27, 18, respectively), 10-15 m (~12, n= 23, 20, 17, respectively), 17-21 m (~18, n= 25, 19, 28, respectively), 23-25 m (~24, n= 22, 24, 8, respectively), and GoF and LoF female mice at 28-35 m of age (~30, n= 19 and 24, respectively) are reported. For each genotype, P value using Chi-square test for trend is indicated.

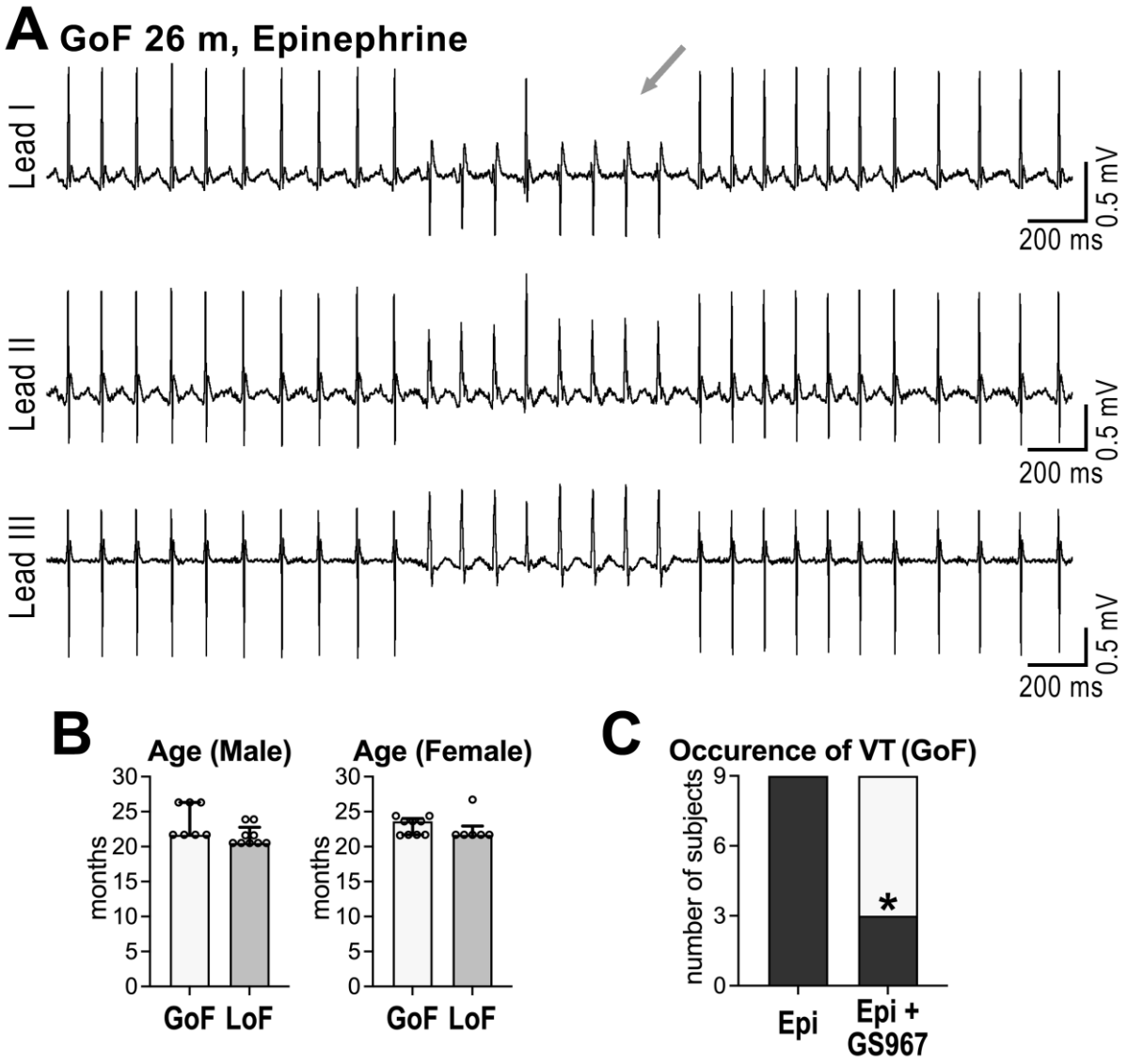

Supplemental Fig S7. Late Na^+ current and occurrence of ventricular ectopic in aged mice events. A, ECG traces for a conscious GoF male mouse at 26 m of age following administration of epinephrine (2 mg/kg body weight, i.p.) showing ventricular tachycardia (VT, gray arrow). **B,** Age of male and female mice included in electrocardiographic studies with epinephrine challenge. **C**, Quantitative data for occurrence of VT for a group of conscious mice exposed to epinephrine challenge in the absence (Epi) and presence of the I_{NaL} inhibitor GS967 (Epi + GS967). GoF mice presenting VT with adrenergic stimulation alone (n=9, male and female mice at 20-28 m) were treated with GS967 on a different day and ~30 min later exposed to epinephrine challenge (Epi+GS967). *P<0.01 vs. Epi using both Fisher's exact test and Chi-square test.

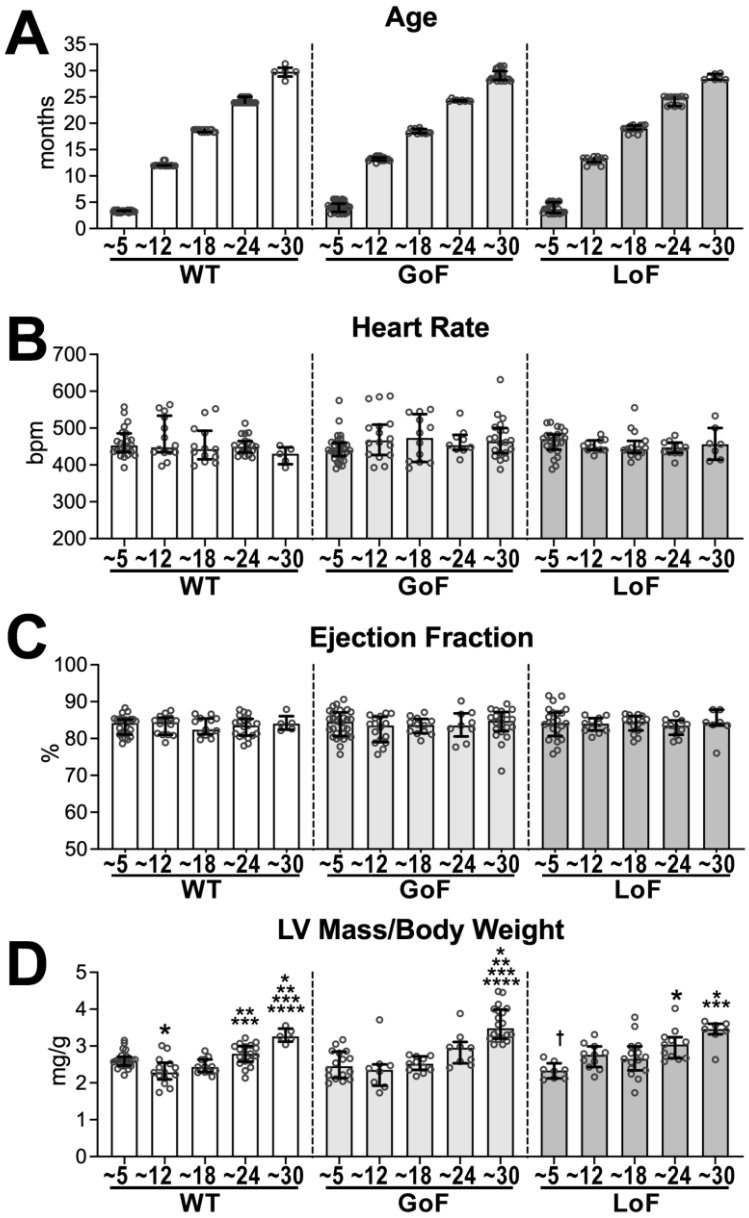

Supplemental Fig S8. Echocardiographic properties of aging male mice. A, Animal age. **B-D,** Quantitative data for heart rate (**B**), LV ejection fraction (**C**), and LV mass normalized by body weight (**D**) obtained by echocardiographic imaging in WT, GoF, and LoF male mice at 3-6 m (~5, n=23, 16-30, 8-23, respectively), 12-14 m (~12, n=14, 8-16, 11, respectively), 18-20 m (~18, n=13, 11-12, 15, respectively), 23-25 m (~24, n=18-19, 9, 11, respectively), and 28-31 m of age (~30, n= 5, 20, 7, respectively). Data are shown as median and interquartile ranges with dot plots. *P<0.05 vs. ~5, **P<0.05 vs. ~12, ***P<0.05 vs. ~18, †P<0.05 vs. age-matched WT. Data were tested by one-way ANOVA, followed by Bonferroni multiple comparison test or by Kruskal-Wallis, followed by Dunn's multiple comparison test.

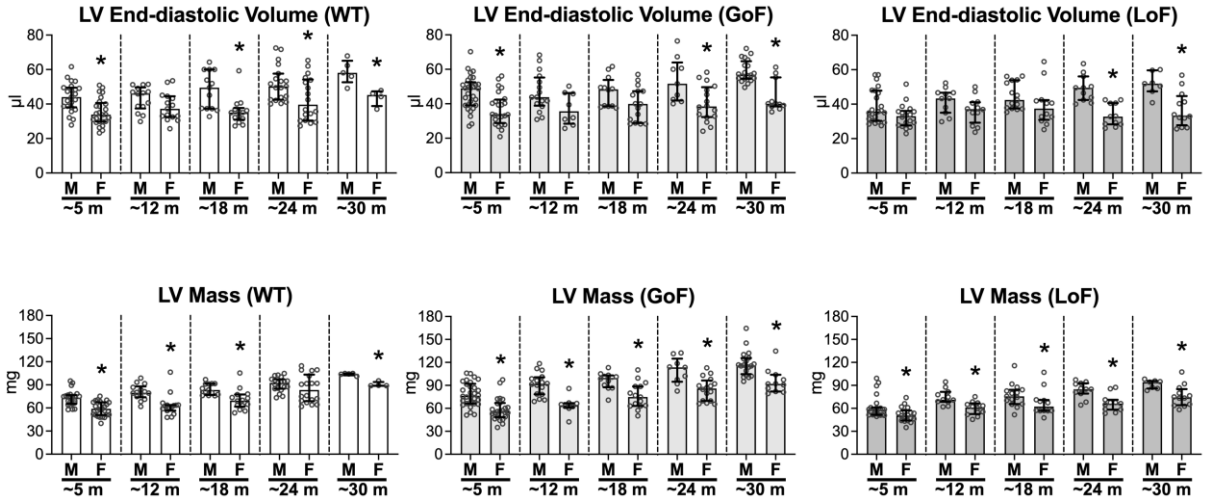

Supplemental Fig S9. Comparison of the echocardiographic properties of age-matched male and female mice. Echocardiographic properties of age-matched male (M) and female (F) mice. Data are shown as median and interquartile ranges with dot plots. *P<0.05 vs. male using unpaired *t*-test or Mann-Whitney test. Presented data is reported in figures illustrating, for each sex, alterations of echocardiographic properties occurring with aging.

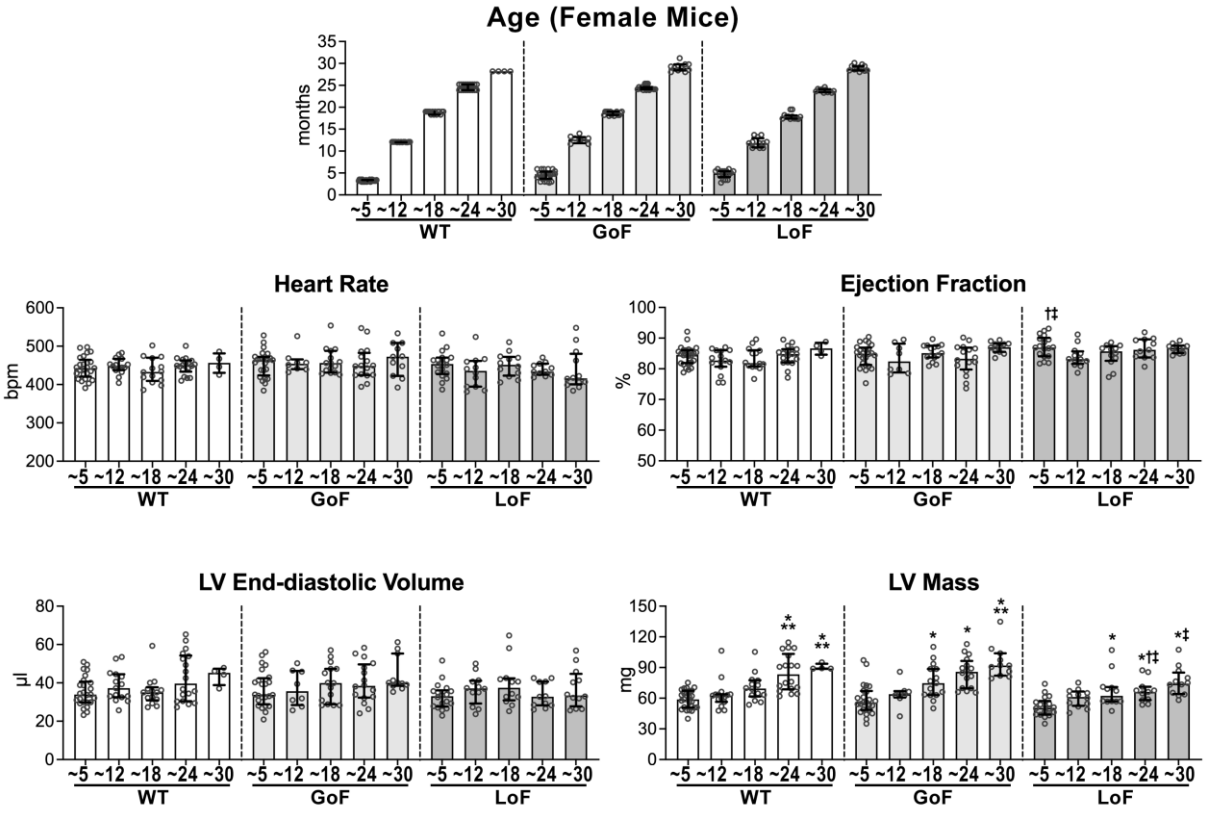

Supplemental Fig S10. Echocardiographic properties of aging female mice. Animal age and quantitative data for functional and anatomical parameters obtained by echocardiographic imaging in WT, GoF, and LoF female mice at 3-6 m (~5, n=25, 24, 18, respectively), 11-14 m (~12, n=15, 8, 12, respectively), 17-20 m (~18, n=14, 15, 12, respectively), 23-25 m (~24, n=18, 16, 12, respectively), and 28-31 m of age (~30, n= 4, 11, 12, respectively). Data are shown as median and interquartile ranges with dot plots. *P<0.05 vs. ~5, **P<0.05 vs. ~12, †P<0.05 vs. age-matched WT, ‡P<0.05 vs. age-matched GoF. Data were tested by one-way ANOVA, followed by Bonferroni multiple comparison test or by Kruskal-Wallis, followed by Dunn's multiple comparison test.

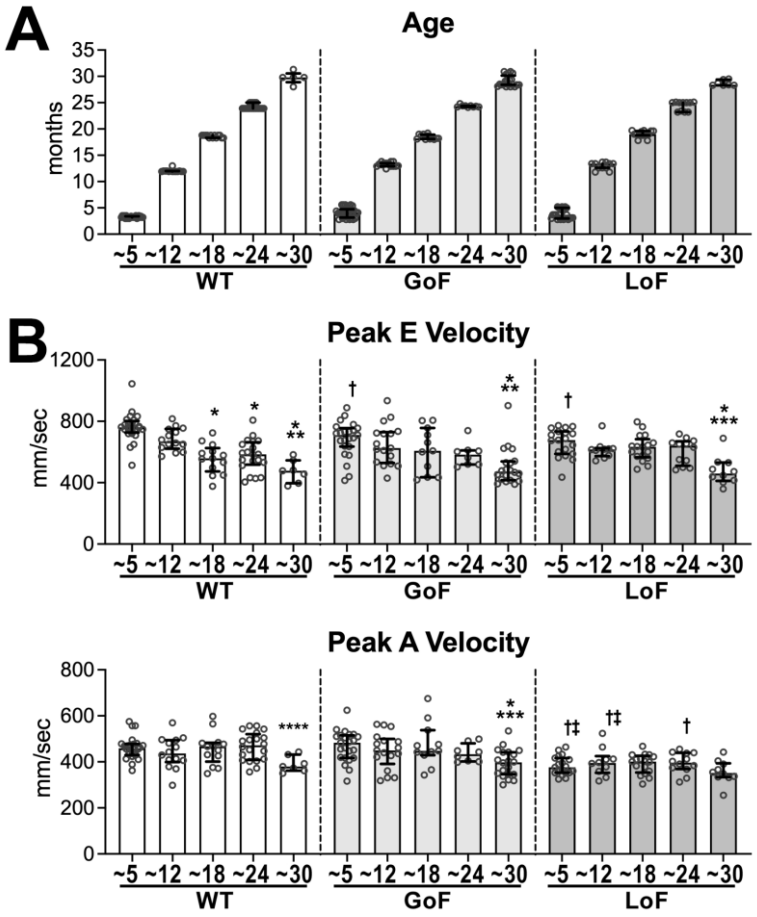

Supplemental Fig S11. Diastolic LV filling properties of aging male mice. Animal age and quantitative data for transmitral flow Doppler echocardiographic parameters obtained in WT, GoF, and LoF male at 3-6 m (~5, n=24, 23, 19, respectively), 12-14 m (~12, n=14, 17, 10, respectively), 18-20 m (~18, n=13, 11, 17, respectively), 23-25 m (~24, n=20, 8, 12, respectively), and 28-31 m of age (~30, n= 7, 20, 10, respectively). Data are shown as median and interquartile ranges with dot plots. *P<0.05 vs. ~5, **P<0.05 vs. ~12, ***P<0.05 vs. ~18, †P<0.05 vs. age-matched WT, ‡P<0.05 vs. age-matched GoF. Data were tested by one-way ANOVA, followed by Bonferroni multiple comparison test or by Kruskal-Wallis, followed by Dunn's multiple comparison test.

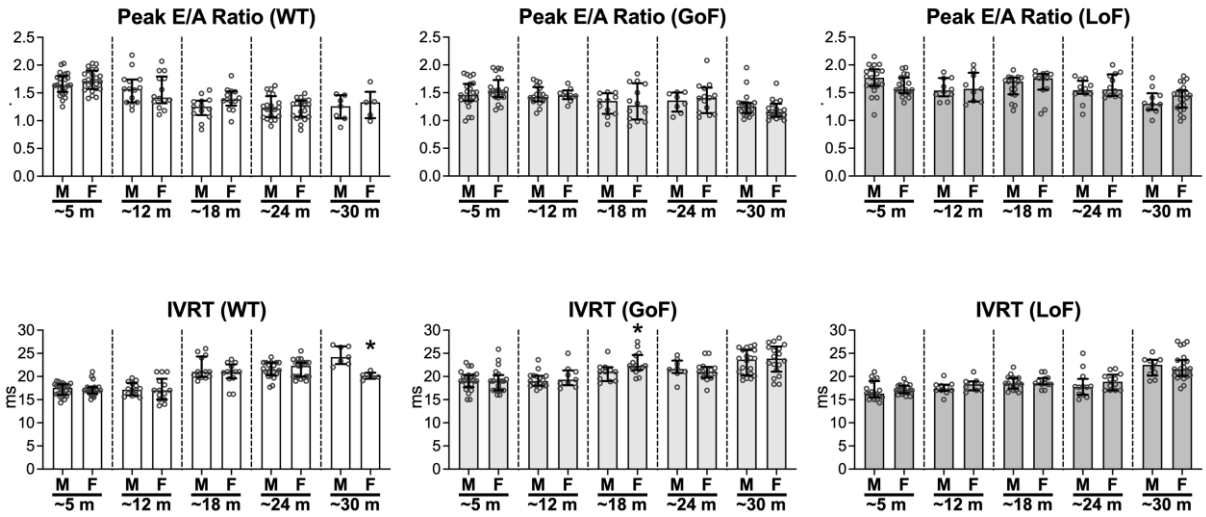

Supplemental Fig S12. Comparison of diastolic LV filling properties of age-matched male and female mice. Data obtained by transmitral flow Doppler echocardiography for age-matched male (M) and female (F) mice. Data are shown as median and interquartile ranges with dot plots. *P<0.05 vs. male using unpaired *t*-test. Presented data is reported in figures illustrating, for each sex, alterations of LV filling properties occurring with aging.

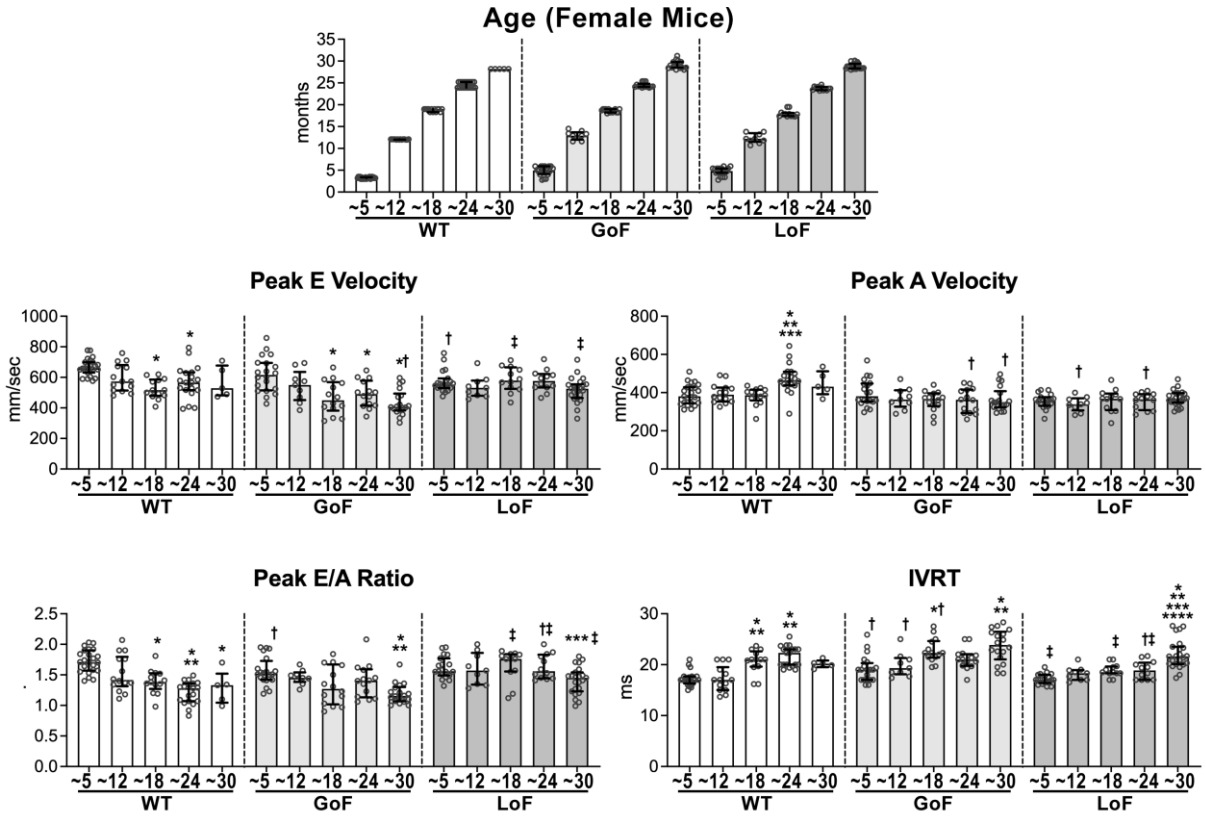

Supplemental Fig S13. Diastolic LV filling properties of aging female mice. Animal age and quantitative data for transmitral flow Doppler echocardiographic parameters obtained in WT, GoF, and LoF female at 3-6 m (~5, n=23, 20, 19, respectively), 11-15 m (~12, n=14, 9, 9, respectively), 17-20 m (~18, n=13, 14, 12, respectively), 23-25 m (~24, n=19, 14, 12, respectively), and 28-31 m of age (~30, n= 5, 18, 23, respectively). Data are shown as median and interquartile ranges with dot plots. *P<0.05 vs. ~5, **P<0.05 vs. ~12, ***P<0.05 vs. ~18, ****P<0.05 vs. ~24, †P<0.05 vs. age-matched WT, ‡P<0.05 vs. age-matched GoF. Data were tested by one-way ANOVA, followed by Bonferroni multiple comparison test or by Kruskal-Wallis, followed by Dunn's multiple comparison test.

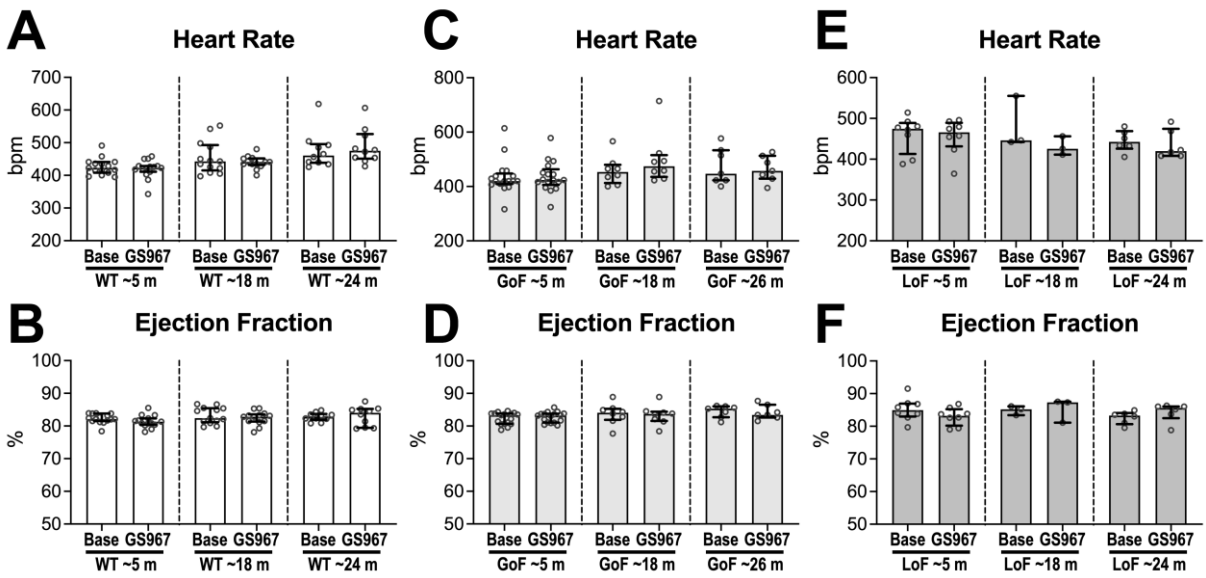

Supplemental Fig S14. Consequences of inhibition of the late Na^+ current on heart rate and ejection fraction. A, B, Quantitative data for two-dimensional echocardiographic parameters obtained in male WT mice at 3-6 m (~5 m, n=15), 18-19 m (~18 m, n=13), and 24-26 m of age (~24 m, n=10) before (base) and after administration of GS967. Data are shown as median and interquartile ranges with dot plots. **C, D,** Quantitative data for two-dimensional echocardiographic parameters obtained in male GoF mice at 5-8 m (~5 m, n=17), 18-19 m (~18 m, n=8), and 26-28 m of age (~26 m, n=7) before (base) and after administration of GS967. Data are shown as median and interquartile ranges with dot plots. **E, F,** Quantitative data for two-dimensional echocardiographic parameters obtained in male LoF mice at 3-5 m (~5 m, n=8), 18-20 m (~18 m, n=3), and 23-25 m of age (~24 m, n=6) before (base) and after administration of GS967. Data are shown as median and interquartile ranges with dot plots.

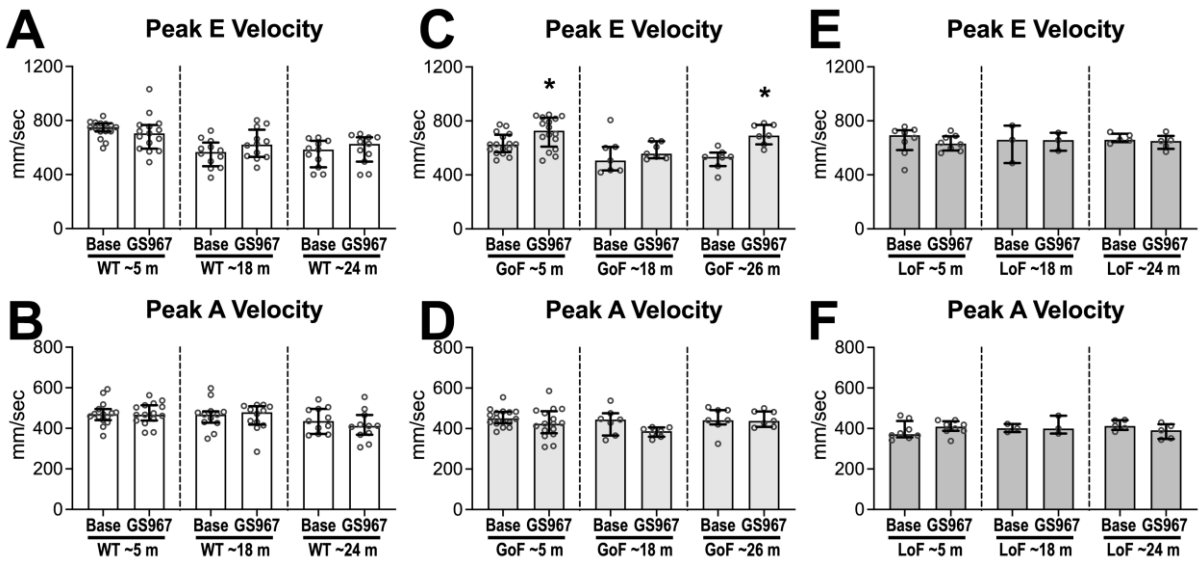

Supplemental Fig S15. Late Na^+ current and LV filling pattern of male mice. A, B, Quantitative data for transmitral flow Doppler echocardiographic parameters obtained in male WT mice at 3-6 m (~5 m, n=15), 18-19 m (~18 m, n=12), and 24-26 m of age (~24 m, n=11) before (base) and after administration of GS967. Data are shown as median and interquartile ranges with dot plots. **C, D,** Quantitative data for transmitral flow Doppler echocardiographic parameters obtained in male GoF mice at 5-8 m (~5 m, n=16), 18-19 m (~18 m, n=7), and 26-28 m of age (~26 m, n=7) before (base) and after administration of GS967. Data are shown as median and interquartile ranges with dot plots. *P<0.05 vs. Base, using paired *t*-test. **E, F,** Quantitative data for transmitral flow Doppler echocardiographic parameters obtained in male LoF mice at 3-5 m (~5 m, n=8), 18-20 m (~18 m, n=3), and 23-25 m of age (~24 m, n=5) before (base) and after administration of GS967. Data are shown as median and interquartile ranges with dot plots.

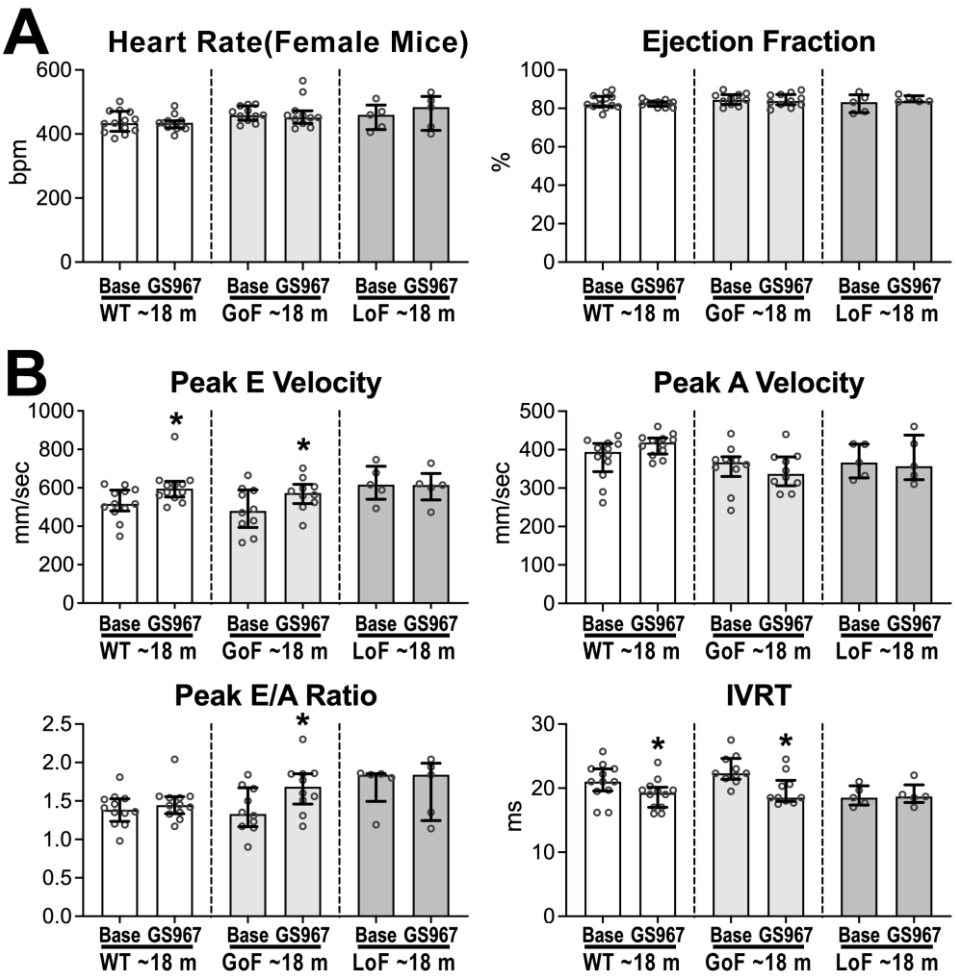

Supplemental Fig S16. Late Na^+ current and LV filling pattern of female mice. A, Quantitative data for two-dimensional echocardiographic parameters obtained in female WT mice at 18-19 m (WT ~18 m, n=13), female GoF mice at 18-21 m (GoF ~18 m, n=11), and female LoF mice at 17-20 m of age (LoF ~18 m, n=5) before (base) and after administration of GS967. Data are shown as median and interquartile ranges with dot plots. **B,** Quantitative data for transmitral flow Doppler echocardiographic parameters obtained in female WT mice at 18-19 m (WT ~18 m, n=12), female GoF mice at 18-19 m (GoF ~18 m, n=10), and female LoF mice at 17-20 m of age (LoF ~18 m, n=5) before (base) and after administration of GS967. Data are shown as median and interquartile ranges with dot plots. *P<0.05 vs. Base, using paired *t*-test or Wilcoxon test.

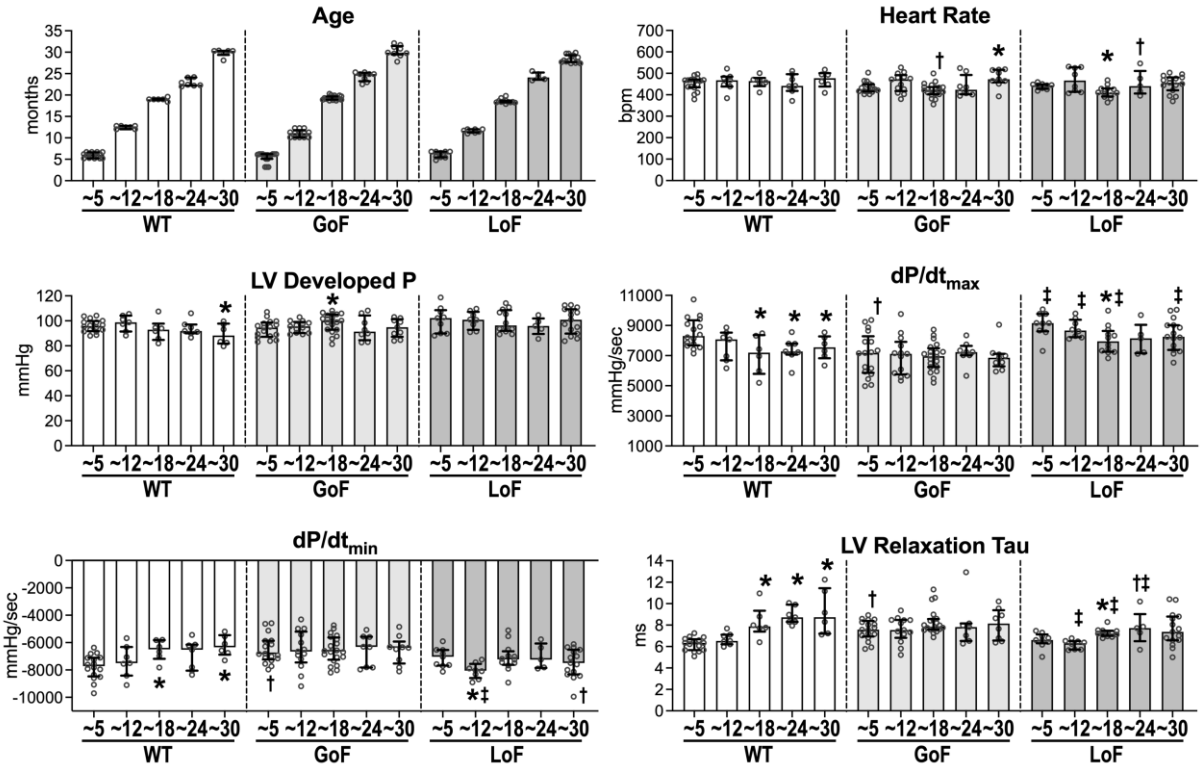

Supplemental Fig S17. LV hemodynamics of aging male mice. Animal age and quantitative data of LV hemodynamics obtained by PV transducer in the closed chest preparation in WT, GoF, and LoF male mice at 3-7 m (~5, n=16, 17, 9, respectively), 10-13 m (~12, n=7, 13, 8, respectively), 18-20 m (~18, n=6, 20, 12, respectively), 22-26 m (~24, n=7, 8, 5, respectively), and 27-32 m of age (~30, n= 6, 9, 15, respectively). Data are shown as median and interquartile ranges with dot plots. *P<0.05 vs. ~5 using *t*-test. †P<0.05 vs. age-matched WT, ‡P<0.05 vs. age-matched GoF, using one-way ANOVA, followed by Bonferroni multiple comparison test or by Kruskal-Wallis, followed by Dunn's multiple comparison test.

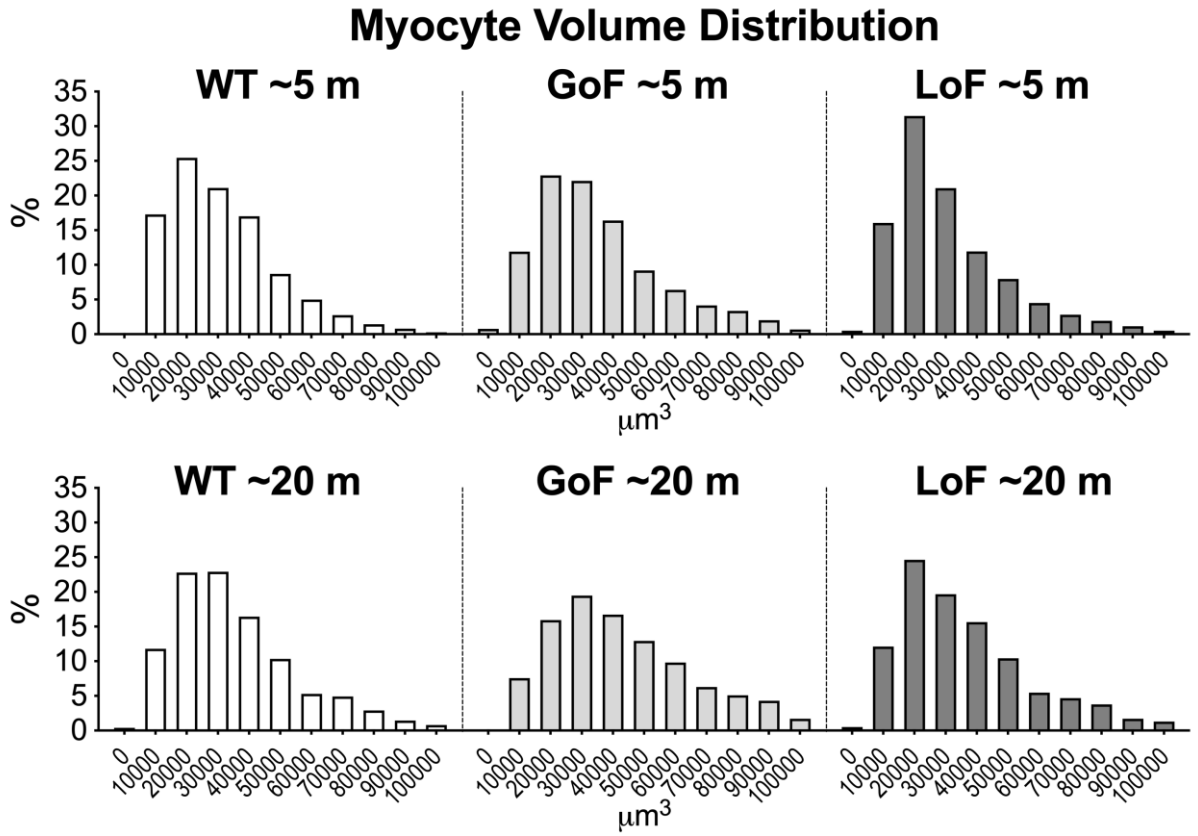

Supplemental Fig S18. Aging alters LV myocytes size of male mice. Distribution of volume of myocytes obtained from WT, GoF, and LoF male mice at 5-7 m (~5, n=757 cells from 5 WT mice, n=889 cells from 6 GoF mice, n= 777 from 5 LoF mice, respectively) and 19-24 m (~20, n=754 cells from 5 WT mice, n=764 cells from 5 GoF mice, n= 766 from 5 LoF mice, respectively).

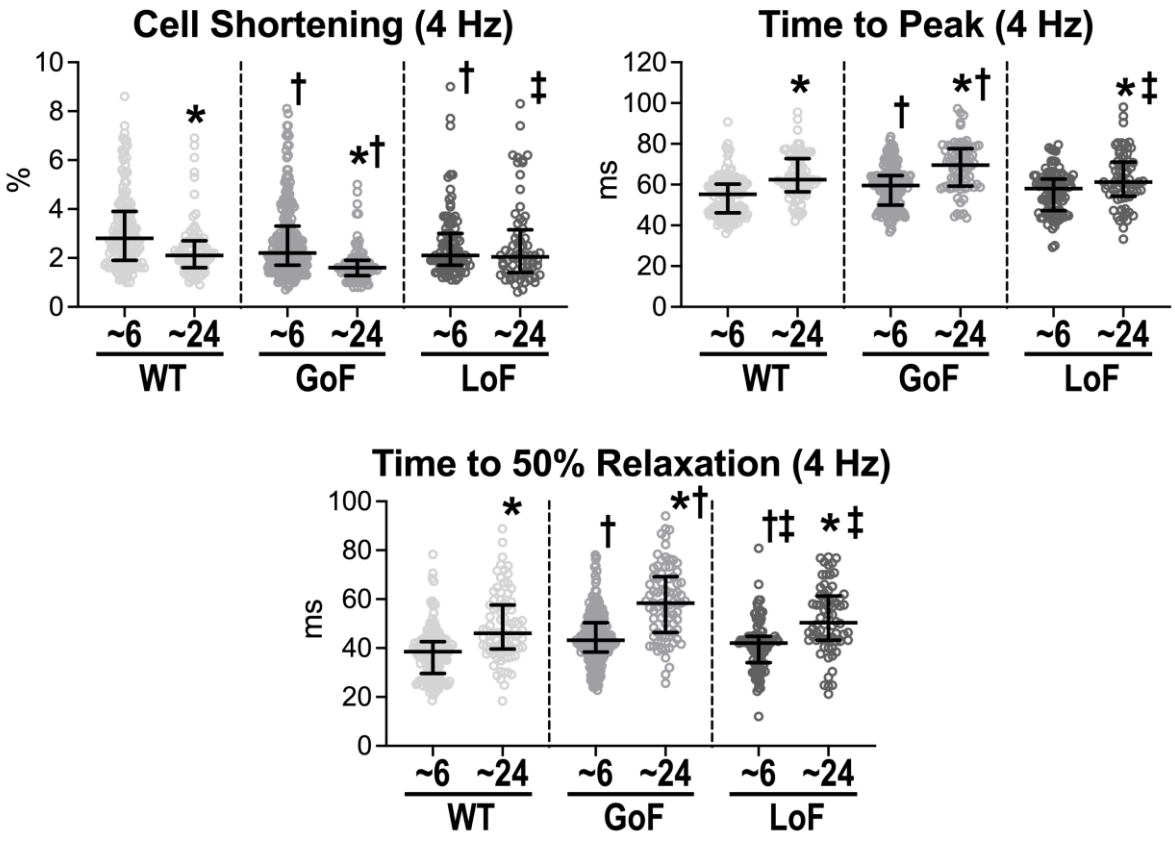

Supplemental Fig S19. Aging and late Na^+ current alter cell mechanics of cardiomyocytes. Quantitative data for cell shortening properties of LV myocytes stimulated at 4 Hz pacing rate obtained. Cells were obtained from WT, GoF, and LoF male mice at 4-7 m (~6, n=169 cells from 5 WT mice, n=233 cells from 9 GoF mice, n=99 from 4 LoF mice, respectively) and 22-28 m (~24, n=83 cells from 4 WT mice, n=78 cells from 5 GoF mice, n=68 from 4 LoF mice, respectively). Data are shown as median and interquartile ranges with dot plots. *P<0.001 vs. ~6 using Mann-Whitney test. †P<0.05 vs. age-matched WT, ‡P<0.05 vs. age-matched GoF, using one-way ANOVA, followed by Bonferroni multiple comparison test or Kruskal-Wallis, followed by Dunn's multiple comparison test.

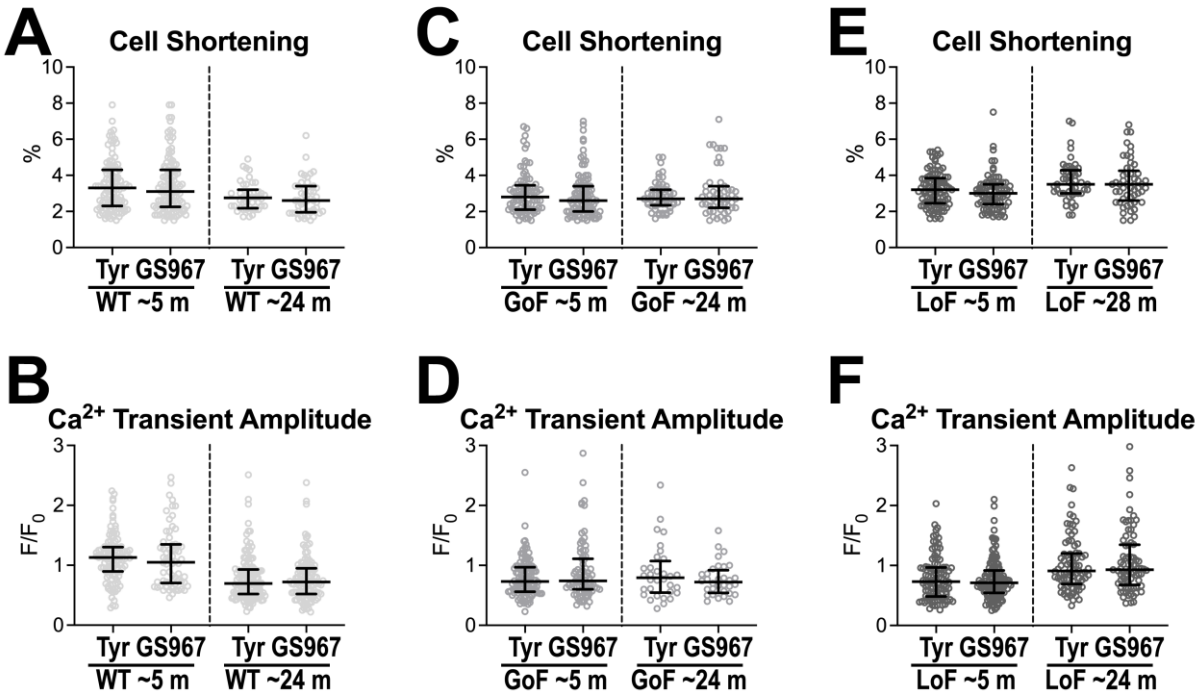

Supplemental Fig S20. Late Na^+ current and properties of Ca^{2+} transients and cell mechanics. Quantitative data for fractional cell shortening and Ca^{2+} transient amplitude of LV myocytes stimulated at 1 Hz pacing rate in the absence (Tyrode solution, Tyr) and presence of the I_{NaL} inhibitor GS967 (300 nmol/L). **A,** Data for cell shortening of myocytes from WT male mice at 4-6 m (~5 m, n=5) in the absence (n=103) and presence of GS967 (n=113) and myocytes from WT male mice at 24-28 m (~24 m, n=2) in the absence (n=42) and presence of GS967 (n=45). **B,** Data for Ca^{2+} transients of myocytes from WT male mice at 5 m (~5 m, n=5) in the absence (n=110) and presence of GS967 (n=64) and myocytes from WT male mice at 21-28 m (~24 m, n=6) in the absence (n=134) and presence of GS967 (n=112). **C,** Data for cell shortening of myocytes from GoF male mice at 5-6 m (~5 m, n=4) in the absence (n=81) and presence of GS967 (n=96) and myocytes from GoF male mice at 24-25 m (~24 m, n=3) in the absence (n=53) and presence of GS967 (n=51). **D,** Data for Ca^{2+} transients of myocytes from GoF male mice at 3-6 m (~5 m, n=4) in the absence (n=108) and presence of GS967 (n=79) and myocytes from GoF male mice at 24-25 m (~24 m, n=3) in the absence (n=32) and presence of GS967 (n=32). **E,** Data for cell shortening of myocytes from LoF male mice at 5-7 m (~5 m, n=4) in the absence (n=101) and presence of GS967 (n=85) and myocytes from LoF male mice at 28 m (~28 m, n=3) in the absence (n=48) and presence of GS967 (n=53). **F,** Data for Ca^{2+} transients of myocytes from LoF male mice at 5-7 m (~5 m, n=4) in the absence

(n=104) and presence of GS967 (n=120) and myocytes from LoF male mice at 21-28 m (~24 m, n=5) in the absence (n=79) and presence of GS967 (n=77). Data are shown as median and interquartile ranges with dot plots.

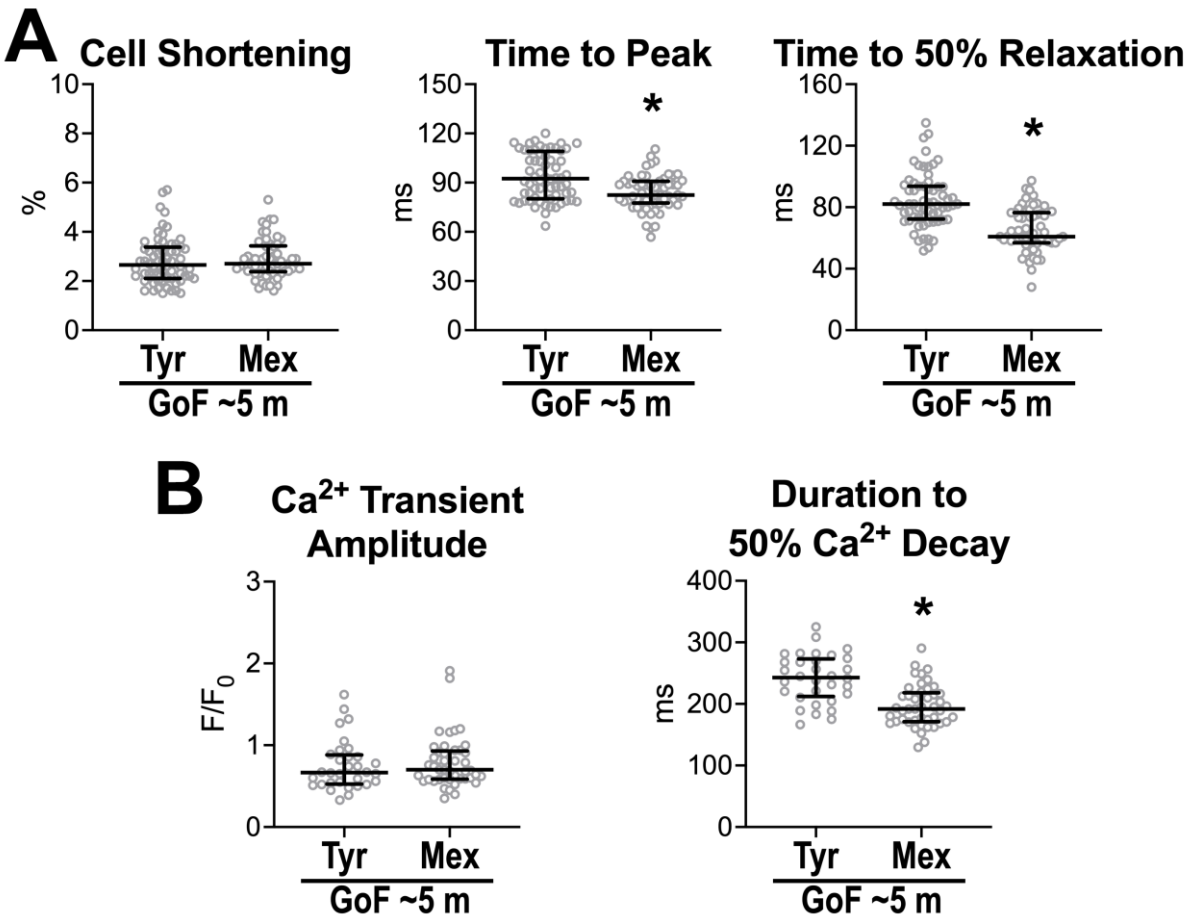

Supplemental Fig S21. Late Na^+ current and kinetics of Ca^{2+} transients and cell mechanics. A, B, Quantitative data for cell shortening and Ca^{2+} transient properties of LV myocytes stimulated at 1 Hz pacing rate in the absence (Tyrode solution, Tyr) and presence of the I_{NaL} inhibitor mexiletine (Mex, 10 µmol/L). **A,** Data for cell shortening of myocytes from GoF male mice at 5 m (~5 m, n=3) in the absence (n=64) and presence of mexiletine (n=58). **B,** Data for Ca^{2+} transients of myocytes from a GoF male mice at 5-6 m (~5 m) in the absence (n=32) and presence of mexiletine (n=45). Data are shown as median and interquartile ranges with dot plots. *P<0.001 vs. Tyr in the same experimental group using unpaired *t*-test or Mann-Whitney test.

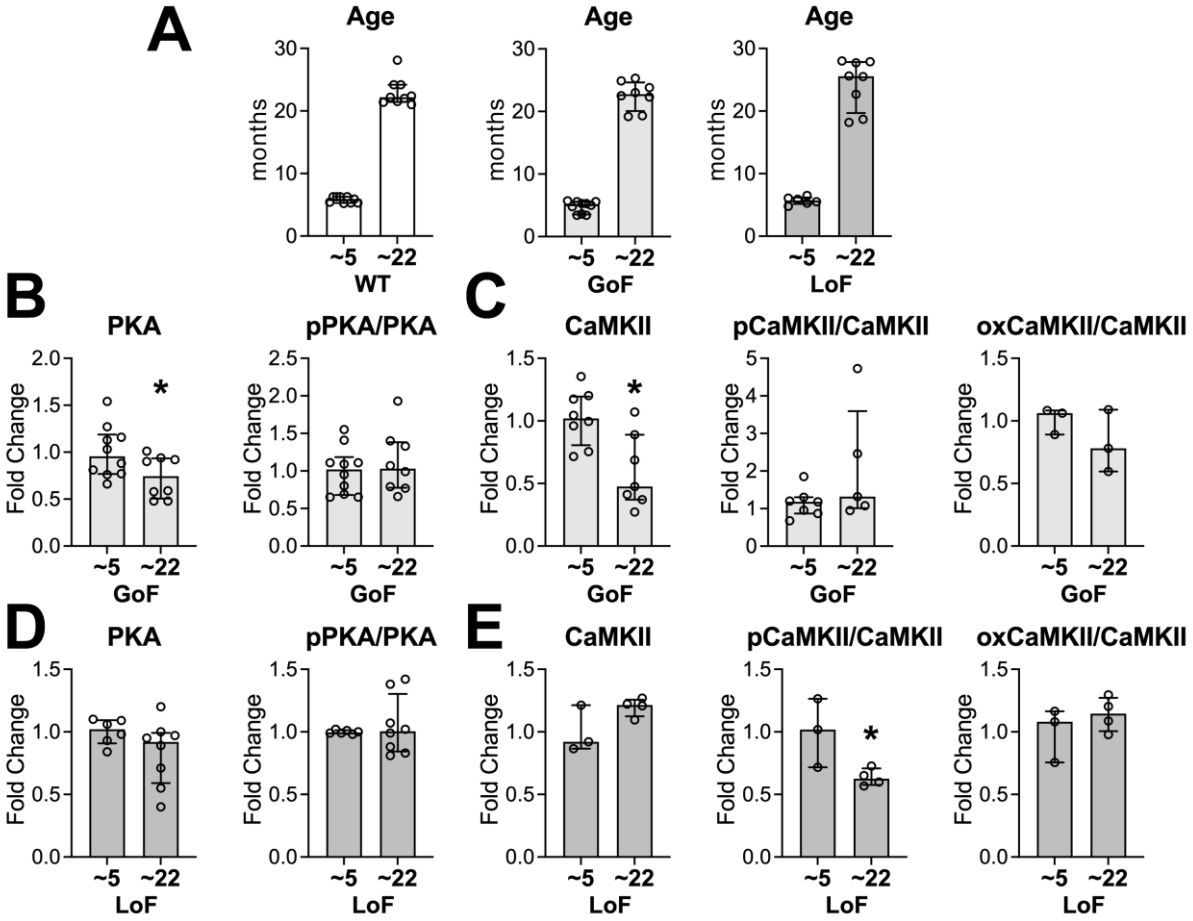

Supplemental Fig S22. Aging, late Na^+ current, and status of key regulatory proteins. A, Age of animals employed to obtain cardiomyocytes utilized for Western blot studies. Cells were collected from WT, GoF, and LoF male mice at 3-7 m (~5, n=9, 10, 6, respectively) and at 18-28 m of age (~22, n=9, 8, 8, respectively). Data are shown as median and interquartile ranges with dot plots. **B**, Quantitative data for expression of total PKA and pPKA-to-PKA ratio in LV myocytes of GoF mice at 3-7 m (~5, n=10) and 18-28 m of age (~22, n=8). Data are reported as median and interquartile ranges with dot plots as fold changes with respect to ~5 m. *P<0.05 vs. ~5 using unpaired *t*-test. **C**, Quantitative data for expression of total CaMKII, pCaMKII-to-CaMKII ratio, and oxCaMKII-to-CaMKII ratio in LV myocytes of GoF mice at 3-7 m (~5, n=3-8) and 18-28 m of age (~22, n=3-7). Data are reported as median and interquartile ranges with dot plots as fold changes with respect to ~5. *P<0.05 vs. ~5 using unpaired *t*-test. **D**, Quantitative data for expression of total PKA and pPKA-to-PKA ratio in LV myocytes of LoF mice at 3-7 m (~5, n=6) and 18-28 m of age (~22, n=8). Data are reported as median and interquartile ranges with dot plots as fold

changes with respect to ~5 m. **E**, Quantitative data for expression of total CaMKII, pCaMKII-to-CaMKII ratio, and oxCaMKII-to-CaMKII ratio in LV myocytes of LoF mice at 3-7 m (~5, n=3) and 18-28 m of age (~22, n=4). Data are reported as median and interquartile ranges with dot plots as fold changes with respect to ~5. *P<0.05 vs. ~5 using unpaired *t*-test. **F,** Quantitative data for expression of total PLN and pPLN-to-PLN ratio in LV myocytes of WT male mice at 3-7 m (~5, n=9) and 18-28 m of age (~22 m, n=9). Data are reported as median and interquartile ranges with dot plots as fold changes with respect to ~5 m.

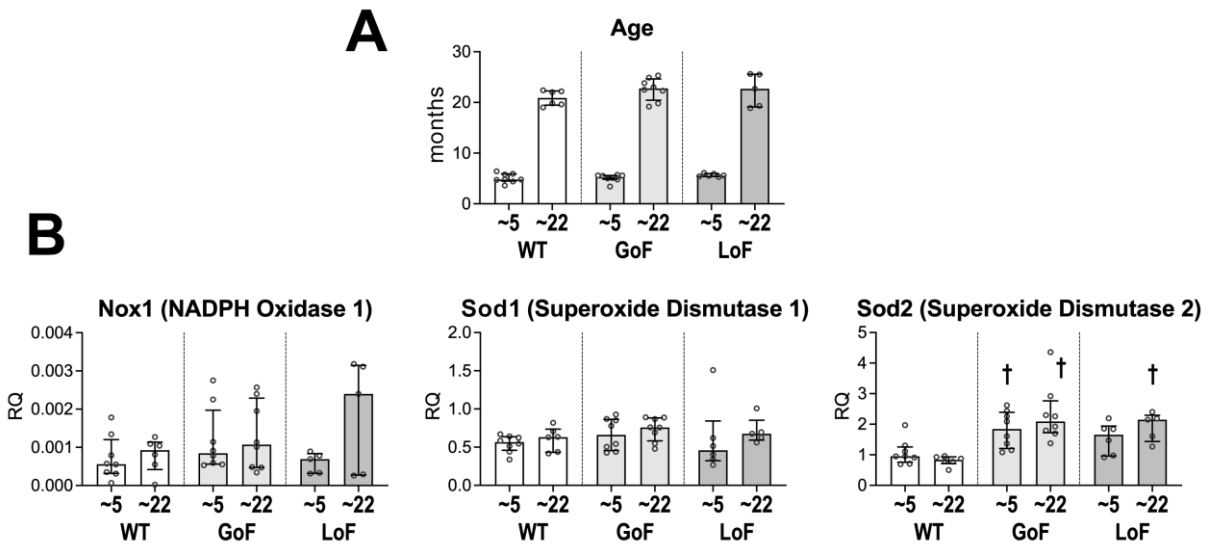

Supplemental Fig S23. Aging, late Na^+ current, and altered expression of ROS-related genes. A, Age of animals employed to obtain cardiomyocytes utilized for RT-PCR studies. Cells were collected from WT, GoF, and LoF male mice at 3-7 m (~5, n=8, 8, 6, respectively) and at 19-26 m of age (~22, n=6, 8, 5, respectively). Data are shown as median and interquartile ranges with dot plots. **B**, Quantitative data for expression of genes related to enzymes involved in ROS production and antioxidant defense in cardiomyocytes from WT, GoF, and LoF male mice at 3-6 m (~5 m, n=8, 8, 6, respectively) and at 19-26 m (~22 m, n=6, 8, 5, respectively). Transcript levels for *Nox1*, encoding for NADPH oxidase 1, *Sod1*, encoding for superoxide dismutase 1, and *Sod2*, encoding for superoxide dismutase 2, are shown as median and interquartile ranges. RQ: relative quantity with respect to hypoxanthine guanine phosphoribosyl transferase (*Hprt*). †P<0.05 vs. age-matched WT using Kruskal-Wallis, followed by Dunn's multiple comparison test.

Supplemental Table S1. Primers for PCR analysis

Gene	Primers
Mouse Hprt	F:5'- AGCCCCAAAATGGTTAAGGT -3'
	R: 5'- CAAGGGCATATCCAACAACA -3'
Mouse *Nox1*	F: 5'- GCTTCCTCATCTGCAATTCCA-3'
	R: 5'- CTTCGCTTTTATCGCTCCCA-3'
Mouse *Nox4*	F: 5'- TTAAACACCTCTGCCTGCTC-3'
	R: 5'- GATGCTCTGCTTAAACACAATCC-3'
Mouse *Sod1*	F: 5'- GTCCTTTCCAGCAGTCACAT-3'
	R: 5'- GGTTCCACGTCCATCAGTATG-3'
Mouse *Sod2*	F: 5'- TGCTCCCACACGTCAATC-3'
	R: 5'- CAAGGTCGCTTACAGATTGCT-3'
Mouse *Homox1*	F: 5'- TTGTGTTCCTCTGTCAGCATC-3'
	R: 5'- ACACTCTGGAGATGACACCT-3'
Mouse *Cybb*	F: 5'- CACCTCCATCTTGAATCCCTT-3'
	R: 5'- TGTTCCTGTACCTTTGTGAGAG-3'
Mouse *Nppa*	F: 5'- ATC ACCCTGGGCTTCTTCCT -3'
	R: 5'- TGTTGGACACCGCACTGTAC -3'
Mouse *Myh7*	F: 5'- ACTGTCAACACTAAGAGGGTCA -3'
	R: 5'- TTGGATGATTTGATCTTCCAGGG -3'

Supplemental Table S2. List of antibodies

Antibody	Dilution	Company	Cat #
Na Channel α-subunit NaV1.5 (SCN5A) Rabbit	1:1000	Custom (Dr. Hund)	n/a
Phosphor-NaV1.5 (Ser571) Rabbit	1:1000	Custom (Dr. Hund)	n/a
CaMKII (pan) (D11A10) Rabbit mAb	1:1000	Cell Signaling Technologies	4436S
Phospho-CaMKII (Thr286) (D21E4) Rabbit mAb	1:1000	Cell Signaling Technologies	12716S
Anti-oxidized-CaM Kinase II (Met281/282) Rabbit pAb	1:1000	Millipore Sigma	07-1387
PKA C-α (D38C6) Rabbit mAb	1:1000	Cell Signaling Technologies	5842S
Phospho-PKA C (Thr197) (D45D3) Rabbit mAb	1:1000	Cell Signaling Technologies	5661
β-Actin (D6A8) Rabbit mAb	1:1000	Cell Signaling Technologies	8457S